AN X-RAY PREIONISED EXCIMER LASER

by

Michael Robert Osborne

Thesis submitted in partial fulfilment of the requirements for the degree of Doctor of Philosophy of the University of London, and for the Diploma of Membership of the Imperial College of Science and Technology.

Blackett Laboratory
Imperial College
London
England.

July 1985

ABSTRACT

An X-ray preionised avalanche discharge pumped laser system has been designed and developed and used to pump the $XeCl^*$ excimer which lases at $\sim$308 nm in the ultra-violet.

The e-beam based X-ray source produces an exposure of $\sim$100 mR, and this has been found to be an order of magnitude greater than required. The versatile pulsed power supply has proved capable of exciting the large, 1 litre, active volume for prolonged periods of time. The voltage peaking effect of a short transmission line section has been demonstrated, and has allowed electrical efficiencies of up to 3.2% to be achieved. The maximum output energy of 4.7J corresponds to 1.2J/l atm and gives a peak power in excess of 50MW.

The duration and temporal shape of the laser output pulse have been found to be strongly dependent on both the electrical excitation rate and the partial pressure of the halogen donor molecule, HCl, in the laser gas mixture. The output pulse duration has been extended to > 250ns F.W.H.M., and this represents the longest pulse yet produced from such a high power discharge pumped laser. However, premature termination of the laser output has been found to occur, and a series of experiments has shown that this is caused by the collapse of the discharge plasma into narrow, columnar channels.

ACKNOWLEDGEMENTS

It is a pleasure to be able to thank my supervisor, Dr. M.H.R. Hutchinson, for his support and encouragement throughout my time at Imperial College, and for his contributions to the work described in this thesis. Special thanks are also due to Dr. P.W. Smith, without whose drive, enthusiasm and considerable expertise the laser system could not have been built.

The technical support given by John Bean and the Optics Workshop has been a major contribution to the rapid progress of the work, and the many useful discussions with other members of the laser group, both past and present, have been a great help.

Finally, I would like to thank my wife and friends, who have made the past three years so enjoyable.

Deanne Eastwood is to be thanked and congratulated for correcting my spelling and grammar and generally typing this thesis more accurately than it was written.

Financial support from the Science and Engineering Research Council is gratefully acknowledged.

CONTENTS

LIST OF FIGURES

LIST OF FIGURES (continued)

Figure Number Page

To my parents

CHAPTER 1

INTRODUCTION

1.1 Introduction

The term 'excimer' is now used to describe both homonuclear and heteronuclear molecules which have bound electronically excited states but dissociative ground states. The broad-band emissions from such molecules were first observed at the turn of the century[1.1], but it was not until 1932 that their structure was identified[1.2]. Since that time many excimer molecules have been identified, and in 1960 their potential as lasing species was recognised[1.3]. However, it was not for another ten years that the first excimer laser was demonstrated by injecting a high energy electron beam (e-beam) into liquid xenon[1.4]. The first rare gas halide excimer laser was operated in 1975[1.5] following earlier observations of fluorescence from these species[1.6,1.7]. There has followed ten years of rapid development to demonstrate the ability of rare gas halide lasers to generate very high peak power radiation in both the near and far U.V. regions of the spectrum - an area in which only the nitrogen laser had previously operated.

In this first chapter we will give a very brief review of the rare gas halide spectroscopy and of the reaction kinetics, illustrating features of their structure which give rise to particular requirements for efficient laser operation. The various ways of meeting these requirements will then be discussed, with particular emphasis on the technique of X-ray preionised avalanche discharge pumping, which will be of particular relevance to the work described in this thesis.

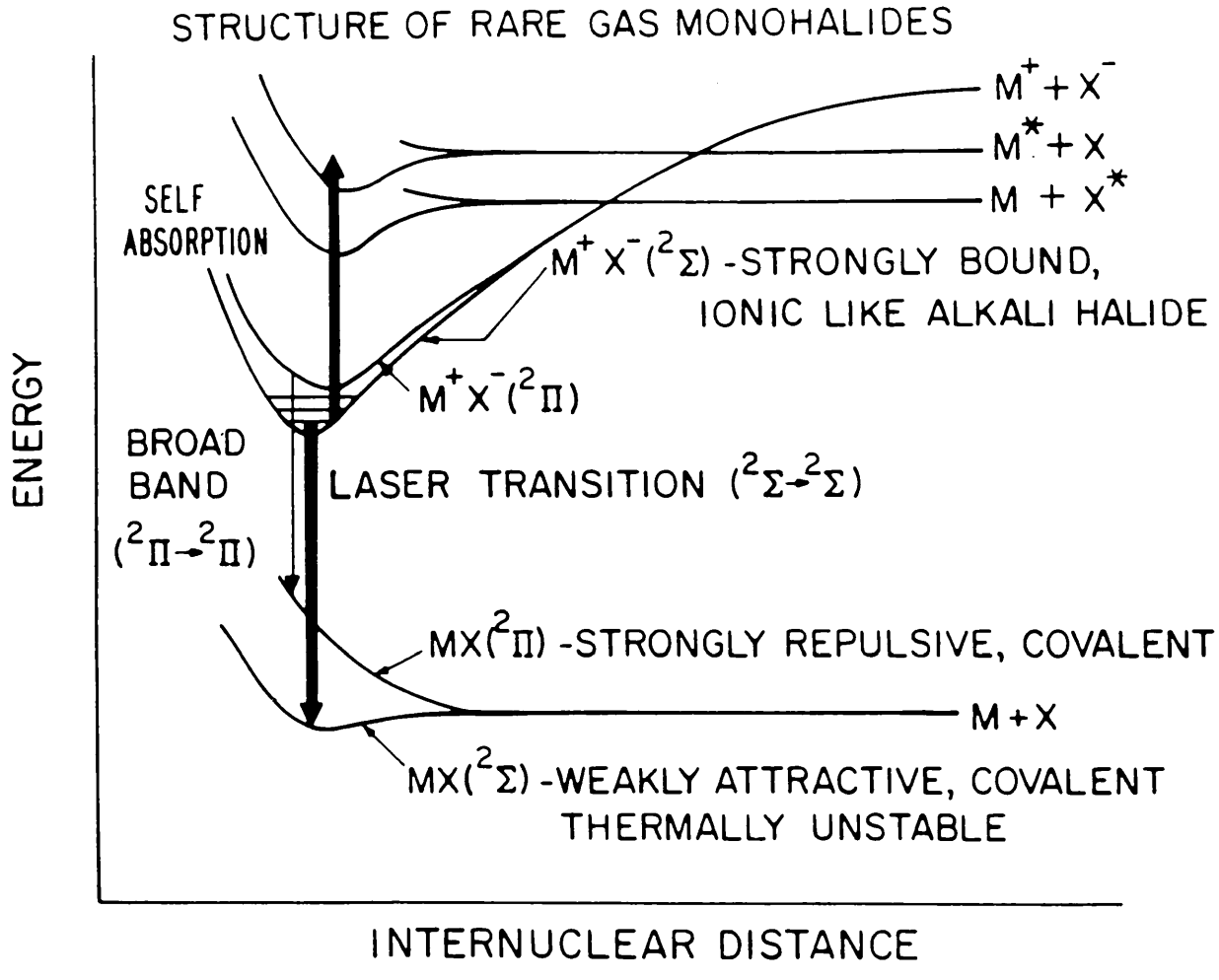

Figure 1.1 Generalised energy level diagram for a rare gas halide molecule. M = rare gas, X = halogen.

1.2 Rare gas halides:- Spectroscopy and Kinetics

The topics covered in this section have received much attention in the recent past, and the reader is referred to the literature for more detailed information than that given here [1.8-1.12].

Figure 1.1 shows a generalised energy level diagram for a rare gas halide molecule formed between the rare gas, M, and the halogen, X. The ground state combines the ^1S state of the rare gas with the ^2P state of the halogen, giving rise to two molecular states. The lowest, or X, state has designation $^2\Sigma$ and is repulsive in most cases, but weakly bound in others such as XeCl, binding energy 255 cm^{-1}, and XeF, binding energy 1065 cm^{-1}. The higher of the two ground states, or A state, has the molecular designation $^2\Pi$ and is always strongly repulsive. The higher lying states which correspond to free ions of the rare gas (^2P) and halogen (^1S) at infinite internuclear separation are, in order of increasing energy, $B^2\Sigma$, $C^2\Pi$, $D^2\Pi$ and so on. Transition rules give allowed radiative transitions of $B \rightarrow X$, $C \rightarrow A$, $D \rightarrow X$ etc. Of these, the $B \rightarrow X$ is generally the most intense. This takes place from a particular vibration level of the upper potential and, in the case of the bound-bound transitions of XeCl and XeF, produces resolvable vibrational and rotational structure. Thus the spectrum usually consists of two to four lines within a total width of $\sim$2 nm. The $C \rightarrow A$ transition, on which laser action has also been produced [1.13, 1.14], is generally less intense and, due to the sloping nature of the lower level potential, is broad-band ($\sim$70 nm). Transitions from higher states, such as the $D \rightarrow X$, have also been observed [1.15], but at much lower intensities due to quenching of the upper level. Figure 1.2 summarises the wave-

		F	Cl	Br	I
Xe	B→X	351	308	282	253
	C→A	450	350	302	263
Kr	B→X	249	222	206	
	C→A	275			
Ar	B→X	193	175		
	C→A	203	199		
Ne	B→X	108			
	C→A	117			

Figure 1.2

Emission wavelengths of B→X and C→A transitions of the rare gas halides. Laser action has been observed on those transitions whose wavelengths have been underlined.

lengths of the B → X and C → A transitions in various rare gas halide molecules, and shows, underlined, the transitions on which laser action has been obtained.

Several important factors governing the operation of excimer lasers may be explained with reference to the energy level diagram in figure 1.1. Firstly, the dissociative or thermally unstable nature of the ground state means that there can be no build-up of population in the lower laser level. This implies that once population is created in the upper level a population inversion will exist. Furthermore, the speed of the dissociation in the ground state, 10^{-13}s, allows a very rapid transfer of molecules to this state, and hence high laser powers. Also, the fact that the laser action takes place down to the ground state produces a laser system of high quantum efficiency.

The excimers are first formed at a large internuclear separation, and so are in a highly excited vibrational level. However, this population will be redistributed among the lower vibrational levels. If a sizeable inversion is to be created, all of this population must be channelled into a small number of levels. This can be done by relaxing the population down into the lowest two or three levels. As this must be achieved before the radiative decay of the excited molecule, the collision rate, and hence laser gas pressure, must be high. The requirement of high gas pressure, whilst less severe for rare gas halide excimers than for the homonuclear excimers, has severe consequences for the discharge pumping of these lasers, as will be described in section 1.4 of this chapter.

The generally short wavelength of the excimer laser transitions and the relatively broad bandwidth place very stringent demands on the electrical excitation of the laser.

It can be shown that[1.16,1.17] the pumping power required to produce unit gain per unit length is given by

$$P = 8\pi \frac{hc^2 \Delta\lambda}{\eta\phi \lambda^5} \qquad (1.1)$$

where ϕ is the quantum efficiency, η is the efficiency of population of the upper state, λ is the wavelength of the laser transition and $\Delta\lambda$ its bandwidth. Taking $\eta\phi = 0.1$ leads to a required power per unit volume to produce a gain of 10% cm^{-1} of $\sim$100kW cm^{-3} for XeCl (308 nm) rising to $\sim$15MW cm^{-3} for Xe_2^* (172 nm). These very high specific input powers have usually been provided electrically either by using an electron beam or by fast transverse discharge excitation, although microwave and R.F. discharge pumping have also been demonstrated. In any case, the formation of the excimer species proceed via two main routes. Taking a typical XeCl laser gas mixture containing xenon, hydrogen chloride as halogen donor and neon as buffer gas, the 'ion-channel' reaction proceeds thus:

$$Xe^+ + Cl^- + Ne \longrightarrow XeCl^* + Ne$$

and is the dominant formation mechanism for all of the discharge pumped rare gas halide excimer lasers. The 'neutral channel' reaction

$$Xe^* + HCl\ (\nu) \longrightarrow XeCl^* + H$$

accounts for up to $\sim$15% of the XeCl* formation[1.18]. The formation of the Xe^+ and Xe* reactants in the two equations above proceeds through various intermediaries, but the reaction

$$HCl + e^- \longrightarrow Cl^- + H$$

has been identified as the major rate determining step in the excimer formation process[1.18]. Further to the formation kinetics, the excimer quenching reactions also have an important

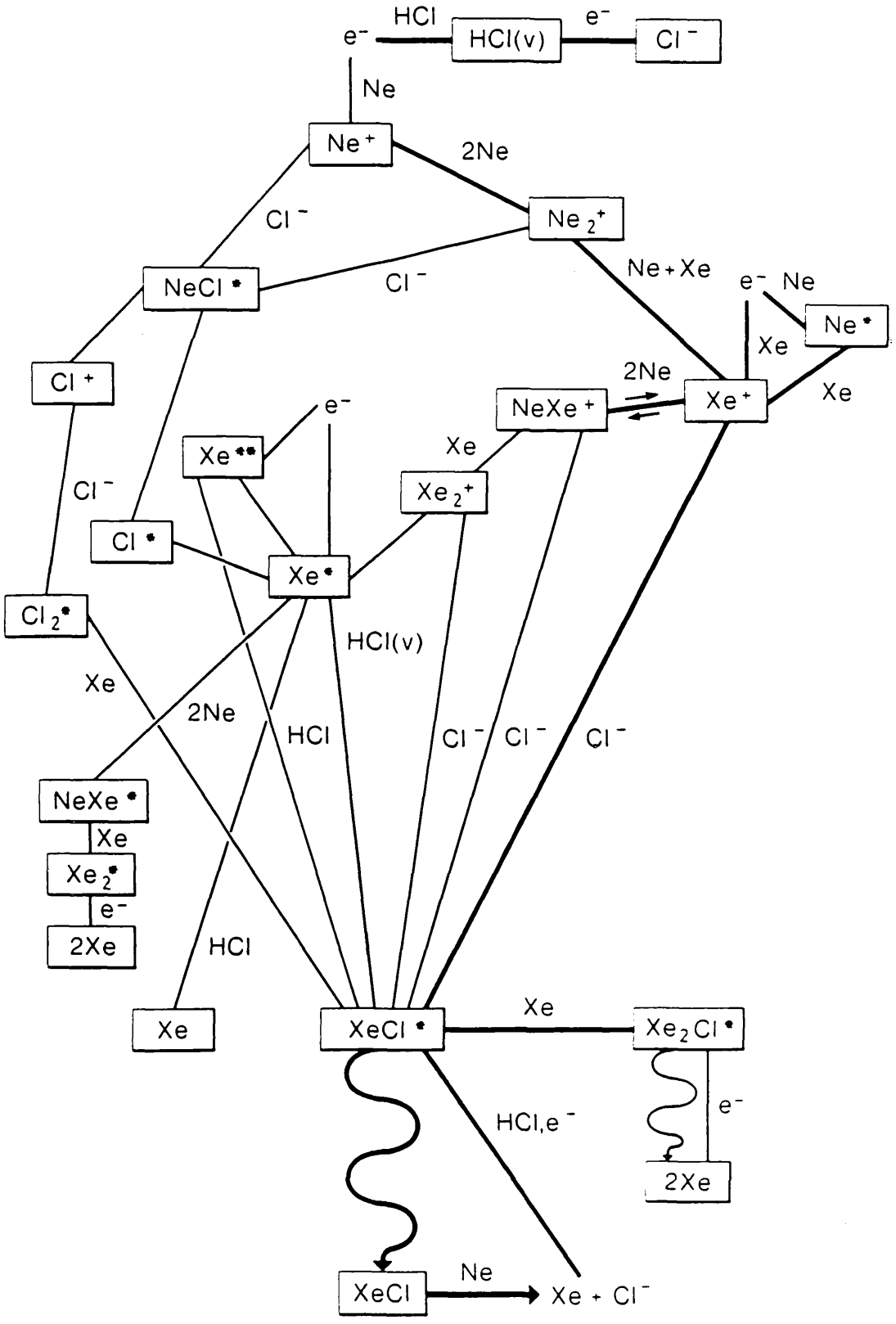

Figure 1.3 Simplified diagram of the main excimer formation reactions.

bearing on the performance of the laser, the main reaction being

$$XeCl^* + HCl\ (\nu),\ e^- \longrightarrow Xe + Cl^-.$$

Figure 1.3 shows these reactions, together with others of importance in a simplified schematic of the main reaction channels similar to that used by Levin et al[1.11] in modelling the kinetics of an e-beam pumped system. The reader is referred to this reference, and to the more recent work of Hokazono et al[1.12] for a more complete discussion of the reaction kinetics.

1.3 Electrical Excitation Schemes

In this section we will briefly review the electrical excitation schemes which have been used to pump excimer lasers. The discussion of the technique of avalanche discharge pumping, which is of most relevance to the work presented in this thesis, is extended into section 1.4. The alternative techniques of e-beam pumping and microwave pumping are included for comparison and completeness.

In e-beam pumping, the high specific input powers required to produce laser action are achieved by injecting a high energy electron beam into the high pressure laser gas. This technique has been shown to work with all excimers which have lased to date, and has the analytical advantage that the power supply is largely decoupled from the kinetics of the laser gas load. However, e-beam pumping has several important practical disadvantages. The high voltage engineering required for the e-beam source is both bulky and expensive. More importantly, the foil which separates the high pressure laser gas from the evacuated e-beam diode and through which all of the e-beam energy must pass, is subject to great mechanical and thermal

stress. This generally results in very low repetition rate, <0.1Hz, operation in the interests of preserving the foil, although complex cooling systems can be used to allow higher rep-rate operation[1.19]. Hence the reliability is always in doubt, and catastrophic failure of the foil is a time-consuming, expensive and potentially hazardous event.

Despite these drawbacks, e-beam excitation is still used for a number of applications. In particular, the homonuclear excimers which operate at higher gas pressure are well suited as the laser gas will stop a significant fraction of even high energy electrons[1.20]. Also, the shortest wavelength excimers, such as Ar_2^* (126 nm), have, to date, only been operated with e-beam excitation[1.21]. Furthermore, e-beams are still used to pump the highest energy excimer lasers[1.22] where large lasing volumes and long pulse durations are required, although recent advances in X-ray preionised avalanche discharge pumped lasers may soon change this. However, for most applications, the size, low repetition rate and poor reliability of e-beam pumped lasers renders them unsuitable.

The performance of excimer lasers may be considerably improved in all of these areas, at least for the longer wavelength excimers, by the adoption of discharge pumping. In this technique the laser gas is excited by running a discharge through it. The high powers and high gas pressures required lead to the adoption of fast, pulsed, transverse discharges. Moreover, the high gas pressures lead to severe problems of discharge stability, and these are discussed in the next section. It is the extent to which these problems can be overcome which determines the performance of the discharge pumped laser. At present, commercial, table-top discharge pumped excimer lasers

are available capable of producing output pulses of several hundred millijoules in pulses of up to 40 ns duration and at repetition rates of hundreds of Hertz. However, the work presented in this thesis, and that done elsewhere, shows that orders of magnitude improvements in this performance are possible.

One way of avoiding the discharge stability problems of a pulsed D.C. discharge is to employ a microwave or R.F. frequency discharge. This also has the advantages that the power deposition is nominally independent of the laser gas composition, and that a breakdown or arc in one part of the pumped region does not compromise the excitation of other regions. Furthermore, the gas lifetime is enhanced as there are no electrode sputtering problems. However, to date, the efficiencies and output energies of such devices have been very low[1.23,1.24] and until such time as they are improved, microwave and R.F. discharge pumping will continue to be of very limited applicability.

1.4 Discharge Stability and Preionisation Requirements

The need to use high pressures of laser gas, as described in section 1.2, leads to severe difficulties in maintaining a stable, large-volume discharge. At lower gas pressures, such as those typical of argon-ion and helium-neon lasers, the mean free path of the electrons and ions is sufficient to distribute, and hence remove, any local inhomogeneities. However, at the pressures of a few atmospheres typically found in excimer lasers, the mean free path is decreased to an extent that non-uniformities will remain localised. This leads to the formation of a narrow arc (rather than a uniform discharge) which does not provide suitable excitation for the laser due

to its small volume, inherent non-uniformity and elevated temperature. Before discussing ways of producing uniform discharges in high pressure gases, we will first review current thinking on the discharge formation mechanism.

It is now generally accepted that low pressure discharges initiated by only marginal overvoltages develop through the mechanism first described by Townsend[1.25,1.26]. In this mechanism the number of secondary ion pairs produced in a small region δx is given by the sum of those produced by negative ions (electrons) $\alpha \delta x$, and by positive ions $\beta \delta x$. This leads to growth in the electron density which is somewhat faster than exponential. This growth is sustained by electrons produced at the cathode by either the collision of positive ions or by photoemission. The approximate condition for the formation of a sustained arc or discharge is

$$\alpha d \simeq 2.5$$

where α is the first Townsend coefficient and d the inter-electrode spacing.

As the Townsend theory of breakdown involves feedback from the discharge electrodes, it predicts a delay between the application of the voltage and the breakdown of some fraction of τ where $\tau = d/v$ and v is the ion drift velocity. This predicted delay of $>10^{-6}$s is not observed in high pressure discharges initiated by large overvoltages where delays as small as 10^{-9}s have been measured. Because of this, an alternative discharge formation mechanism has been proposed which is generally held to apply to high pressure discharges [1.27-1.30], although other workers believe that the Townsend theory is still applicable[1.31,1.32]. It is this alternative theory, which has been applied to the case of excimer lasers

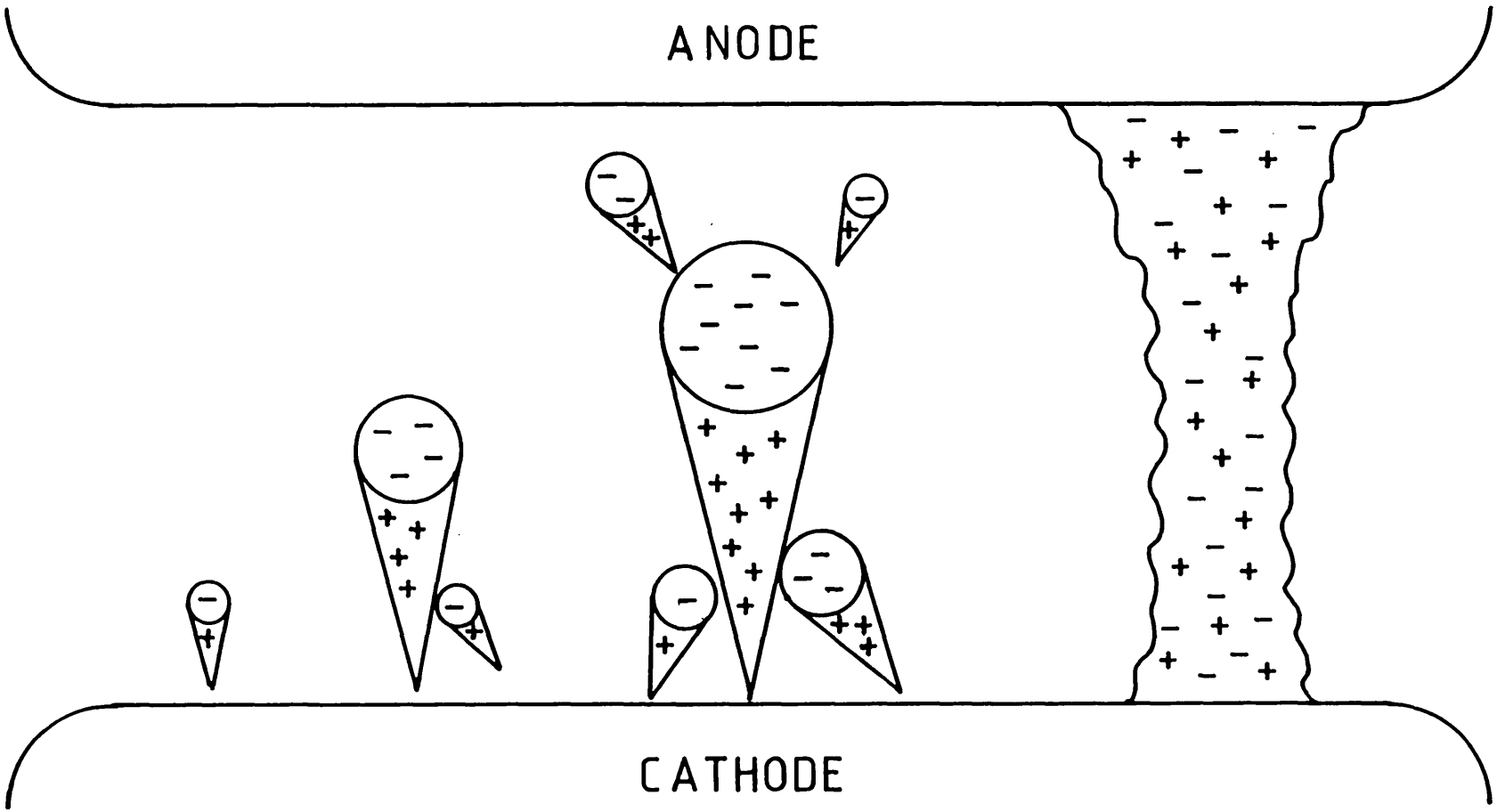

Figure 1.4 Diagrammatic representation of the formation of a 'Kanal' or 'streamer' discharge.

(1.8,1.33,1.34), and which will be discussed in the remainder of this section.

The 'Kanal' or 'streamer' theory of breakdown is based on the effects of the space-charge induced electric field produced within the gas by the differential motions of the positive ions and electrons. This is assumed to be small and is neglected in the Townsend theory. On the application of the electric field, electrons will avalanche towards the anode, leaving the low mobility positive ions essentially stationary. These separated charges will produce a local field, which grows as the avalanche develops. At some point, when this space-charge induced field is comparable to the applied field, the local field will itself give rise to secondary avalanches, as shown in figure 1.4. These will be predominantly parallel to the original avalanche, as it is in this direction that the applied field supplements the space-charge field. The by now enhanced fields between the negatively charged avalanche head and anode, and the positive tail and cathode, result in ever more rapid repetitions of this process until the discharge plasma spans the entire inter-electrode gap. Hence, in the Kanal theory, the breakdown originates from a single electron avalanche which induces other avalanches both in front of and behind it. Feedback or electron emission from the discharge electrodes is not required for breakdown, and hence the formative delay between the application of the voltage and the electrical breakdown does not depend on any one species crossing the inter-electrode gap. This leads to the prediction of very short formation times, $\sim 10^{-9}$s, in agreement with experiment. The approximate condition for the observation of Kanal breakdown[1.27]

$$\propto d \simeq 20$$

is more severe than for Townsend breakdown, but is generally met in excimer lasers.

The electrical breakdown mechanism in excimer lasers is, therefore, essentially localised as it originates from a single avalanche. If something approaching a 'uniform' discharge is to be produced from such a mechanism, it is clear that there must be a large number of 'original' avalanches, and that these must be sufficiently close together to have considerable spatial overlap. One way of ensuring that this is the case is to 'preionise' the laser gas, that is to introduce a uniform distribution of electrons throughout the discharge volume before the discharge voltage is applied. The number of preionisation electrons required to produce a uniform discharge has been estimated by several authors[1.33,1.34,1.35], generally using the assumption that each preionisation electron gives rise to one original avalanche. Assuming that a uniform discharge is produced when the initial electron number density is sufficient to produce overlap of neighbouring avalanches before the space-charge field becomes high enough for the production of secondary avalanches, values of the minimum preionisation electron density of $\sim 10^4$ cm^{-3} have been obtained[1.33]. However, this value is subject to a large uncertainty due to the arbitrary nature of the criterion for uniformity, and the difficulty in assigning dimensions to an individual avalanche. Furthermore, this work assumes that the discharge voltage is applied to the electrodes instantaneously. In practice, the non-zero voltage risetime will cause preionisation electrons to drift away from the discharge cathode immediately prior to breakdown. This will reduce their effective number density, and therefore necessitate a higher than previously predicted initial number density for uniform discharge formation. Taking

this fact into account, other authors have shown that an initial density of $\sim 10^5$ cm^{-3} should be adequate, assuming a sub-microsecond voltage risetime[1.34].

It should be stressed that the above theories rely on many simplifying assumptions, including what constitutes a uniform discharge, and the numerical predictions are therefore in doubt. However, the descriptions they offer of the discharge formation mechanism, and of the role of the preionisation in preventing arc formation, are quite compelling.

1.5 Types of Preionisation

The most commonly used form of preionisation is that which is referred to as 'U.V. preionisation'. In this technique, the initial electron number density is produced by irradiating the laser gas mixture with ultra-violet radiation which photoionises a fraction of the constituents. Usually the ultra-violet radiation has been produced by one of three techniques.

In 'corona preionisation' a high voltage is applied between two electrodes separated by some dielectric material. The corona produced may be surface or volume generated, and provides sufficient ultra-violet radiation to adequately preionise a reasonably sized excimer laser[1.36,1.37]. This technique has the advantage of being inherently simple, although much care is required to produce preionisation of acceptable uniformity.

The second technique, and the one most frequently employed, uses a series of sparks to generate the U.V. These must be placed close to the active volume to produce adequate preionisation, but need not require a separate electrical driving circuit as, by ingenious design, they may be incorporated

in the main discharge circuit[1.38], thereby also easing synchronisation problems. This has become the technique used by all of the major commercial rare gas halide laser manufacturers, and provides devices capable of output energies of several hundred millijoules in pulses of ~20 ns duration. However, this form of preionisation has several major disadvantages. Firstly, the penetration of the U.V. light produced is very limited (~2 cm) in typical laser gas mixtures[1.39]. This severely limits the volumes which can be preionised, and hence the laser output energies. It also necessitates the use of many sparks quite closely spaced (2-3 cm) along the length of the laser. The presence of these sparks reduces the lifetime of the laser gas mixture. Also, due to the poor penetration and localised source of the U.V., the uniformity of preionisation is not good. This leads to output beams of poor spatial quality, and to discharge instabilities which rapidly terminate the laser, limiting the pulse duration and further restricting the energy which can be extracted.

These problems may be overcome to a large degree by using U.V. laser preionisation. In this technique a U.V. laser, usually either ArF (193 nm) or KrF (248 nm), is directed along the volume to be preionised and produces emission of photoelectrons either from species within the normal laser gas mixture or from the easily photoionised molecules of an additive molecule (C_6H_6, C_6H_5F etc.)[1.40]. A preionisation laser flux of only ~1 mJ/cm^2 is sufficient for adequate preionisation, and the low attenuation of the preionising radiation in the laser gas mixture suggests that the application of this technique to wide-aperture large-volume systems may be possible. However, it has been suggested that the additive molecules do not reform after photoionisation[1.41], and hence

their expense may be an important factor. Also, the economics of using one rare gas halide laser to preionise another will probably not prove to be viable in the majority of applications.

An alternative way of avoiding the problems associated with conventional U.V. preionisation is to use X-rays as the preionisation source. The shorter wavelength of the X-rays gives much greater penetration in the laser gas, typically 20m for 100 keV X-rays[1.42]. The greater penetration also allows the X-rays to be generated externally to the laser chamber and directed into the laser gas through an X-ray 'window'. This reduces contamination of the laser gas and hence improves its lifetime. Furthermore, the X-rays can be produced from an extended source and this fact, together with the possibility of placing the source a large distance from the active volume, ensures good uniformity of preionisation with the consequent benefits of good beam quality, long output pulse duration and high output energy. The first demonstration of X-ray preionisation was by Sumida et al[1.43] in 1978, since which time there has been much further development and many significant advances. The work described in this thesis forms part of this body of research.

While not strictly relevant to the present work, mention should be made of the technique of sustained discharge pumping of excimer lasers. This is done by injecting an electron beam into the laser gas before and during the duration of the discharge. In the early stages of the discharge formation this performs a similar function to the preionisation described earlier, but in the later stages it has a different effect. The preionisation electron density in avalanche discharge pumped excimer lasers is several orders of magnitude lower than the electron density in the fully formed discharge. Therefore,

the influence of the preionisation source ceases once the discharge has commenced as it provides only a negligible fraction of the total ionisation. In a sustained discharge, however, this is not the case. The sustaining source produces an electron density comparable to the running discharge electron density. This allows continuing control of the discharge uniformity. Furthermore, the discharge E/P (electric field/gas pressure) may be adjusted to give optimum excitation of the desired excimer species in the knowledge that any shortfall in electron production can be made up from the sustaining source.

E-beam sustained excimer lasers range in performance from those in which the majority of the energy is supplied by the e-beam, where output energies of $\sim$90J in pulses of $\sim$1 µs have been produced[1.44], to those where the e-beam is used only to control the discharge and supplies little energy[1.45].

E-beam sustained lasers, however, suffer from all of the disadvantages of e-beam pumped systems, although to a lesser extent, and this severely limits their usefulness. Other methods of sustaining discharges have been suggested, such as photo-ionisation sustaining[1.46] and X-ray sustaining[1.47], but have not yet been demonstrated in the open literature.

1.6 The Present Work

The work described in this thesis describes the design and development of an avalanche discharge pumped laser system built to demonstrate the advantages of using X-ray preionisation for rare gas halide lasers.

Chapter two describes the X-ray source developed for this

purpose in some detail, while chapter three is devoted to the discharge circuit and includes the relevant pulse forming line (P.F.L.) and transmission line theory. Chapter four presents the operating characteristics of the completed laser system, including an optimisation of the performance with respect to output energy. Chapter five addresses the problem of obtaining high electrical efficiency operation and reports results comparable with the best yet produced from a discharge pumped excimer laser. These have been published elsewhere[1.48,1.49]. In chapter six the output pulse duration of the laser system is extended beyond that produced by any other similar high-power laser, and a detailed investigation of the output pulse terminating mechanism is undertaken. Again, these results have already been published in outline[1.50,1.51]. Finally, in chapter seven a review of the present work is given, with the emphasis on the relevance of the results obtained and on possibilities for future work and further development. A very brief summary is to be found at the end of chapter seven, which, together with figure 7.1, covers the more important results of the present work.

CHAPTER 2

THE X-RAY SOURCE

2.1 Introduction

The potential advantages of using X-rays to preionise excimer lasers have been outlined in the previous chapter. The following two chapters cover the design and construction of a laser system built to demonstrate these advantages. This chapter deals with the X-ray source covering the performance requirements, the design of a unit to meet these requirements and the performance testing of the completed unit. Towards the end of the chapter the laser chamber is described, together with its associated X-ray window. In the following chapter the discharge circuit built to provide the pumping power for the long-pulse, large-volume laser is detailed. Careful consideration is given to designing a circuit to meet the peculiar needs of the excimer laser. The theoretical background to the chosen circuit is given, as are the practical difficulties encountered in attaining the predicted performance.

2.2 X-ray Source Requirements

The X-ray exposure, dose* and uniformity required to preionise adequately the excimer laser gas mixture was not known at the time of the design of the X-ray source. In previous work, Sumida et al[2.1] had used a point source of X-rays, giving an exposure of $\sim$ 5mR to preionise a small volume (180 cm^3). In other work, Lin, Bao et al[2.2] used an exposure between 500 to 1000 mR in a similar volume (190 cm^3), and Lin and Levatter[2.3]

---

* See Appendix I for definitions of the terms 'dose' and 'exposure'.

preionised a much larger volume (1000 cm^3), using an unspecified exposure, probably similar to that of Lin, Bao et al. On the basis of these results it was deemed prudent to construct an X-ray source capable of producing exposures of at least several tens of mR. Furthermore, because of the nature of the gases in a typical rare gas halide laser mixture, it is not only the total time integrated X-ray dose which is of importance. The dissociative attachment of the preionisation electrons to the halogen donor molecule is extremely rapid. Reactions such as

$$HCl(\nu) + e^- \longrightarrow H + Cl^-$$
$$F_2 + e^- \longrightarrow F + F^-$$

have rates which are dependent on the electron energy and vibrational quantum number (ν), but typically take place in a few tens of nanoseconds[2.4,2.5]. These reactions remove the preionising electrons, replacing them with much less effective, low mobility, negative ions. It is therefore the instantaneous preionisation electron production rate which is important as a large number density of preionisation electrons cannot be produced from a long exposure to low intensity X-rays. What is required is short burst, lasting perhaps 10 ns, of high intensity X-rays. Using longer pulses than this is wasteful of energy, but will, however, allow for greater ease of synchronisation between preionisation source and discharge circuit.

The optimum value of the energy of the individual X-ray photons is a compromise between the low energies which will be readily absorbed by the laser gas, thus producing many preionisation electrons, and high energies, which will ensure little absorption of the X-rays and hence no depletion in dose

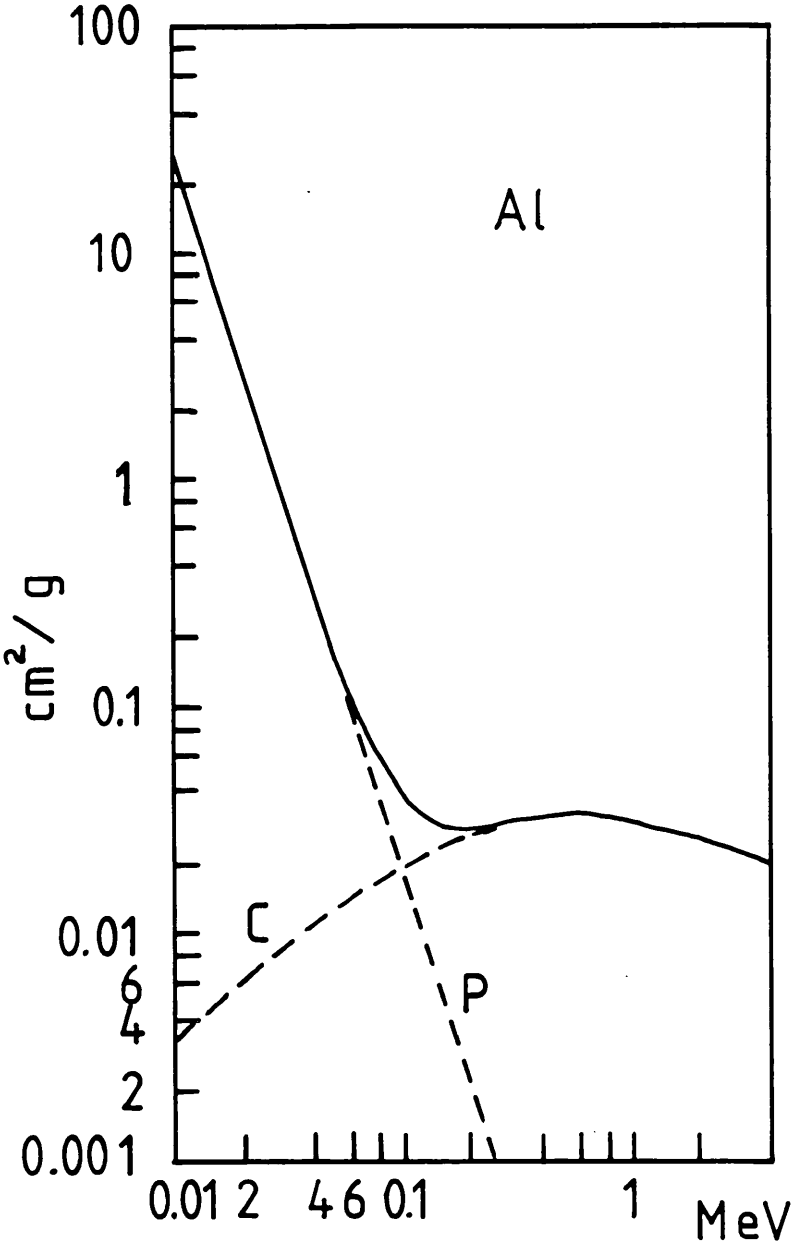

Figure 2.1 Total X-ray absorption coefficient (full line) for element Z = 13 (Al). Contributions from Compton effect (C) and photoionisation (P) are shown dotted.

in the direction of the X-ray propagation, thereby giving good uniformity of preionisation. The gross X-ray attenuation characteristics of an element vary smoothly with atomic number (Z), and the mass absorption coefficient for element Z=13 (Aluminium) is shown in figure 2.1[2.6]. This shows that for X-rays of energy less than 1 MeV the total absorption is produced by the photoelectric and Compton effects, both efficient means of producing preionisation electrons. The rapid rise in absorption at low X-ray energies leads to an increase in the energy deposited in the material, even though the individual photon energy is lower. The mass absorption diagram for neon (Z=10), a frequently used excimer laser buffer gas, is of the same form as that shown in figure 2.1, although the photoelectric effect is marginally less important. For X-rays of energy 12.4 keV (λ = 1Å), the mass absorption coefficient of neon is μ/ρ = 6.476 cm^2/g[2.7]. This implies that the transmission of 12.4 keV X-rays through 5 cm of neon gas at 5 atmospheres pressure will follow

$$I = I_o \exp\left[-6.476 \times 0.839 \times 10^{-3} \times 5 \times 5\right]$$

$$\frac{I}{I_o} = 87\%$$

where the density of neon at S.T.P. is 0.839×10^{-3} g/cm^3. This shows that there is ~13% absorption, slightly higher than desirable for optimum preionisation uniformity. This suggests that higher X-ray photon energies should be used, perhaps around 20 keV. However, this optimum value will be greatly affected by the practical problem of transmitting the X-rays into the laser gas through the walls of the pressure chamber. As figure 2.2 shows, even 2 mm of Aluminium will

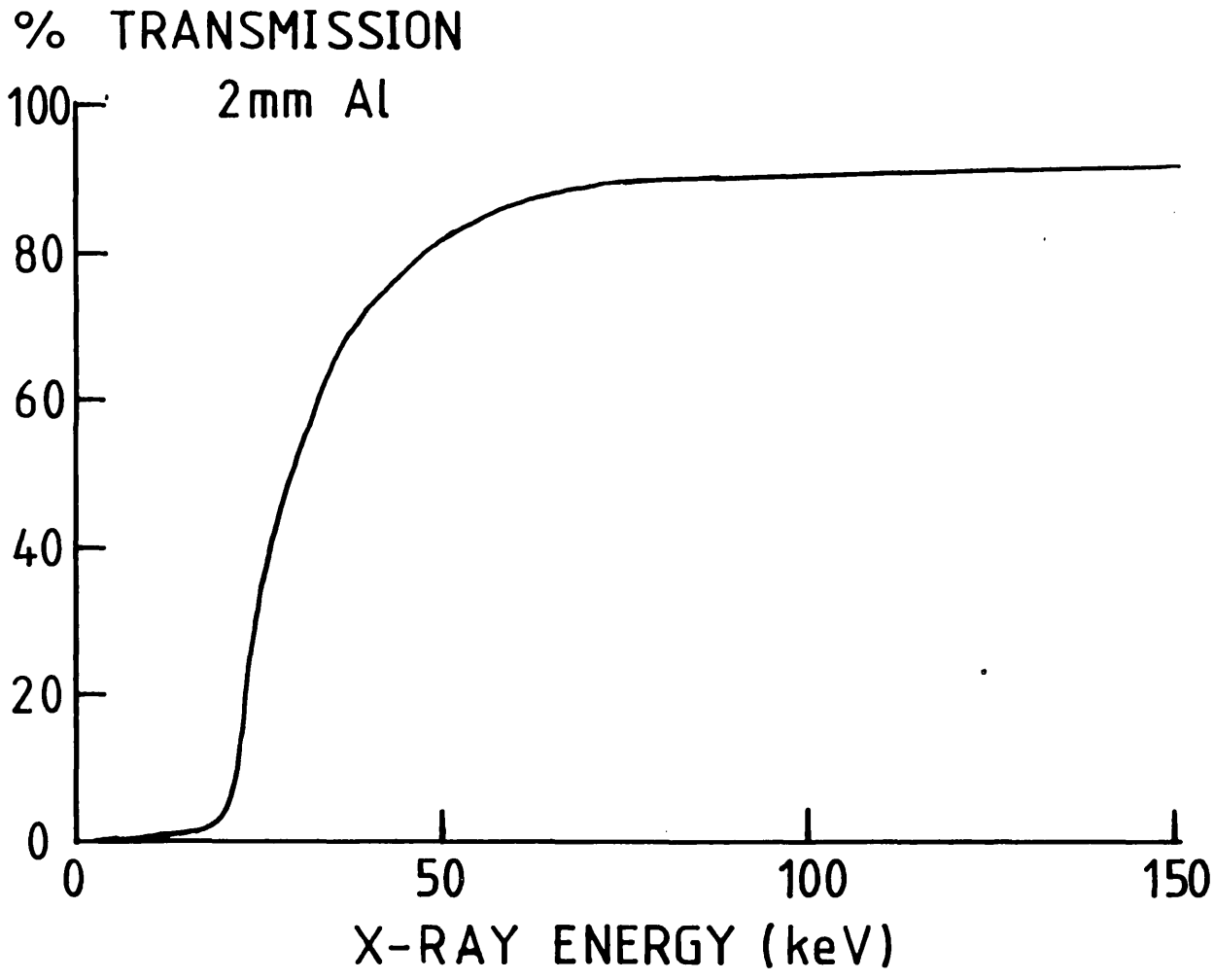

Figure 2.2 X-ray transmission through 2 mm of aluminium as a function of X-ray energy.

seriously attenuate any X-rays below 50 keV. It is, therefore, extremely important to keep the X-ray 'window' of the pressure chamber as transparent as possible. This consideration rules out one, otherwise very attractive, preionisation geometry, namely that of injecting a beam of X-rays into the cavity along the laser axis through one of the end windows[2.8]. This technique has the major advantage of requiring an X-ray beam which is uniform over an area equal to only the smallest cross-section of the discharge volume. It does, however, need the X-rays to be collimated, and of high photon energy leading to low efficiency of preionisation electron production and possible damage to the laser optics.

With preionisation along this axis of the chamber excluded, the remaining options are through either the insulating wall of the chamber or through one of the electrodes. Comparing X-ray attenuation coefficients, mechanical strengths and respective dimensions shows the metallic electrode to be the better window option. This approach has the unfortunate consequence that the dimension along which the preionisation uniformity is most easily assured, i.e. along the direction of X-ray propagation, is the dimension in which it is least required, i.e. perpendicular to the electrode surface[2.9]. Preionisation uniformity in the more important directions parallel to the electrode surfaces must be produced by using an X-ray source with good uniformity over a large area, in the case of the present laser some 100 x 4 cm^2. The development of such a source is described in the next section.

2.3 X-ray Source

Of the various methods of X-ray production, the one which appeared to be the best suited to the physical dimensions and

System Efficiency

Stored Energy -E-beam	5%
E-beam-X-rays	0.5%
Transmission to laser gas	50%
X-ray absorption in laser gas	1%

Overall Efficiency = 1.25×10^{-6}

Laser Volume	1000 cm^3
Laser gas ionisation ptl.	20 eV

Energy required to produce 10^9 e^-/cm^3 = 3×10^{-6} J

$$\text{Stored Energy Required} = \frac{3 \times 10^{-6}}{1.25 \times 10^{-6}} \simeq 2J$$

Figure 2.3 Order of magnitude calculation of X-ray source requirements

timescales required, and the one in which there was most expertise in our laboratory, involved the use of an electron beam (e-beam).

A beam of high energy electrons is allowed to impinge on a target material which slows the electrons and produces bremsstrahlung radiation. If the energy of the electrons is initially several tens of kiloelectronvolts, then the radiation produced will be in the form of a continuum up to this energy, with a peak in the distribution at approximately half of the maximum energy, and therefore be in the X-ray region of the spectrum. In addition to this continuum, some of the characteristic X-ray lines of the target material will also be excited. The ratio between electron energy loss by collisions, to energy loss from bremsstrahlung production, is given approximately by

$$\eta \simeq \frac{EZ}{700} \qquad (2.1)$$

where E is the electron energy in MeV, and Z is the atomic number of target material[2.10].

This equation may be thought of as indicating the efficiency of X-ray production by bremsstrahlung, showing that a high Z target material is desirable. Using this equation and reasonable estimates of E,Z, laser gas ionisation potential, and efficiency of e-beam production indicates that only a relatively modest e-beam is required to produce the X-ray exposures used by Sumida[2.1]. The approximate calculation shown in figure 2.3 opposite shows how a stored energy of only 2 Joules should be sufficient to provide adequate preionisation (10^9 e^-/cm^3), neglecting the loss of electrons due to dissociative attachment to HCl.

Therefore a relatively simple e-beam source was constructed,

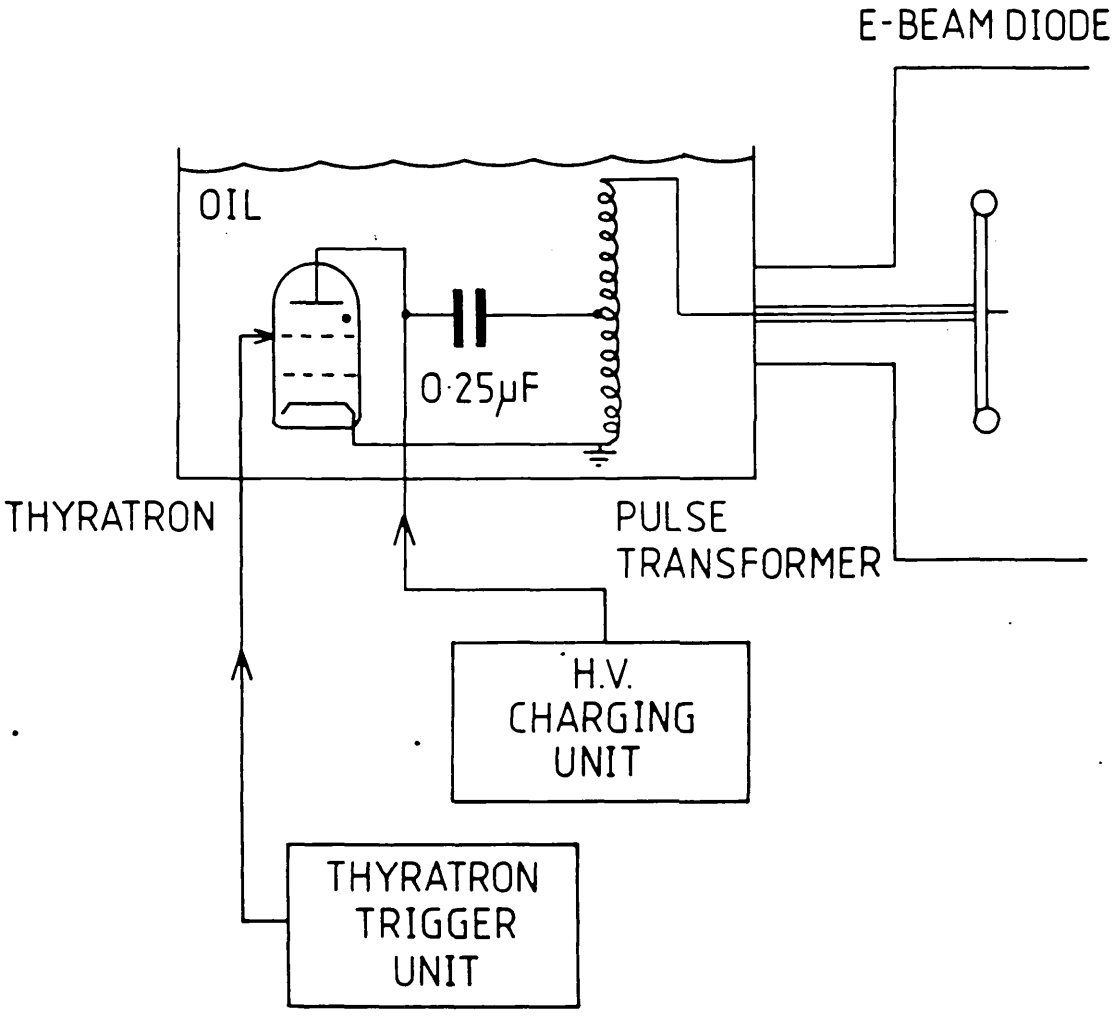

Figure 2.4 Schematic diagram of X-ray source.

using a cold cathode e-beam diode powered from a small capacitor (Maxwell 0.25 μF, 50 kV) switched through an auto-transformer by a hydrogen thyratron (E.E.V. CX1538) as is shown in figure 2.4. In order to produce a sufficiently fast voltage rise on the cold cathode using this simple circuit, the inductances of the home-made autotransformer and circuit layout were kept to a minimum.

The 'air-cored' autotransformer[2.11,2.12] has a two turn primary and twenty turn secondary and is wound from 50 x 0.13 mm^2 copper with 200 x 0.25 mm^2 mylar insulation around a large (250 mm) diameter, perspex former. A larger (300 mm) diameter concentric perspex tube completes the housing, the two primary windings being accessible through the side of the tube, while the high voltage output is taken out along the axis of the cylinders. The windings are vacuum impregnated with transformer oil. The low inductance transformer (L_p = 1.6 μH, L_s = 160 μH) is connected to the thyratron and capacitor using copper plates 120 mm wide and 1.5 mm thick, and the whole assembly immersed in oil for insulation. The gain of the transformer was found to be approximately 13.5 into a nominally open circuit, close to that calculated using a computer code. Into a load of 130Ω, the estimated value of the e-beam diode impedance[2.13], the gain falls to 4.5, somewhat lower than the 6.5 predicted by the same computer code. This shortfall is due in part to the tolerances in the construction of the transformer, but is mainly due to the non-ideal switching of the thyratron - in the code perfect switching is assumed. The transformer was tested up to output voltages of 200 kV without electrical breakdown, and the voltage risetime into 130 Ω was found to be 200 ns, adequate for its application.

The output from the transformer is taken through a field

Element	Cu	Ta	Pb
Atomic Number	29	73	82
Melting Point	1083	2996	327
Resistivity ($\mu\Omega$ cm)	1.69	13.5	21.7
Thermal Conductivity cal/(sec)(cm^2)(°C/m)	0.94	0.13	0.08
Tensile Strength (p.s.i.)	30 000	50 000	3000

Figure 2.5 Comparative data for possible e-beam target materials

graded oil to vacuum bushing and onto the e-beam cathode which consists of a one metre long razor blade attached to an aluminium back plate, the edges of which are blended into 1" diameter copper tubing which encircles the cathode. The cathode assembly is rigidly mounted on the earthed plate which carries the foil e-beam target. This allows accurate adjustment of the blade-foil separation over the entire blade length. The earthed mounting plate is fabricated from 13 mm thick Dural and forms an O-ring seal onto the similarly constructed vacuum chamber. The tubular high voltage connector on the rear of the cathode is located into a socket on the bushing by means of leaf springs. The vacuum chamber is generally evacuated to a pressure of less than 2×10^{-5} torr using a small 50 c.c. charge oil diffusion pump (Edwards 203B) and rotary backing pump (Edwards ES200).

2.4 E-beam Target Material

The optimum target material is one which will efficiently produce X-rays in stopping the electrons incident upon it, and then transmit these X-rays without significant absorption. As shown by equation 2.1, the most efficient X-ray producers are high Z materials, just those materials which also exhibit the highest X-ray absorption. It is for this reason that a thin foil of high Z material is used, but this brings with it quite severe mechanical and thermal criteria. The material with perhaps the best combination of strength, thermal conductivity and high atomic number is tantalum (fig. 2.5).

The optimum target thickness for a given material is governed by its absorption and attenuation coefficients for both X-rays and electrons. A comprehensive calculation (which will not be carried out) includes the steps depicted in figure

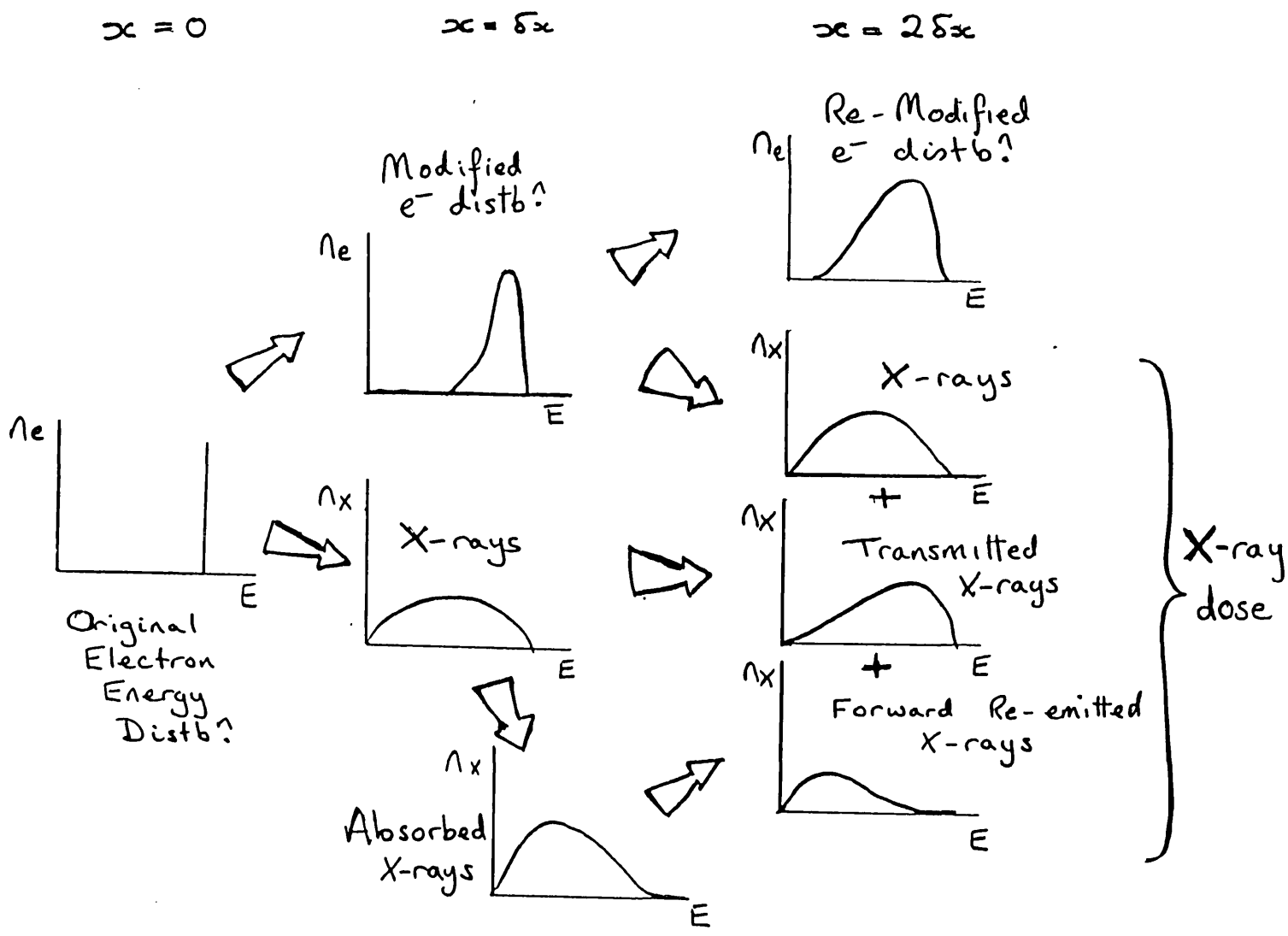

Figure 2.6 Schematic representation of the steps involved in a rigorous calculation of the production and transmission of X-rays through a small thickness of e-beam target material.

2.6. Of the electrons incident on the foil, a number $n_e(E)$ of them would have an energy E. On traversing a small distance, δx, of foil, the energy of these electrons will be modified, giving rise to a distribution similar to that shown in the second column of fig. 2.6, and a range of X-rays of various energies will be produced. The modified electron distribution will produce a slightly different range of X-rays in the next small region, δx, while being re-modified itself. The X-rays produced in this region will be added to those which have been transmitted forward from the previous region without absorption. Also to be added is that fraction of the absorbed X-rays which are subsequently re-emitted in the forward direction.

As can be seen, this calculation rapidly becomes extremely complex. Moreover, small inaccuracies in the assumed interactions between electrons, X-rays and target material will lead to sizeable errors after many compound iterations.

Faced with these problems, a more empirical approach to determining the optimum target thickness was taken. Commercially available 8 μm Ta foil will stop over 90% of even the highest energy electrons liable to impinge on it (100 keV)[2.14, 2.15]. This same thickness of foil will transmit more than 85% of the lowest energy X-rays which will pass relatively unattenuated through the aluminium X-ray window, i.e. ~60 keV (see figure 2.2). This represents a good compromise between X-ray transparency and electron opacity, and together with the properties listed in figure 2.5, leads to 8 μm thick Tantalum foil being chosen as the e-beam target material.

2.5 X-ray Source - Performance

The spacing between blade and foil was set to 30 ± 1 mm and all non-emitting surfaces of the cathode were coated with

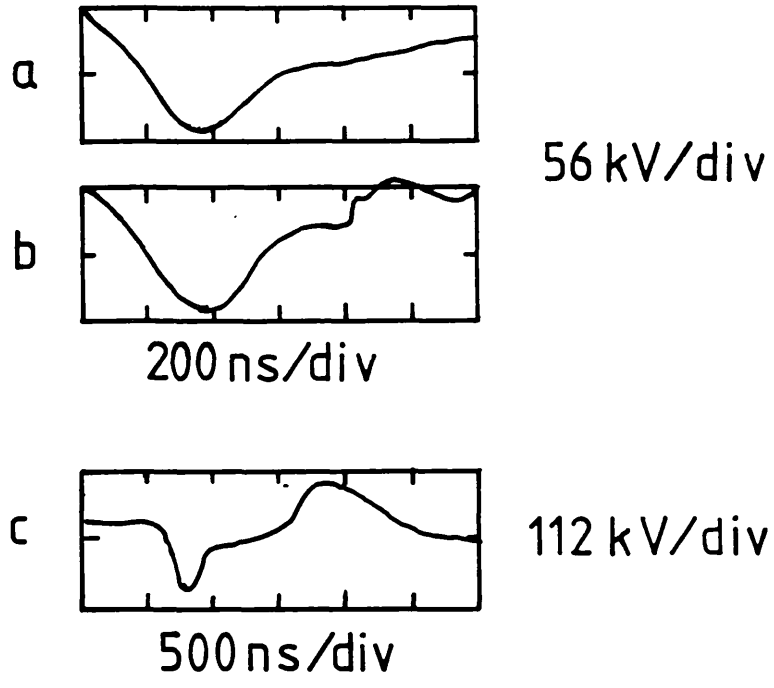

Figure 2.7 Voltage on e-beam cathode, a) normal, b) with breakdown, c) showing voltage reversal.

diffusion pump oil. The voltage on the cathode was monitored through a copper sulphate resistive divider and found to be closely related to the sound of the e-beam gun, a smoothly varying voltage, figure 2.7a, producing a quiet, dull sound whereas any rapid voltage jump, such as that in figure 2.7b, due perhaps to tracking or arcing, could clearly be heard as a sharp crack. Thus, the sound of the diode provides a useful, if somewhat crude, continuous check on its performance. It was found that in order to avoid 'hard' sounding shots it was necessary to increase the operating voltage of the cathode gradually over the first few shots. The X-ray exposure produced was measured through two layers of 1 mm thick aluminium, forming the X-ray window and the laser discharge cathode (which will be described in section 2.7), using quartz fibre exposure meters.

On first using a new blade, approximately one hundred shots were required before the X-ray exposure became repeatable from shot to shot. After this conditioning it was found that the exposure was higher both in the centre of the X-ray window and at the ends, and fell to approximately 10% of its maximum value in the areas between. Inspection of the blade showed that electron emission was indeed taking place preferentially from the centre of the blade where the high voltage feed was attached to the cathode, and from the ends of the blade where the field enhancement was obviously greater. These problems were solved by a combination of curving the blade to increase the blade/foil separation in the centre, and by embedding the ends of the blade in electrically conducting epoxy (R.S. Silver loaded epoxy, $\rho \sim 500\ \mu\Omega\,cm$). With an anode-cathode spacing of 29 mm (edge) and 31 mm (centre), relatively uniform X-ray exposures were obtained, with $\pm$ 20% variation spatially across the X-ray window and $\pm$ 5% variation from shot to shot.

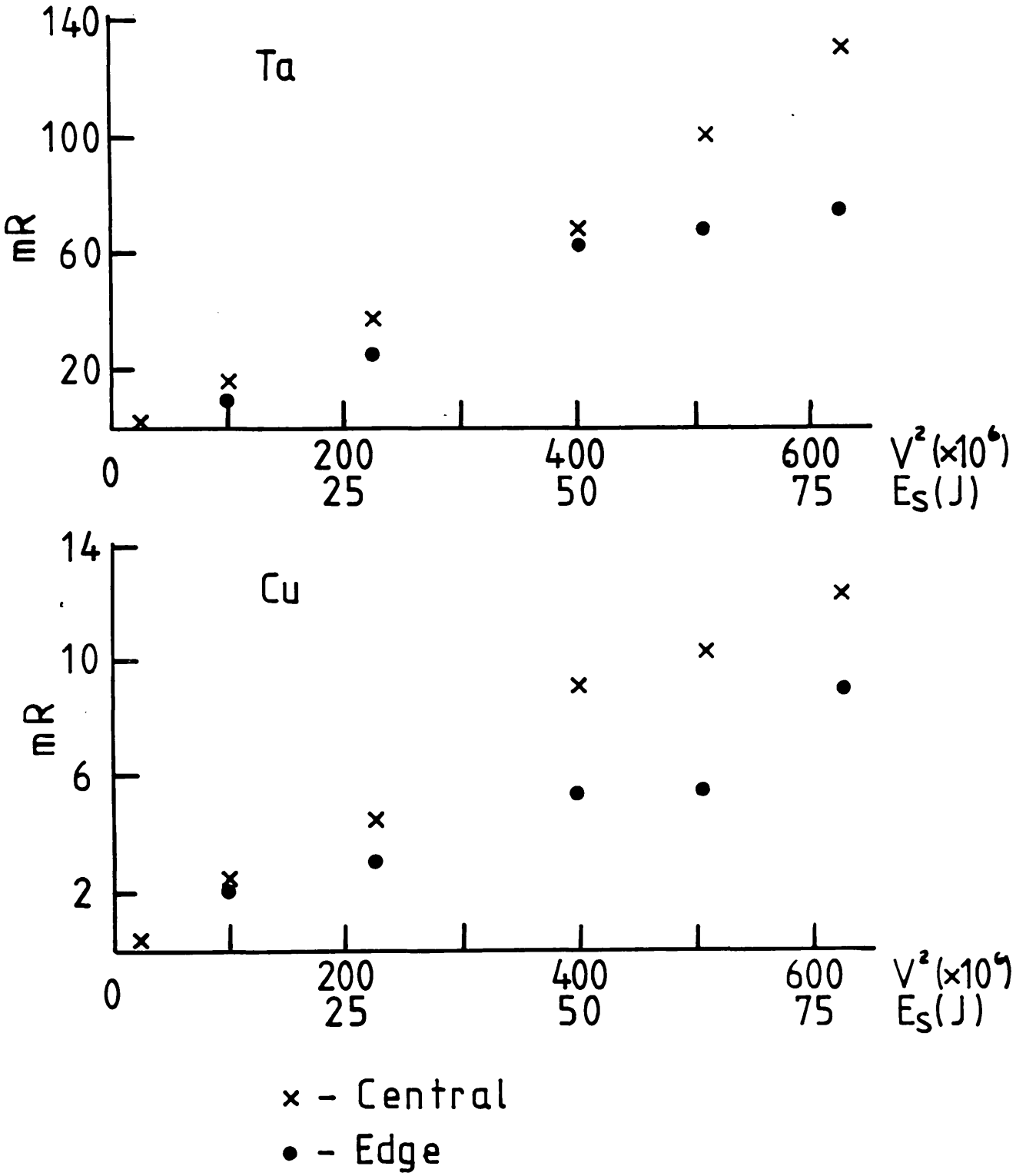

Figure 2.8 Measured X-ray exposure through X-ray windown and discharge electrode as a function of energy stored in the X-ray source (E_s) or the square of the capacitor charging voltage (V). Results for two target materials, Ta and Cu, are shown.

Greater uniformity of exposure could undoubtedly be achieved by increasing the rate of rise of voltage on the e-beam cathode and thereby producing more uniform e-beam emission. This could be done by including a peaking capacitor and spark gap on the high voltage circuit after the autotransformer. However, at the high exposures produced ($\sim$100 mR) the uniformity was considered 'adequate until proved otherwise'.

The impedance of the e-beam diode was estimated from the decay of the voltage across it to be 115Ω, slightly lower than the predicted 130Ω. With a charging voltage of 25 kV, close to the limit set by the thyratron, the transformer gain was 4.4, giving a maximum voltage on the e-beam cathode of 110 kV. Figure 2.8 shows how the X-ray exposure measured through the X-ray window and discharge electrode varies as a function of the energy stored in the capacitor, or alternatively the square of the capacitor charging voltage. Results are also shown for a later experiment using a copper rather than tantalum target. The difference between the exposures from the centre and the edge of the discharge region gives some indication of the spatial variation.

As the capacitor charging voltage is increased, so then is the energy of the electrons in the e-beam. This increases the efficiency of the bremsstrahlung production according to equation 2.1, and excites more of the characteristic lines of the target material. Also, the average energy of the X-rays produced is increased, thereby significantly increasing the fraction of the X-rays which penetrate through the X-ray window and discharge electrode. The combination of these two factors leads to the X-ray exposure in the present system being

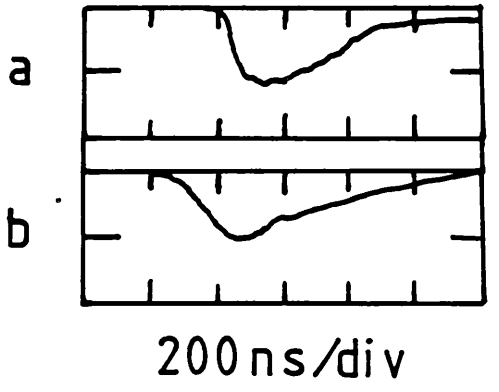

Figure 2.9 a) Measured X-ray intensity shown synchronised with, b) the e-beam cathode voltage.

approximately proportional to the square of the charging voltage, or alternatively the stored energy.

The lower exposures produced by the copper target are explained by two factors. Firstly, the lower atomic number reduces the efficiency of X-ray production by a factor of $\frac{Z_{Cu}}{Z_{Ta}} = \frac{29}{73}$, and secondly, the 80 μm thickness of the foil, which gives similar X-ray attenuation to the 8 μm tantalum foil, stops only about 20% of the incident electrons at 100 keV, hence the overall X-ray exposure is reduced to approximately $\frac{29}{73} \times \frac{20}{90} \simeq \frac{1}{10}$ of that produced with the tantalum (excluding the negligible production of X-rays in the Aluminium window).

The temporal behaviour of the X-ray emission was monitored using a photomultiplier (E.M.I. TUVP56). This was shielded from electromagnetic noise using mild steel foil around all but the photocathode entrance port, and kept in darkness using an aluminium case with three layers of black cloth covering the entrance port. Lead shielding prevented X-rays from entering the photomultiplier except through the normal entrance. The X-rays were detected both directly, using the photomultiplier alone, and indirectly, using a disc of scintillator (NE 110) over the photocathode, the results being identical. A sheet of mild steel across the entrance port severely reduced the signal, whereas a similar thickness of lead removed the signal altogether, revealing a low noise background. The detected X-rays are shown, together with the e-beam cathode voltage in figure 2.9. The start of the X-ray emission is quite abrupt and occurs some 100 ns after the start of the voltage waveform, but after this time the two curves follow each other quite closely, giving an X-ray pulse of $\sim$300 ns duration. This pulse is much longer than is needed

for preionisation, but eases the synchronisation requirements between the X-ray source and the discharge circuit.

2.6 X-ray Source Lifetime

Although the present X-ray source was designed for use on a low repetition rate laser ($\sim$0.1 Hz), it is informative to investigate the lifetime of the various components in the system to discover where the present system could be improved, and assess whether it could be used on a higher repetition rate laser. In normal use the storage capacitor is charged to 25 kV giving a stored energy of $\sim$78J and a peak cathode voltage of 110 kV, and the pressure at the e-beam diode is lower than 2×10^{-5} τ. Under these conditions a few thousand shots produces small but noticeable wear in the form of slight pitting of the blade edge and thermal distortion and colouring of the tantalum foil. The X-ray performance does not suffer because of this. However, using a less good vacuum ($\sim 10^{-3}$ τ), a similar number of shots severely erodes the blade and produces small perforations in the foil. Eventually the blade becomes sufficiently eroded for the e-beam emission, and hence X-ray dose, to become very non-uniform, giving almost zero dose in places. Thus the lifetimes of the foil and, more particularly, the blade, are clearly strongly dependent on the quality of the vacuum which can be maintained, and are, in any case, shorter than the lifetimes of the other components. With a good vacuum (2×10^{-5} τ) over ten thousand shots have been demonstrated without degradation in performance, giving an estimated blade lifetime of a few tens of thousands of shots ($\sim 3 \times 10^{4}$). While this lifetime is more than sufficient for a 'single-shot' prototype laser it is clearly insufficient for a laser of a few hundred Hertz repetition rate, comparable

to the currently available U.V. preionised excimer lasers. For such systems X-ray sources using carbon felt cold cathode emitters, thermionic emitters or wire-ion-plasma (W.I.P.) sources may prove more suitable[2.16,2.17,2.18].

After the electron emitting surface the component with the most limited lifetime will be the thyratron which, when used in this circuit, is subject to a large voltage reversal ($\sim$70%) shown in figure 2.7.c, a few microseconds after it is fired. This will reduce the lifetime from the 10^8-10^{10} shots expected otherwise.

2.7 Laser Chamber

One of the main advantages of X-ray preionisation that this laser system was designed to demonstrate is the ability to preionise large volumes of laser gas. It was therefore necessary to use a large volume discharge chamber, but, as the constituents of the excimer laser gas mixtures are relatively expensive, the smallest total volume consistent with the large active volume was sought. Internal dimensions of 120 x 11 x 11 cm^3 were chosen, giving a total volume of some 14.5 litres, significantly less than virtually all commercial lasers (cf Lambda Physik EMG 101, 40 litres). The laser chamber was constructed from halogen compatible materials, the main body being formed from four 1" thick slabs of poly-vinyl difluoride (P.V.D.F.) welded together to form the top, bottom and ends of the chamber.

The P.D.V.F. was O-ring sealed onto the earthed mounting plate, which carries both the tantalum foil and the discharge cathode. The solid brass discharge anode was attached to a Dural mounting plate, using twenty one M4 bolts, each with its own O-ring seal, and the mounting plate was similarly sealed

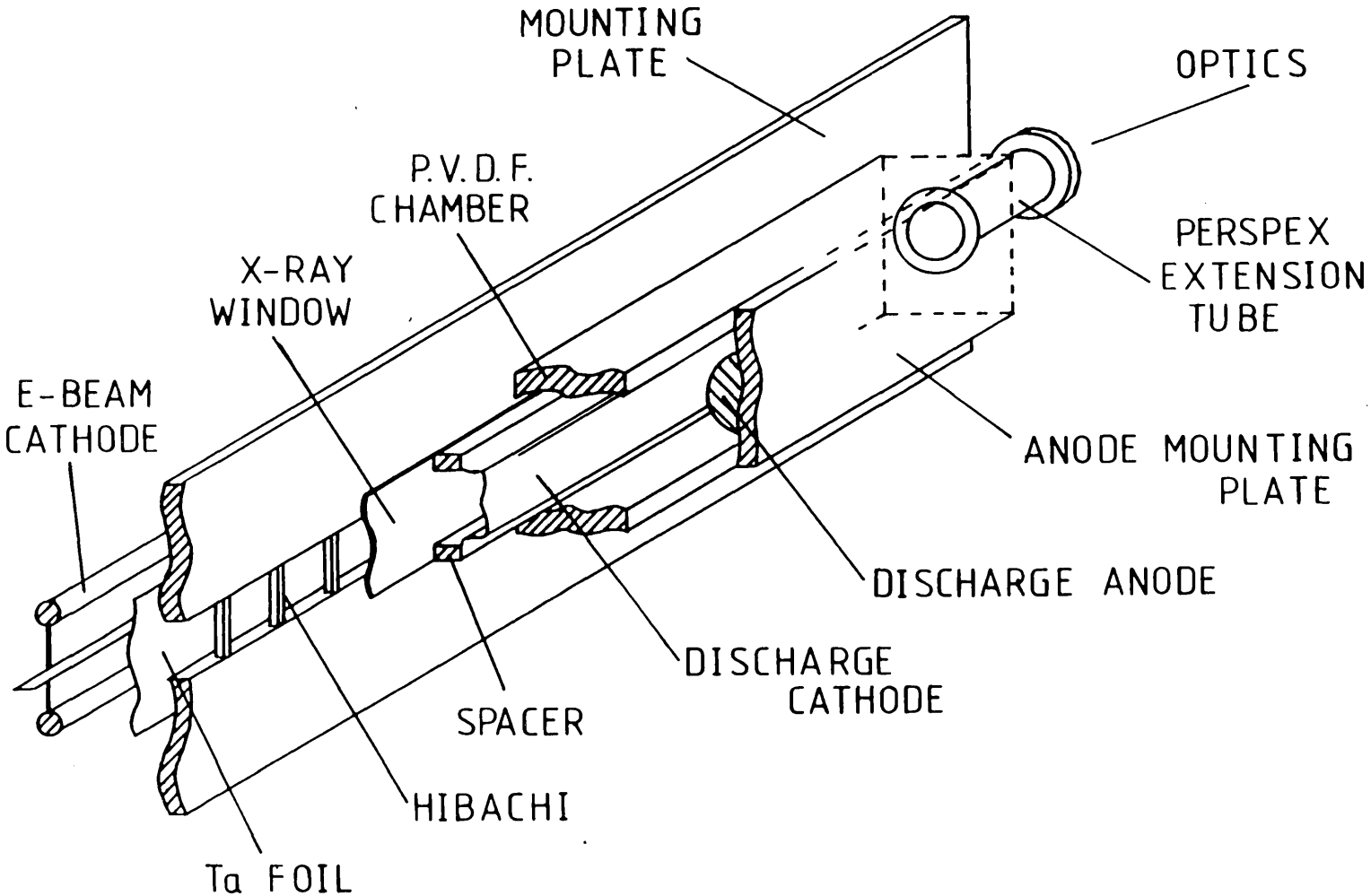

Figure 2.10 Sectional view of laser chamber.

onto the remaining open side of the P.V.D.F., completing the laser chamber (Fig. 2.10). The fused quartz optics were mounted on 20 cm long perspex spacing tubes, clear aperture 2", protruding from the ends of the chamber. This was to distance them from the discharge region, and hence reduce the frequency at which the optics must be cleaned.

As was mentioned in section 2.2, the optimum X-ray energy is only $\sim$20 keV, higher energies than this being less efficient at producing preionisation electrons. These X-rays have to be transmitted through the X-ray window, but this window must also be capable of withstanding the pressure differential of several atmospheres between the laser chamber and the e-beam diode chamber over a large ($\sim$100 x 10 cm^2) area. These requirements of strength and X-ray transparency obviously conflict, and some compromise must be made. Initially a single sheet of 1 mm aluminium was used as both X-ray window and discharge cathode. This gives a 38% transmission of 20 keV X-rays, and 59% of 25 keV. However, at discharge chamber pressures of more than one atmosphere the aluminium began to bend, producing distortion of the electrode, and at a pressure of approximately two atmospheres catastrophic failure occurred, the aluminium being literally torn apart. After this a two layer structure was employed. The pressure bearing component consists of a 1 mm thick aluminium sheet supported at 4 cm intervals along its length by a Hibachi grill. Bowing of this structure under pressure is unimportant as the discharge cathode is fabricated from a completely separate piece of 1 mm aluminium, attached to the mounting plate through spacers to permit simple variation of the discharge anode-cathode separation. It is this structure which is shown in figures 2.10 and 2.11.

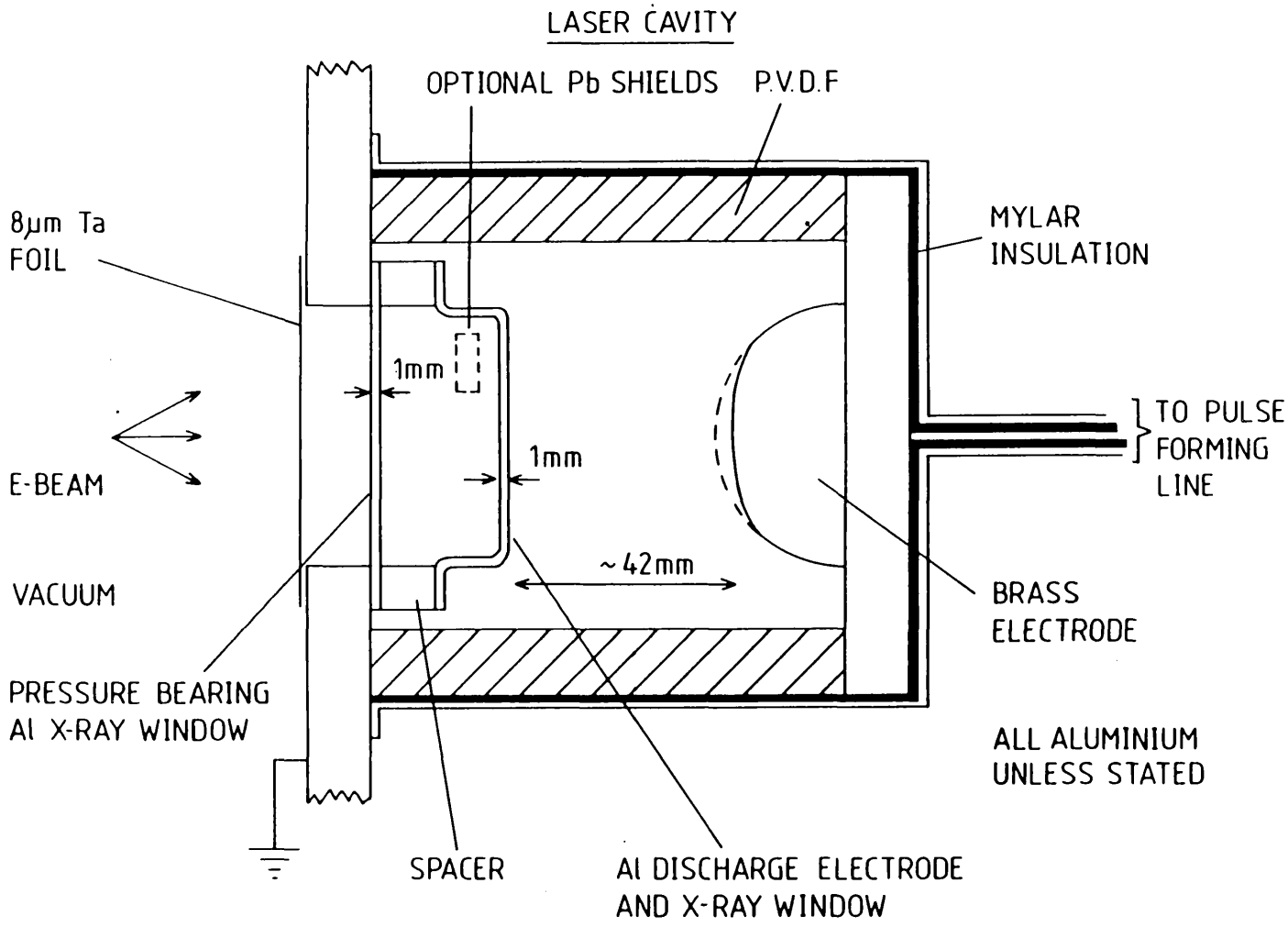

Figure 2.11 Cross-sectional view of laser chamber.

A further advantage of this arrangement is that the X-ray exposure may be spatially modulated by placing lead shields in the space between the X-ray window and discharge cathode. However, the transmission of low energy X-rays is decreased to that shown in figure 2.2, giving only 14% transmission at 20 keV and 35% at 25 keV. It was through this two layer structure that the X-ray exposure measurements of section 2.5 were made, showing more than adequate X-ray flux. The maximum pressure limit of the discharge chamber is now no longer governed by the X-ray window, but by the perspex extension, tubes and pressures up to 3.5 atmospheres are routinely used.

Due to the corrosive nature of the halogen donor gases, all O-rings are made of Viton, and are smeared with Fluorocarbon Vacuum Grease. The only exposed bolts within the chamber are those connecting the discharge cathode through the spacer and onto the mounting plate, and these are made of stainless steel. All other exposed metal is aluminium, with the exception of the brass discharge anode. The profiling of the anode, and its separation from the flat cathode, was adjusted with reference to the laser output beam, and this will be described in Chapter 4.

CHAPTER 3

THE DISCHARGE CIRCUIT

3.1 Discharge Circuit Requirements

As outlined in Chapter 1, excimer lasers, due to their broad bandwidth and short wavelength, require very high specific input powers in order to produce significant gain. Typically several hundred kilowatts per cubic centimetre are required, which, in the present system of projected volume 1000 cm^3, implies a total input power of almost 1 GW. This input power level cannot be sustained continuously for two reasons; firstly, the magnitude of the power supply necessary, and secondly, the more fundamental problem of cooling the laser gas when subjected to such input powers. In fact, not only does gas heating rule out C.W. operation, the thermal gradients caused by it are sufficient to place a limit of around 5 μs[3.1] on the laser output pulse duration. However, as there is no obvious kinetic reason why excimer lasers should not run for periods of time comparable to this, it is desirable to provide electrical excitation for as large a fraction of this time as is practicable.

Before the introduction of X-ray preionisation avalanche discharge pumped excimer lasers had demonstrated only short (10 ~ 20 ns) output pulse durations, severely limiting their output energy, beam quality and general utility. The greater uniformity of preionisation provided by X-rays rapidly demonstrated the ability to produce pulse durations an order of magnitude greater than had previously been possible[3.2]. In order to demonstrate this advantage of X-ray preionisation, and investigate the possibility of extending the pulse durations still further, a discharge circuit capable of providing

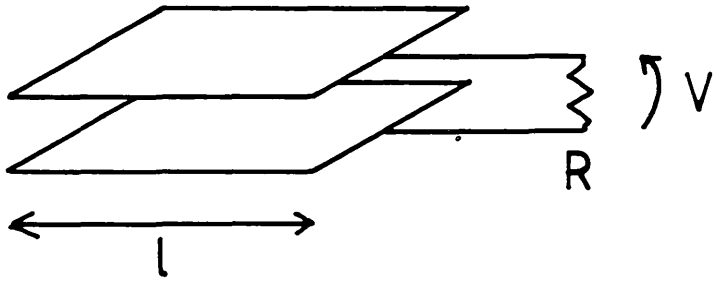

Figure 3.1 Parallel plate capacitor of dimension l and voltage V_o, with load R connected at one end.

excitation over a time of >150 ns was required, implying an energy deposition in the laser discharge plasma of around 100J, and so a stored energy somewhat greater than this.

Of the various forms in which this energy can be stored (electrostatic, electromagnetic, kinetic, thermal, etc.), the one which allows quickest access to the energy is the charging of a low inductance capacitor. This energy may then be directly transferred to the discharge at a rate limited by the inductance in the circuit. However, the exponential or ringing waveform characteristic of an L-C circuit cannot provide a constant power deposition in the laser discharge. This leads to inefficient use of the stored energy and possibly to instability within the discharge.

There is, however, a way in which all of the stored energy can be deposited into a resistive load at a constant rate in a well specified period of time, and the theory of this technique is described in the next section.

3.2 Transmission Line and Pulse Forming Line Theory

The pulse forming line (P.F.L.) is closely related to the capacitor which, indeed, is its low frequency counterpart. Consider a parallel plate capacitor (figure 3.1) charged to a voltage V_o. If a resistance, R, is connected as shown across one end of the plates, the voltage across the capacitor will decay with time constant RC according to the familiar formula

$$V = V_0 \exp(-t/RC) \qquad (3.1)$$

where V is the voltage between any two points on the plates.

If R is reduced, then the decay becomes more rapid. However, as R is further reduced there will come a time when

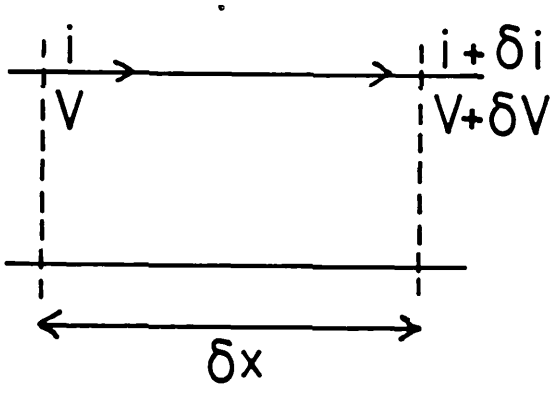

Figure 3.2 Currents and voltages on a transmission line consisting of two one-dimensional conductors.

the decay predicted by Eqn. 3.1 occurs in a shorter time than it takes for the electric field to travel between the plates from the resistor to the far end,

$$\text{i.e.} \qquad RC < \left(\frac{c_o}{\sqrt{\varepsilon}\, l}\right)^{-1} \qquad (3.2)$$

where C_o is the speed of light and ε is the dielectric constant of the material between the plates. Obviously at this point the voltage between the plates cannot be described by the single valued variable V, but is a spatially varying function. It is not sufficient to consider the capacitor as a single, lumped component, the spatial transmissions of voltage within it must be taken into account, and this requires the use of transmission line theory.

The theory of transmission lines is well covered in text books[3.3,3.4,3.5], but generally in respect of signal transmission, or continuous A.C. power transmission, and it will therefore be useful to present here a review of the theory and derive some of the equations of particular relevance to P.F.L.'s and pulsed power supply. A rigorous treatment involves the solution of Maxwell's equations in three spatial and one temporal dimension, using the particular boundary conditions; however, much physical insight can be gained from a two dimensional analysis, where the wave nature of the solutions is assumed.

Considering the one dimensional conductors shown in figure 3.2, the change of voltage over a length δx is given by

$$\delta V = -\left(ri + L\,\frac{\partial i}{\partial t}\right)\delta x \qquad (3.3)$$

where r is the resistance of the conductors and L is the

inductance, both per unit length.

Similarly,

$$\delta i = -\left(gV + C \frac{\partial V}{\partial t} \right) \delta x \qquad (3.4)$$

where g is the conductance of the dielectric separating the conductors and C is the capacitance between them, again per unit length. As we will be concerned with only relatively short lengths of transmission line, we will assume it to be lossless, i.e. r = g = 0. This yields

$$\frac{\partial V}{\partial x} = - L \frac{\partial i}{\partial t} \qquad (3.5a)$$

and

$$\frac{\partial i}{\partial x} = - C \frac{\partial V}{\partial t} \qquad (3.5b)$$

which, on differentiation, lead to

$$\frac{\partial^2 V}{\partial x^2} = LC \frac{\partial^2 V}{\partial t^2} \qquad (3.6a)$$

$$\frac{\partial^2 i}{\partial x^2} = LC \frac{\partial^2 i}{\partial t^2} \qquad (3.6b)$$

These equations have solutions of the form

$$V = V_1 (x-st) + V_2 (x+st)$$

$$i = i_1 (x-st) + i_2 (x+st) \qquad (3.7)$$

$$\text{where} \qquad s = 1 / (LC)^{\frac{1}{2}} \qquad (3.8)$$

These solutions represent two arbitrary waves, one travelling in the positive x direction (x-st), and one in the opposite direction (x+st), both with speed s.

The relation between the voltage and current may be

obtained in the following way. Integrating Eqn. 3.5b, one obtains

$$\int \frac{\partial i}{\partial x}\, dx = - C \int \frac{\partial V}{\partial t}\, dx = i \qquad (3.9)$$

Now, considering (for simplicity), V to be a wave travelling in the positive x direction, then

$$V = V_1 (x-st) \Rightarrow \frac{\partial V}{\partial x} = \dot{V}_1$$

and

$$\frac{\partial V}{\partial t} = - s\dot{V}_1$$

So

$$\frac{\partial V}{\partial x} = - \frac{1}{s} \frac{\partial V}{\partial t} = - (LC)^{\frac{1}{2}} \frac{\partial V}{\partial t} \qquad (3.10)$$

Substituting $\frac{\partial V}{\partial t}$ from Eqn. 3.10 into Eqn. 3.9 produces

$$i_1 = - C \int \frac{\partial V_1}{\partial t}\, dx = C / (LC)^{\frac{1}{2}} \int \frac{\partial V_1}{\partial x}\, dx = (C/L)^{\frac{1}{2}} V_1$$

$$Z = \frac{V_1}{i_1} = (L/C)^{\frac{1}{2}} \qquad (3.11)$$

So V and i are related by the simple equation 3.11, which shows that on a transmission line there exists a characteristic impedance Z resulting from reactive components which nevertheless shows the phase relationship of a pure resistance.

From equations 3.8 and 3.11 the capacitance and inductance per unit length of the line may be expressed in the two useful formulae

$$C = \frac{1}{Z s} \quad \text{and} \quad L = \frac{Z}{s} \qquad (3.12)$$

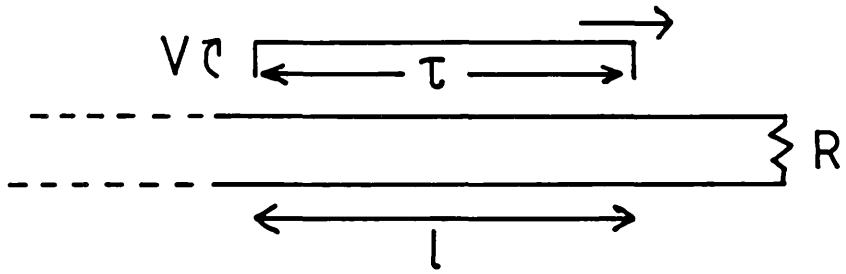

Figure 3.3 Rectangular voltage pulse of magnitude V and duration τ travelling down an infinite transmission line towards a load R.

We now move on to consider how much of an incident wave travelling along the line is reflected from a terminating load of resistance R. The incident voltage and current are related, from Eqn. 3.11, by V=ZI, and similarly any reflected wave must obey $V_r = -ZI_r$, the negative sign indicating that the current is now in the opposite direction. The total voltage and current across and through the load are equal to the sum of the incident and reflected waves, so that

$$\begin{aligned} V_1 &= V + V_r \\ \text{and} \qquad I_1 &= I + I_r \end{aligned} \qquad (3.13)$$

But

$$R = \frac{V_1}{I_1} = \frac{V + V_r}{I + I_r} = \frac{V + V_r}{(V/Z) - (V_r/Z)} \qquad (3.14)$$

using the equations in the text. Therefore, from Eqn. 3.14,

$$V_r = V\,\frac{R-Z}{R+Z} \equiv \rho V \qquad (3.15)$$

where the reflection coefficient ρ is given by

$$\rho = \frac{R-Z}{R+Z} \qquad (3.16)$$

With the formulae derived it is now possible to analyse the power transfer from a transmission line into a resistance R. Consider the case of an incident rectangular pulse of voltage V and duration τ travelling down a line of infinite length towards a load R, as in figure 3.3. The energy stored in the travelling wave is given by (3.6)

$$S = (\tfrac{1}{2}CV^2 + \tfrac{1}{2}LI^2) \times \text{length } l$$

Substituting for C and L from Eqn. 3.12 and setting I = V/Z gives

$$S = \tfrac{1}{2}V^2 l/Zs + \tfrac{1}{2}(V^2/Z^2)(Zl/s) = \frac{V^2 l}{Z s} = \frac{VIl}{s} \qquad (3.17)$$

The energy deposited in the load is given by

$$D = V_l I_l \tau$$

but $$V_l = V + V_r = (1+\rho)V$$

and $$I_l = I + I_r = (1-\rho)I \qquad (3.18)$$

$$\text{and} \quad \tau = l/s$$

so

$$D = VI\,(1+\rho)(1-\rho)l/s = \frac{VIl}{s}(1-\rho^2) \qquad (3.19)$$

Therefore the efficiency of energy transfer (equal to the energy deposited, D, divided by the energy stored, S) is

$$\eta = D/S = 1-\rho^2 \qquad \left(= \frac{4RZ}{(R+Z)^2}\right) \qquad (3.20)$$

It is easily shown that the reflected energy

$$(\tfrac{1}{2}CV_r^2 + \tfrac{1}{2}LI_r^2) \times \text{length } l$$

is equal to S-D.

Formula 3.20 gives the efficiency of energy transfer from a wave on a transmission line into a load of resistance R, and it can be seen that where R=Z then this is unity. This arrangement therefore offers the possibility of 100% energy transfer into the load in a well specified time τ. However,

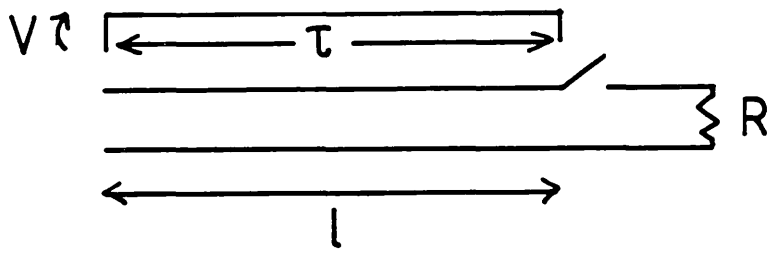

Figure 3.4 Pulse forming line arrangement with finite transmission line charged to voltage V over its entire length l, and then switched onto load, R.

it does require the use of a travelling wave which must be sent down the transmission line. In general, such a wave cannot be launched onto the line with a similar high efficiency from an energy storage capacitor. An alternative approach, not requiring an initial travelling wave, is to use a pulse forming line (P.F.L.). As was mentioned at the beginning of this section, a P.F.L. is similar to a capacitor in that it is charged along its entire length before operation (figure 3.4). Under these circumstances the energy stored is simply

$$S = \tfrac{1}{2}CV^2 = \tfrac{1}{2}\frac{V^2 \tau}{Z s} \qquad (3.21)$$

If a load of resistance R is then suddenly connected across one end, then the voltage appearing across it will initially be given by the simple resistive divider formula

$$V_\tau = VR/(R + Z) \qquad (3.22)$$

However, the relation between V, V_r and V_i, as given by Eqn. 3.18, will still be obeyed, giving

$$V_r = V_\tau - V = V\left(\frac{R}{R+Z} - 1\right) = -\frac{V Z}{R + Z} \qquad (3.23)$$

thereby producing a reflected wave of magnitude V_r, which travels between the conductors in transmission line fashion away from the load R. At the far end of the line the open circuit represents an infinite load, producing a reflection coefficient of $\rho = 1$, as given by Eqn. 3.16. This completely reflects the wave V_r and sends it back towards the load R, where it returns after a time $t = 2\tau$. Here the wave is again reflected, this time with coefficient

$$\rho = (R - Z)/(R + Z)$$

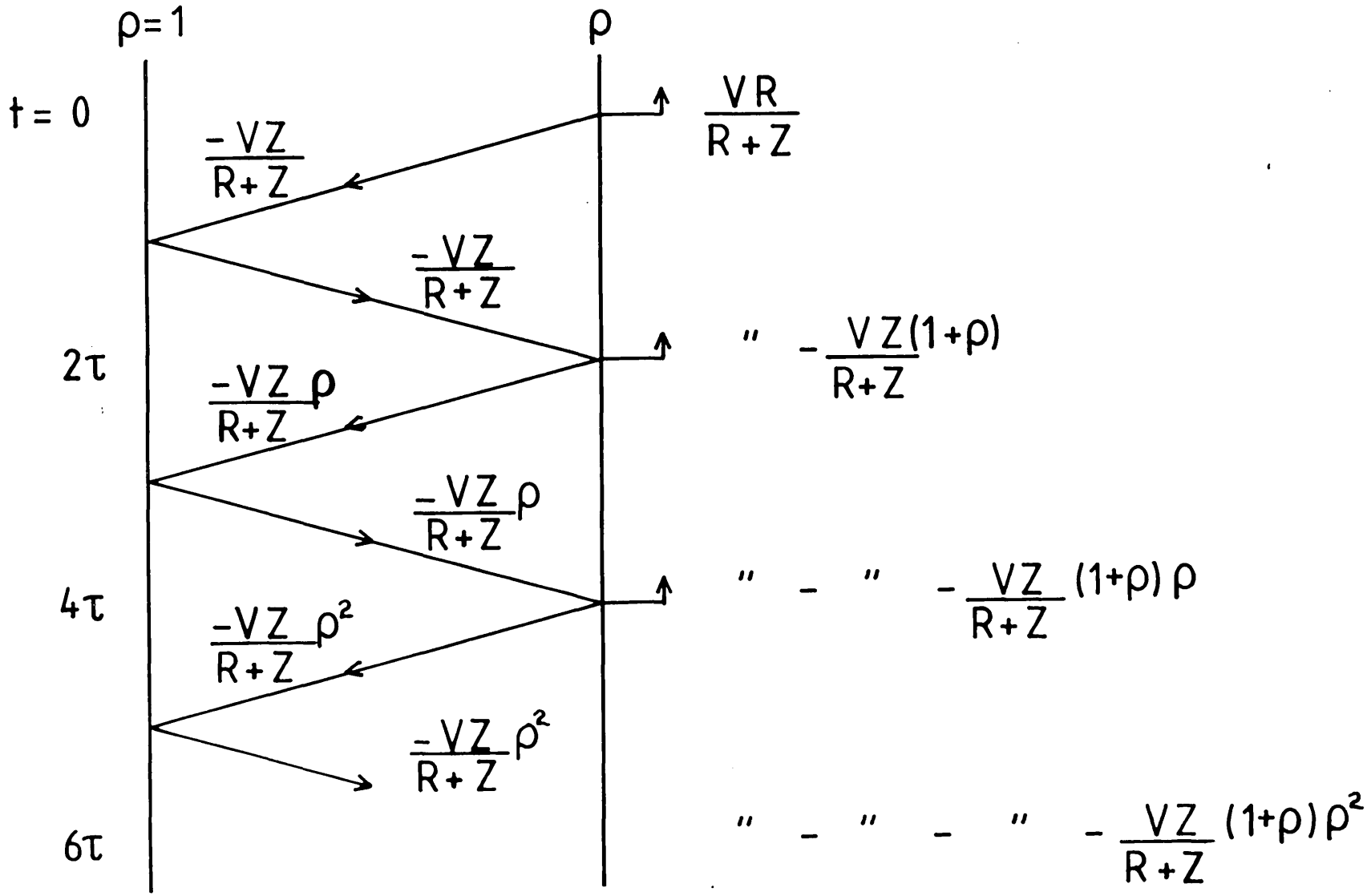

Figure 3.5 Lattice diagram showing successive voltage reflections from load, ρ , and open end of line, ρ = 1. The voltage at the load is shown to be incremental at time intervals of 2τ.

and in doing so adds a further contribution of $(1 + \rho) V_r$ to the voltage appearing across the load. This process of successive reflections continues, as is shown in the lattice diagram in figure 3.5, incrementing the voltage across the load at intervals of 2τ. Hence the voltage across the load follows the equation

$$V_1 = V \left[\frac{R}{R+Z} - \frac{Z}{R+Z} (1+\rho) \left\{ 1(t=2\tau) + \rho(t=4\tau) + \rho^2(t=6\tau) + \ldots \right\} \right] \qquad (3.24)$$

Figure 3.6 shows the form of this voltage for R greater than, equal to, and less than Z. The current waveforms are identical in form except that the R>Z voltage waveform becomes the R<Z current, and vice versa. It can be seen that when R=Z all of the energy stored on the P.F.L. is transferred into the load at a constant rate over a well defined time of 2τ. For $R \neq Z$ there are voltage and current reflections from the load. In a perfect, loss-free, line all of the energy will eventually be deposited in the load, but over a much longer time and at a decreasing rate. However, when used as a pulsed power source, it is the fraction of the stored energy which is deposited at a constant rate during the first time interval 2τ which is of importance.

The energy deposited in this time will be

$$D\ (t = 0,2\tau) = V_1 I_1\ 2\tau$$

$$= \frac{V\ R}{R+Z} \cdot \frac{V}{R+Z} \cdot \frac{2l}{s}$$

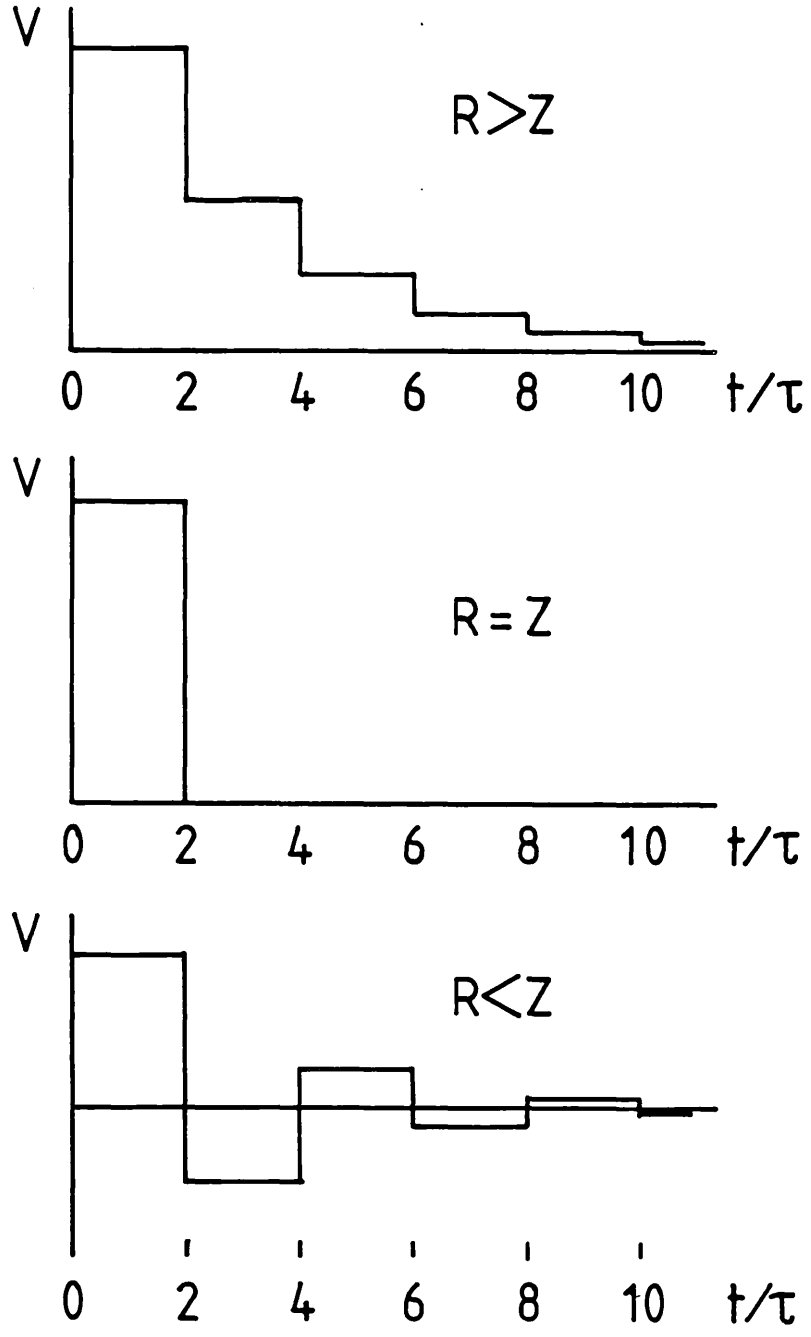

Figure 3.6 Voltage across P.F.L. load, a) for R>Z, b) for R=Z and c) for R<Z.

Therefore, defining an efficiency η as the fraction of the stored energy deposited in this time,

$$\eta \equiv \frac{D(t = 0,2\tau)}{S} = \frac{2IV^2R}{s(R+Z)^2} \cdot \frac{2}{CV^2}$$

$$= \frac{4RZ}{(R+Z)^2} = 1 - \rho^2 \qquad (3.25)$$

the same form as the equation relating to the infinite transmission line (eqn. 3.20). This equation will be used again in a modified form in Chapter 5, but the present concern is the design of a system in which R=Z in order to maximise the efficiency.

3.3 P.F.L. Modifications for Excimer Laser

The foregoing analysis of the PFL in the previous section shows that 100% energy deposition within the load at a constant rate for a specific time is possible. However, this only applies to a purely resistive load of constant value. In the case of an excimer laser the load consists of the laser head and the discharge plasma contained within it. This necessarily has an inductance which must be minimised by careful design if classical P.F.L. behaviour is to be approached. Moreover, the laser discharge does not provide a constant resistance. Before the discharge plasma is formed it presents an almost infinite resistance, after the plasma has formed the impedance rapidly falls to a low value ($\sim 0.1\Omega$), strongly dependent on the parameters of the electrical circuit driving the discharge. The change in the discharge impedance, and its dependence on the driving circuit, make it impossible to achieve good impedance matching between load and P.F.L. without using some additional technique. Furthermore, the fact that the voltage

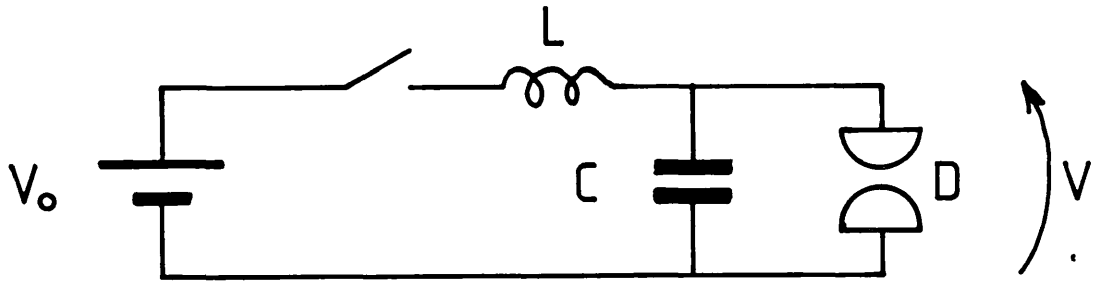

Figure 3.7 P.F.L. equivalent circuit over short timescales. Main P.F.L. is represented by constant voltage source, V_o; rail-gap by switch and inductor L; and short section of transmission line by capacitor C.

required to initiate the discharge plasma is several times that required to sustain it makes the efficient use of simple P.F.L. almost impossible. What is required is a means of very rapidly producing a high voltage across the discharge electrodes to promote rapid and uniform discharge formation before the main energy from the P.F.L. is delivered. This can be provided by a separate external circuit[3.7], but a more elegant and simple method was employed in the present work[3.8].

As mentioned at the start of section 3.2, a P.F.L. or section of transmission line will act as a capacitor if its physical dimensions are small enough for the conductors to be considered as equipotentials. This fact can be used to advantage by placing a short section of transmission line between the P.F.L. switch and the laser head. On short time-scales this section will be kept separate from the rest of the P.F.L. by the inductance inherent in the P.F.L. switch. Also, for the short period of time of interest the P.F.L. will provide a constant voltage. Therefore the equivalent circuit is as shown in figure 3.7, where V_o is the constant voltage source, C is the capacitance of the short section of line, and L is the switch inductance, D being the discharge electrodes. This circuit will produce a voltage across the discharge electrodes of

$$V = V_0 (1 - \cos\omega t) \qquad (3.26)$$

where $\omega^2 = 1/LC$ (see Appendix II for derivation). Therefore after the short time $t = \pi (LC)^{\frac{1}{2}}$ the voltage appearing across the electrodes will be double that on the P.F.L., providing voltage gain to break down the discharge gap D. When breakdown does occur, the excess voltage will be rapidly discharged through the laser plasma (improving the current

risetime) and the short section of line is then left merely as a continuation of the main P.F.L.

Thus, this technique provides a means of producing rapid, transient voltage gain to break down the laser gas, without changing the impedance of the driving circuit at any point. This greatly reduces the amount of reflected energy compared to the more conventional methods of providing voltage gain such as the capacitor transfer circuit, or using an increase in the impedance of the P.F.L. at a junction. Furthermore, it is a self-synchronising technique requiring no external power supply or trigger. The inductance required for operation of the circuit, although undesirable in other ways, is merely that of the P.F.L. switch, which is unavoidable, but is kept to a minimum.

3.4 P.F.L. Experimental

The energy and time requirements outlined in section 3.1 must be incorporated into the P.F.L. design discussed in sections 3.2 and 3.3. The pulse duration of >150 ns requires, from section 3.2, a P.F.L. of length

$$l > \frac{150\,ns}{2}\, s$$

But from eqn. 3.8, $s=(LC)^{-\frac{1}{2}}$ which is easily shown to be equal to $s = c(\varepsilon_r u_r)^{-\frac{1}{2}}$ and so, for non-magnetic materials,

$$l > \frac{\tau\, c}{2(\varepsilon_r)^{\frac{1}{2}}} \quad \Rightarrow \quad l > \frac{22.5}{(\varepsilon_r)^{\frac{1}{2}}} \text{ metres.}$$

Because of this relationship it is obviously necessary to use a dielectric of high ε_r in order to make the P.F.L. a reasonable size. In the present prototype system, where versatility is an important factor, the chosen dielectric was water,

which has $\varepsilon_r \simeq 80$ at frequencies up to about 1 GHz. Ceramic materials with their much higher ε_r's ($\sim$1000) could be used on a more 'commercial' system. Using water dielectric the chosen length of P.F.L. of 2.75 m gives a pulse duration of 164 ns. As mentioned earlier, if the full advantages of using a P.F.L. are to be realised, the inductance of the load must be kept to a minimum. Appendix III shows that the inductance of two parallel plates is given by

$$L = \mu \, l \, \frac{\Delta}{W} \qquad (3.27)$$

where l is the length, W the width and Δ the separation of the plates ($W >> \Delta$). The width of the plates, W, is to a large extent governed by the length of the discharge electrodes. However, the effective width may be doubled, and hence the inductance halved, by using another plate connected in parallel with the first. This can be done by using two earth return plates, one above and one below the high voltage plate, and this is referred to as a double P.F.L.

Using a width of one metre and length of 2.75 metres, the stored energy requirement of >150J gives

$$150 < \frac{1}{2} CV^2 = \frac{V^2}{2} \frac{l}{Zs} \times 2 \text{ for double P.F.L.}$$

With $s = c(80)^{-\frac{1}{2}}$ this leads to

$$\frac{V^2}{Z} > 1.8 \times 10^9$$

So for a reasonable charging voltage of $V \simeq 30$ kV, then $Z < 0.5\,\Omega$, indicating that low impedances must be used. This is commensurate with the matching of the P.F.L. to the projected laser plasma impedance of $\sim 0.1\Omega$. Appendix III shows that for

non-magnetic materials the impedance of the double P.F.L. is given by

$$Z = \tfrac{1}{2} \frac{377}{(\varepsilon_r)^{\frac{1}{2}}} \frac{\Delta}{W} \qquad (3.28)$$

This indicates a plate separation of 4.8 mm for $Z = 0.1\,\Omega$, not easy to maintain over an area of 2750 x 1000 mm^2, but significantly easier than the 2.4 mm which would have been necessary, had a single P.F.L. been used. The placing of such large area plates so close together places strict limits on the conductivity of the water dielectric if energy is to be stored on them for any significant time. The resistance between the central plate and the two outer ones is

$$R = \tfrac{1}{2} \frac{\varrho \Delta}{l W}$$

and the capacitance between them is

$$C = 2 \varepsilon_0 \varepsilon_r \frac{l W}{\Delta}$$

and so the relevant time constant is

$$RC = \varepsilon_r \varepsilon_0 \varrho$$

where ϱ is the resistivity of the water. If the energy is to be stored for $\sim 1\ \mu s$, we require $RC \sim 10\ \mu s$, i.e. $\varrho \sim 1\ M\Omega$ cm. This is irrespective of the separation between the plates, and far higher than the $\sim 300\,\Omega$ cm of local tap water. In order to achieve this resistivity the P.F.L. water is constantly circulated through a resin ion-exchange deionising cylinder (ELGA C124).

The P.F.L. is constructed from 2 mm thick aluminium plates separated by perspex spacers and immersed in a perspex water tank. The plates are laid horizontally and were initially

bolted together through the perspex spacers, using OBA nylon bolts. However, this led to electrical breakdowns occurring along the bolts, possibly due to air entrained in the screw thread. Removal of the bolts alleviated this problem, and, as long as the plates are supported evenly over their surface, without detriment to the accuracy of the plate spacings.

In order for the benefits of using a P.F.L. to be realised, and to produce the fastest transient voltage gain on the short transmission line section, it is necessary to keep the inductance of the switch connecting this line to the P.F.L. to a minimum. Given that current enters and leaves the switch uniformly distributed along 1m wide conductors, any decrease in the width through which this current passes in the switch, or increase in separation from the earth plates, will give the switch a higher inductance than the surrounding circuit (Eqn. 3.27). It is therefore practically impossible to make the inductance of the switch comparable to that of the P.F.L., and hence remove the voltage peaking effect. To keep the inductance to a minimum the switch used is a 1m long rail gap with one round brass electrode (anode) and one knife edge brass electrode (cathode) contained in a sealed, annealed perspex tube. The 'hold-off' voltage of the switch is varied by changing the pressure of dry air within the tube. Such a switch would be expected to give multichannel operation, an inductance of $\sim$5-10 nH and jitter of $\sim$5 ns when the voltage risetime across it is of the order of 100 ns[3.9]. In order to avoid tracking within the rail-gap the electrode separation is $\sim$1.5 cm while the tube internal diameter is 3.0 cm. This forces the separation between the earth return plates to be increased by 4 cm over the separation elsewhere to clear the switch. The short transmission line section is constructed

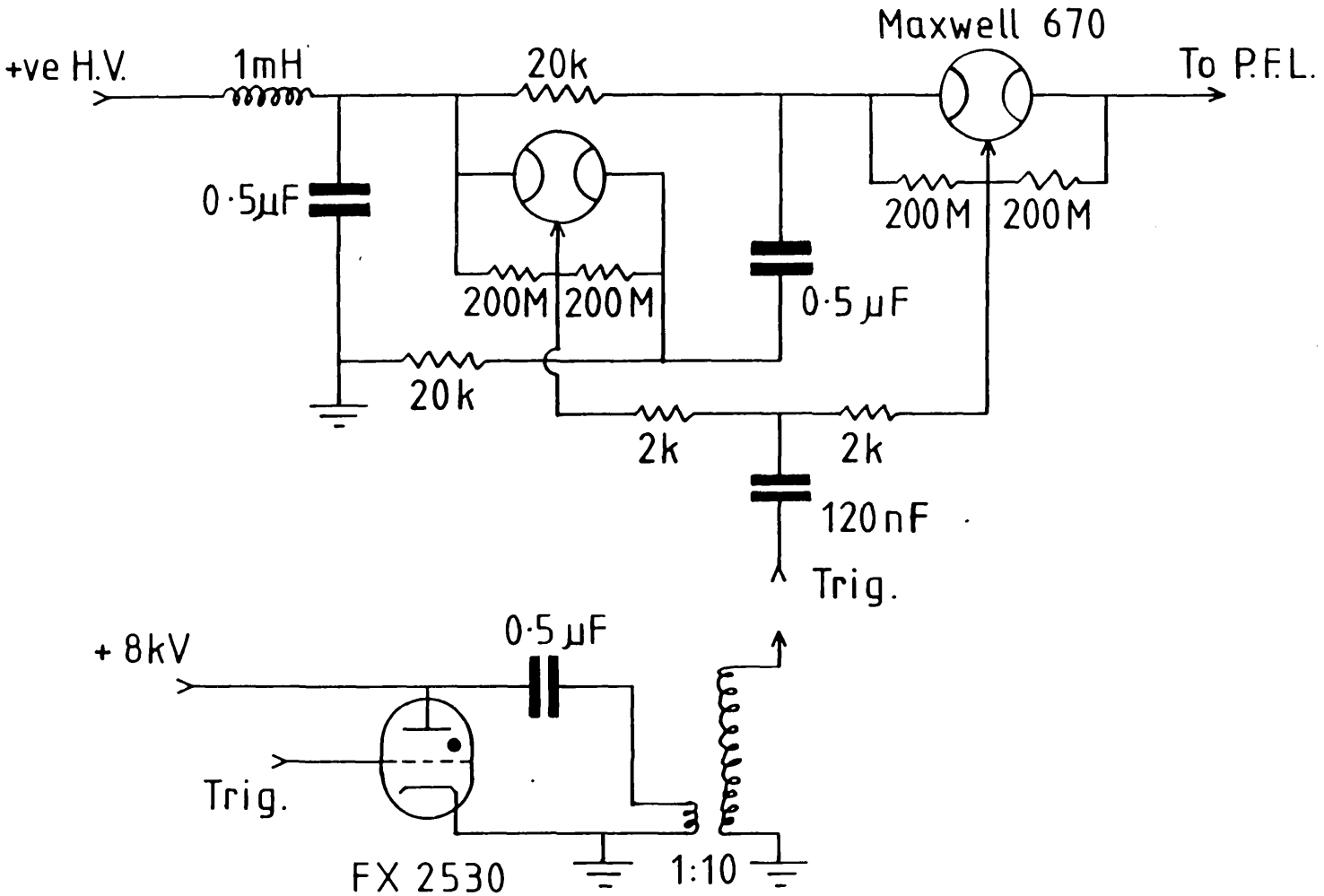

Figure 3.8 Marx bank circuit, top, operated under oil and trigger circuit; bottom, operated in air.

from the same materials as the P.F.L. and is 0.5 m (15 ns single transit time) in length. It is connected to the laser head by 0.9m wide aluminium sheet insulated with Mylar, the physical length of these dry feeds being kept to a minimum, and their electrical length being significantly shorter than the equivalent dimensions with water dielectric.

3.5 The Marx Bank

As the P.F.L. is suitable for storing energy for only short periods of time due to its low interplate resistance, it must be pulse charged from a primary energy store. In the present system this consists of two 0.5 μF, 50 kV low inductance (20 nH) Maxwell capacitors connected in a Marx bank configuration as shown in figure 3.8. The 2kΩ and 20kΩ resistors are of the copper sulphate variety and the entire Marx is immersed in oil for insulation. Initially only the first spark-gap was triggered, but this led to unacceptable jitter of ~400 ns, triggering both gaps from the same low inductance source reduced this to < 5 ns.

It is required to charge the P.F.L. quite quickly in order to both reduce the energy loss into the P.F.L. water and to improve the operation of the rail-gap in terms of both inductance (number of spark channels) and jitter. The circuit governing the charging of the P.F.L. is shown in figure 3.9, where C_1 is the erected capacitance of the Marx, C_2 is the capacitance of the P.F.L. and L is the inductance of the Marx bank (Capacitors, Spark gaps, connections) and feeds to the P.F.L. As is shown in Appendix II, this circuit obeys the equation,

$$V(t) = V_0 \frac{C_1}{C_1+C_2} (1 - \cos\omega t) \qquad (3.29)$$

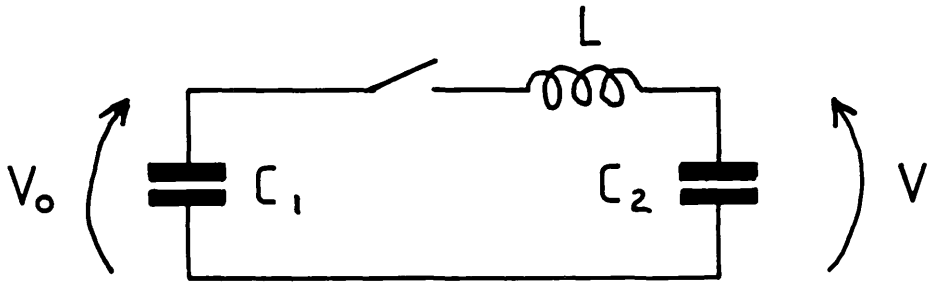

Figure 3.9 Equivalent charging circuit of P.F.L. C_1 is erected Marx capacitance, C_2 the P.F.L. capacitance and L the inductance between the two.

where $\omega^2 = (1/LC_1) + (1/LC_2)$ giving a risetime of voltage on the P.F.L. of

$$t_r = \pi\sqrt{\frac{L\,C_1C_2}{C_1 + C_2}} \qquad (3.20)$$

Therefore, to minimise t_r, the inductance of the Marx Bank was kept as low as geometrically possible and was measured as being ~ 200 nH, giving voltage risetimes of the order of half a microsecond.

3.6 P.F.L. Performance

Initial tests were carried out at line separations of 6.6 and 13.5 mm, giving P.F.L. impedances of 0.13 and 0.28 Ω respectively. At first the gross field between the plates could not be reliably raised above 10^6V/m before electrical breakdown between the plates occurred. This corresponds to only ~ 7 kV on the 0.13 Ω line and is a significantly lower field than the normal breakdown strength of water of $\sim 10^9$V/m[3.9]. Even allowing for field enhancement effects, it was felt that the performance should be better. Close inspection of the line revealed small air bubbles clinging to the metal surfaces which, it was suspected, could contribute to the low observed breakdown strength. Tilting and vibrating the plates failed to remove the bubbles, but degassing the water quickly solved the problem. This was done by placing the water being circulated through the deioniser under a partial vacuum by constricting the flow close to the pump inlet (figure 3.10). This causes some of the gas dissolved in the water to form into bubbles, which are then pumped along with the water into a settling chamber placed immediately after the pump. Here the bubbles rise to

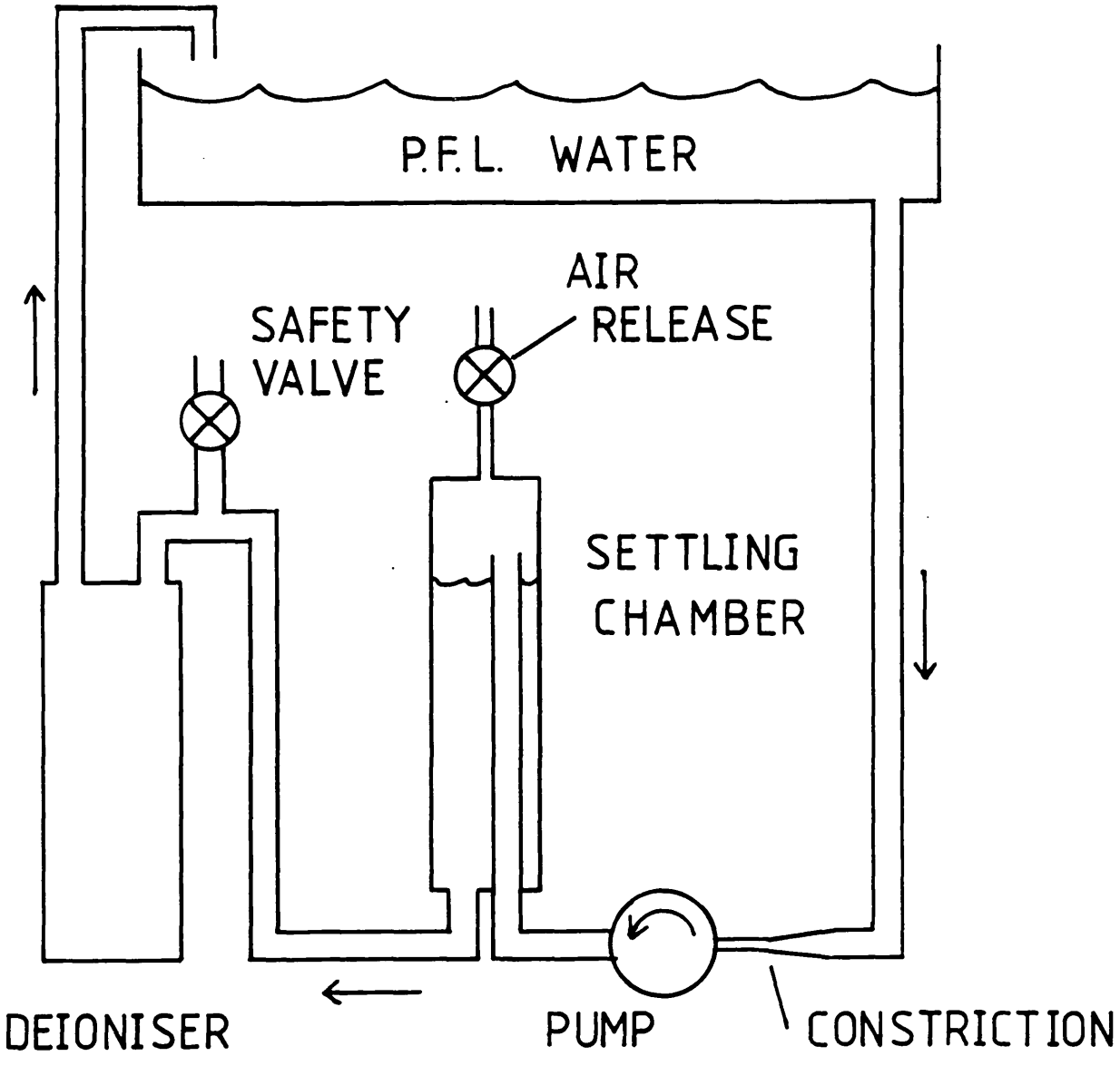

Figure 3.10 Schematic diagram of the P.F.L. water circulation system, showing degassing and deionising phases.

the top, and the degassed water is drawn from the bottom. The gases collected in the settling chamber are forced through the release valve by the excess pressure created by the pump, while gas reabsorption under this pressure is minimised by the high water flow rate and low water surface area. When operated with previously untreated water this system releases ~20 litres of gas in the first hour, falling to ~½ l/h after 24 hours operation.

The degassed water entering the P.F.L. tank absorbs the small bubbles, resulting in their complete disappearance within ~36 hours. With the removal of the bubbles, and by offsetting the edges of the plates much higher breakdown strengths can now be achieved, up to the limit of 4×10^6 V/m set by the charging units.

The initial performance tests voltages were measured using a homemade, ~300X, 50Ω output impedance aluminium chloride resistive divider similar to that used to measure the voltage on the e-beam cathode. While being perfectly adequate for most voltage measurements, the results of measuring the voltage between the discharge electrodes by this method are liable to error, firstly due to the rapidly varying nature of this voltage and the unknown frequency bandwidth of the probe, and secondly due to the very close proximity of very high rates of change of currents ($\frac{dI}{dt} \simeq 10^{12} A\ s^{-1}$) leading to electromagnetic pickup. A novel method of more accurately measuring this particular voltage was developed at a later stage, and will be presented in Chapter 4.

The output current from the P.F.L., as measured through various gases in the laser cavity, was monitored in two ways. The first method uses a Rogowski coil current transformer (EEV type MA459) surrounding part of one of the earth return loops.

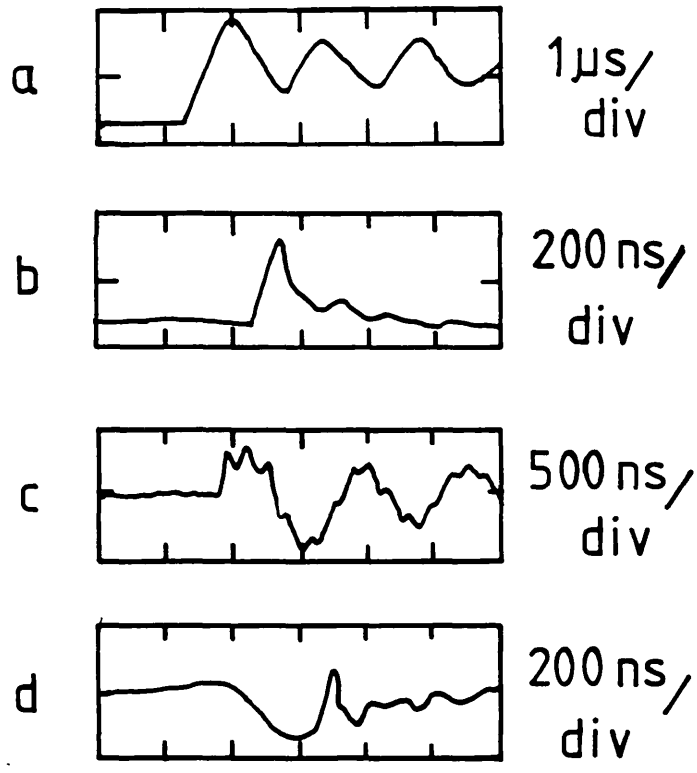

Figure 3.11

a) P.F.L. charging voltage.

b) P.F.L. output voltage across a load of two atmospheres of neon.

c) Discharge current through two atmospheres of neon.

d) P.F.L. output voltage superposed on e-beam cathode voltage showing relative synchronisation between preionisation and discharge voltage.

Although the calibrated output of the current transformer is a measure of only part of the discharge current, its total value may be estimated from the fraction of the earth return loop encircled. To obtain a fully calibrated current waveform a nichrome foil current viewing resistance was included in one of the earth returns; however, the uncertainty introduced by the unknown contact resistances produced results no more accurately calibrated than with the current transformer. Moreover, the susceptibility of the foil shunt to electrical noise led to the Rogowski coil being chosen for all routine current measurements.

Using a P.F.L. of impedance 0.28 Ω, and hence capacitance of 290 nF, the voltage and current waveforms of figure 3.11 were obtained. Figure 3.11a shows the voltage on the P.F.L. when charged from the Marx bank. Under these circumstances the voltage risetime is seen to be $\sim$600 ns, and the peak voltage is over 90% of that predicted by equation 3.29. The rate of decay of the ringing waveform may be used to estimate the resistivity of the P.F.L. water, giving a value of 1.0 $\pm$ 0.2 M Ω cm.

When the P.F.L. is discharged through the rail gap and into two atmospheres of neon in the laser head, the voltage between the discharge electrodes is as shown in figure 3.11b. The peak voltage of 38 kV is reached in about 70 ns from a P.F.L. charged to only 20 kV. Hence the voltage gain is 1.9, very close to the predicted optimum of 2. However, it should be noted that any increase in circuit impedance between P.F.L. and discharge electrodes, such as where the feeds meet the laser head, will also result in voltage gain, but at the expense of reflected energy. The rate of fall of the voltage

after the peak, and the subsequent behaviour, is better recorded using the technique described in the next chapter.

The current waveform, as shown in figure 3.11c, shows a period of oscillation longer than any characteristic time of the P.F.L., indicating that it is largely determined by the inductance of the load. The period of the oscillation is used in Chapter 5 to calculate this inductance, and the results obtained are in good agreement with other observations. The current risetime is very fast ($\sim$50 ns), demonstrating a further advantage of using the short transmission line between the rail gap and laser head - the current risetime being determined by the inductance of the laser head alone, and not including the rail gap.

The synchronisation between the preionisation and the discharge is measured by superposing the discharge voltage waveform (figure 3.11b) and the e-beam cathode voltage waveform (figure 2.9) to produce a composite similar to that in figure 3.11d. The close temporal link between the e-beam cathode voltage and X-ray output observed in the previous chapter allows very accurate positioning of the discharge voltage within the X-ray dose.

CHAPTER 4

INITIAL LASER TESTS

4.1 Discharge Electrode Configuration

The discharge circuit described in Chapter 3, when brought together with the X-ray source of Chapter 2, completes the laser system. This chapter details the initial tests performed on the laser.

The optical cavity employed consisted of an aluminium flat reflector, nominally 100%, mounted as one of the end 'windows' of the laser chamber, as shown in figure 2.10, and an uncoated quartz flat output coupler mounted as the other window. The laser gas mixture used was varied slightly, but generally consisted of ~5 τ HCl, ~40 τ Xe, with argon as buffer gas, similar to the mixture used previously in an e-beam sustained XeCl laser[4.1]. The discharge electrodes consisted of a 110 cm long earthed cathode with a 9 cm wide flat cross section and rounded edges, fabricated from 1 mm thick aluminium, and a contoured, solid brass anode. The anode was smoothly curved to avoid any significant field enhancement, and was, at 90 cm in length, shorter than the cathode. This was to avoid emission from the rather sharp ends of the folded aluminium cathode. This electrode arrangement is shown in figure 4.1a, which is drawn to scale, the numbers indicating the horizontal dimension (in mm) of the relevant component. A ratio 'r' may be defined as the possible surface tracking distance divided by the discharge path length, and may be used as an indicator of the likelihood of tracking. In this case we have:

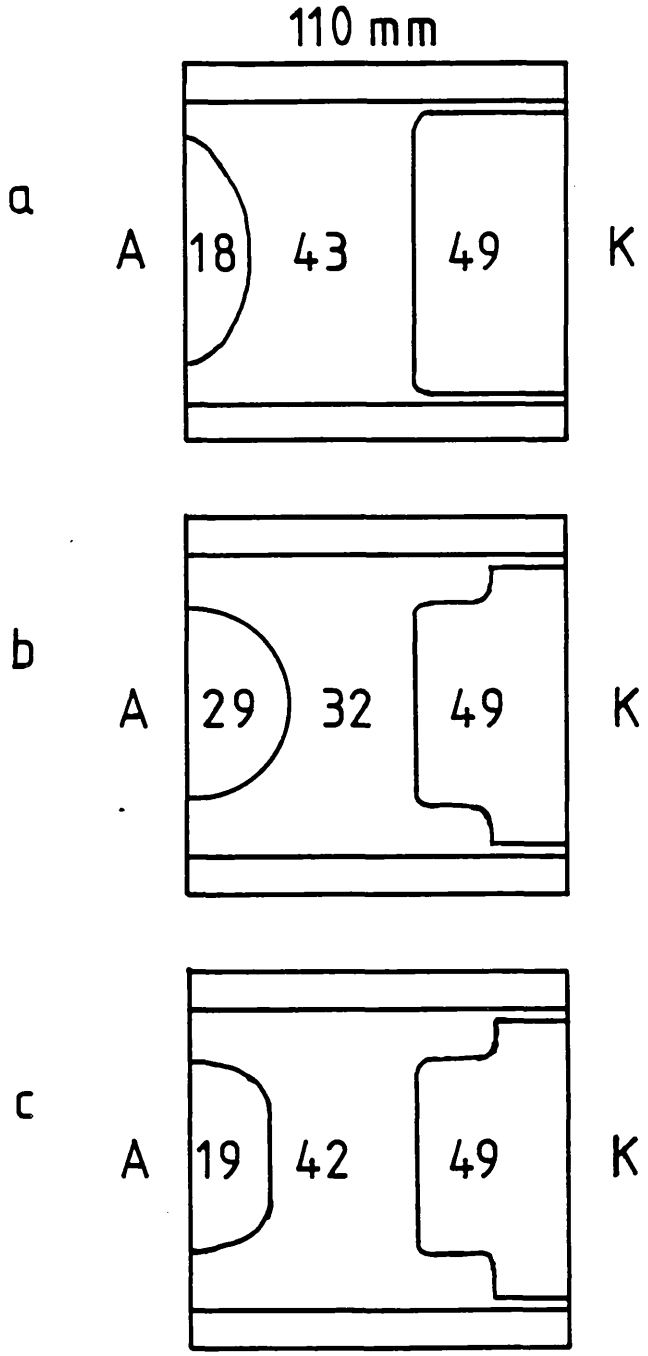

Figure 4.1 Cross-sectional views of discharge electrodes and laser chamber. The anode, A, on the left and the cathode, K, on the right are separated by the P.V.D.F., horizontal, of length 110 mm. All other numbers refer to the horizontal width, in millimetres, of the relevant component.

$$r \equiv \frac{\text{tracking distance}}{\text{discharge gap}} = \frac{110}{43} \simeq 2.6$$

This value of 'r' is similar to that typically found in commercial discharge pumped excimer lasers[4.2], and was thought, therefore, to be sufficiently high to prevent tracking occurring. However, using the argon buffered laser gas mixture, no laser action was obtained from this electrode configuration and dark trails of carbon on the inside surface of the P.V.D.F. laser body indicated that tracking was indeed taking place. Closer inspection of these marks revealed that they did not extend continuously from the anode plate to the cathode mounting plate (from A to K in figure 4.1), but stopped short of the cathode plate, where the discharge cathode closely approached the P.V.D.F. body, suggesting that it was a combination of arcing across the small gap, and tracking along the surface of the P.V.D.F., which was responsible for the lack of laser output. Measuring along this path, the 'effective r' is only

$$r' = \frac{63}{43} \simeq 1.4$$

understandably leading to tracking problems. In order to increase 'r', the discharge cathode was reshaped to the form shown in figure 4.1b; reducing the flat central portion to 7.5 cm, and recessing the point at which the cathode most closely approaches the P.V.D.F. This measure on its own proved to be insufficient to completely eliminate tracking, and so the anode was replaced with a 'half-round' brass bar of radius 29 mm, narrowing the discharge gap to 32 mm, as shown in figure 4.1b. This gives an 'r' of $\sim$3.4, and a minimum

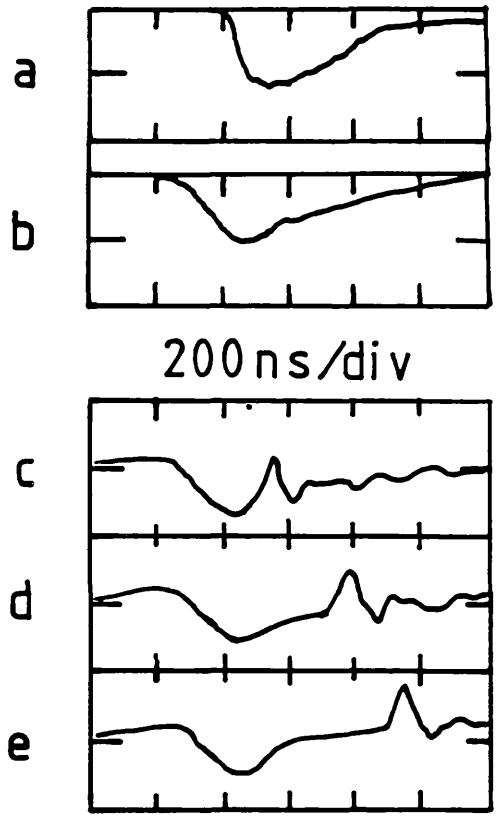

Figure 4.2 Synchronised record of

a) Measured X-ray emission

b) E-beam cathode voltage

c,d,e) E-beam cathode voltage with discharge voltage superposed. c), d) lasing, e) non-lasing.

'effective r' of ~3.0, high enough to preclude tracking.

It was with this electrode configuration using one atmosphere of laser gas driven from the 0.28Ω P.F.L. that laser action was first obtained, giving an output pulse energy of up to 350 mJ. The effect of the X-ray preionisation intensity and synchronisation on the laser output energy was investigated, and is described in the next section.

4.2 Preionisation Dependence

In the preliminary experiments to produce laser action the X-ray preionisation source was operated close to its maximum output with a stored energy of ~78J (25 kV), producing an average X-ray exposure of ~110 mR (see figure 2.7) throughout the discharge volume. Also, the voltage between the discharge electrodes was synchronised to occur close to the peak of the X-ray emission. Figure 4.2a shows the measured X-ray emission with respect to figure 4.2b, the voltage on the e-beam cathode (see Chapter 2). The synchronisation used in the early experiments is displayed in 4.2c, which shows the e-beam cathode voltage (similar to 4.2b) on which is superimposed the voltage appearing between the discharge electrodes, showing that this voltage does indeed appear close to the time of maximum X-ray flux. If the discharge voltage appears at, or before, the start of the X-ray emission, then no laser output is produced. However, delaying the discharge voltage to the position shown in figure 4.2d has no measurable effect on the laser output, although at a position near to that shown in 4.2e the laser output falls rapidly to zero. This shows that a delay of ~400 ns between the peak of the X-ray emission and the discharge voltage is sufficient to prevent laser action using the argon buffered laser gas mixture, and

therefore sets an upper limit on the time for which the preionisation remains active. With the present X-ray source in which the total X-ray exposure is spread over quite a long period of time, ~300 ns, it is difficult to be more precise about the time for which the preionisation is active. In any case, it is for a significantly shorter period than that found by Shields et al[4.3,4.4], where delays of up to 2 μs could be tolerated before laser action ceased. However, these authors have shown[4.4] that this maximum allowable delay is strongly dependent on the voltage between the discharge electrodes. If, before the discharge plasma forms, there is a significant voltage between these electrodes, this will tend to destroy the preionisation both by sweeping the electrons away from the discharge cathode, leaving a region with a very low density of preionisation electrons[4.8], and also by raising the energy of the free electrons and thereby increasing their attachment rate to HCl[4.4]. It is therefore possible that the smaller maximum permissible delay in the present system is due to a larger electrical prepulse before the discharge is initiated. Alternatively, the many modifications and changes of gas mixture in the present system may have an effect. The 2 μs delays tolerated by Shields et al were obtained on a laser system which had been operating under constant conditions for several months. After disassembly a long 're-passivation' period was required before a similar performance could again be attained[4.6]. This may explain the shorter maximum delay found in this, and other[4.11] systems.

Nevertheless, the time 'window' of ~300 ns is ample to allow easy synchronisation between the discharge and X-ray source.

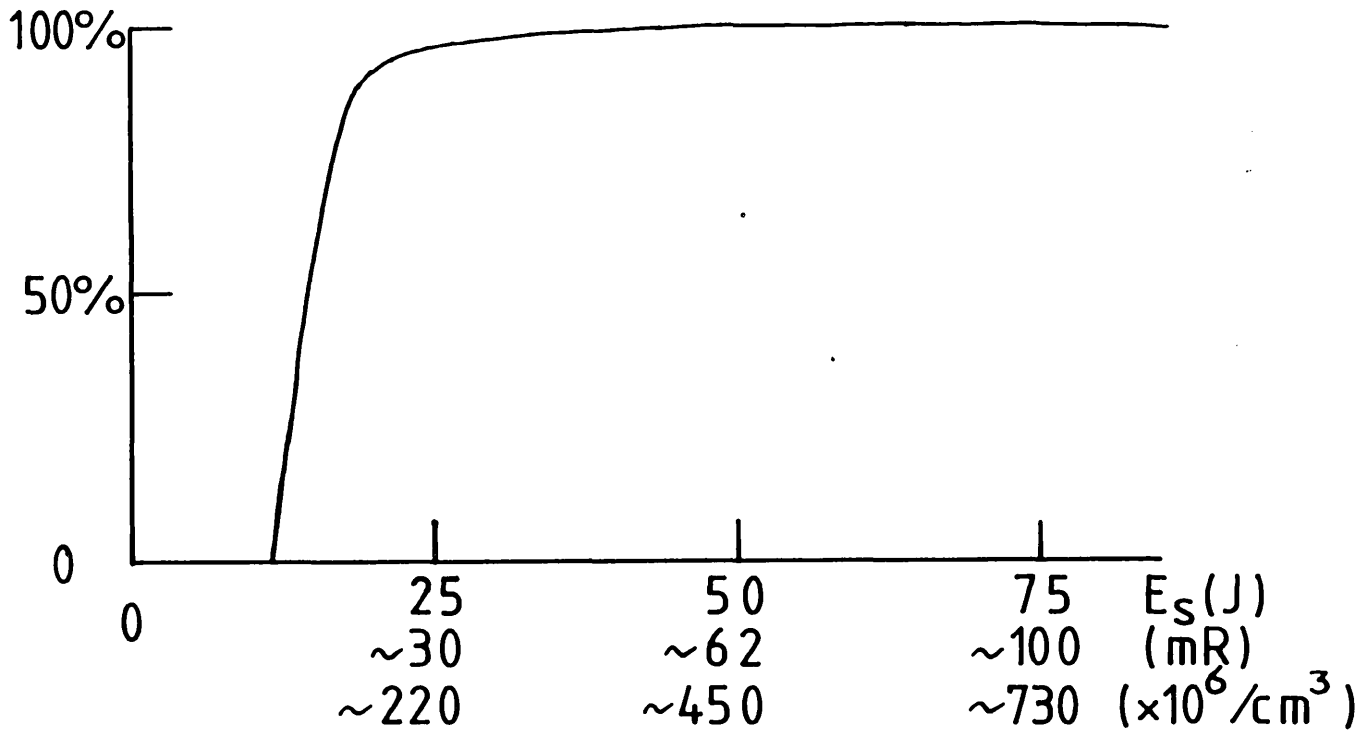

Figure 4.3 Normalised laser output energy as a function of the energy stored in X-ray source. Also shown is the X-ray exposure, taken from figure 2.8, and the calculated preionisation electron number density produced.

Using the 'optimum' synchronisation of figure 4.2c, it is possible to reduce the energy stored in the X-ray generator by a factor of four to $\sim$20J ($\sim$12.5 kV) corresponding to a decrease in X-ray exposure by a factor of over five to $\sim$20 mR before any decline in laser output energy is observed. This is shown in figure 4.3, where the laser output energy is plotted against the energy stored in the X-ray source (and the X-ray exposure obtained from figure 2.7). Also shown is the number of preionisation electrons per cubic centimetre that such an exposure would produce in 3.5 atmospheres of neon[4.7,4.11], the buffer gas used in much of this work. The critical electron density is shown to lie between 100 and 200 x 10^6 electrons/cm^3. This is much higher than the predicted minimum requirement of $\sim 10^4$ electrons/cm^3 [4.8,4.9], but is in general agreement with the experimental value of $\sim 10^8$ electrons/cm^3 found by other workers[4.10]. Any loss of electrons during the duration of the X-ray pulse, or electrons created after the full discharge voltage is applied, or any non-uniformity of the preionisation electron distribution, especially close to the cathode, will result in a higher than theoretically predicted average electron number density being required.

Using the copper, rather than tantalum, foil in the X-ray generator did not produce sufficient X-rays to allow laser action. The results in figure 2.7 show a maximum exposure of around 11 mR, just below the threshold shown on figure 4.3.

In spite of this evidence showing that the amount of preionisation has little effect on the laser performance above a threshold value easily attainable with the present preionisation source, the X-ray generator was still operated close to its

maximum output for most of the experiments to be described in the remainder of this thesis.

4.3 Laser Performance Optimisation

The laser output energy was measured by sampling the output beam using a 1 cm aperture calorimeter (Laser Instrumentation 14/142 L.R.) and then scaling to the full beam size by reference to polaroid burn marks. At this stage of the laser development this technique was not very accurate as the output beam was of poor spatial quality. However, at later stages of development beams of excellent uniformity were produced, as will be described in section 4.4. Sampling of these beams with a larger aperture (1.8 cm) calorimeter (Quantronix 501/504) produced much more reliable results. These were calibrated against the energy measured using a 6 inch aperture GenTec calorimeter* capable of measuring the whole beam, and were found to be in agreement to better than 15%.

Using the argon buffered laser gas mixture, increasing the total gas pressure by increasing the pressure of argon produced gains in output energy for pressures up to 1.3 atmospheres. Above 1.5 atmospheres, however, the laser output declined again. This was due to small parasitic tracking which, while not directly detrimental to laser performance, did release small particles, probably of carbon, into the laser gas, causing it to become cloudy, and hence obscuring and scattering the laser beam. At these gas pressures, the first shot on a particular gas fill would

---

* Thanks are due to Dr. M. Shaw and the Rutherford Appleton Laboratory for the loan of this equipment.

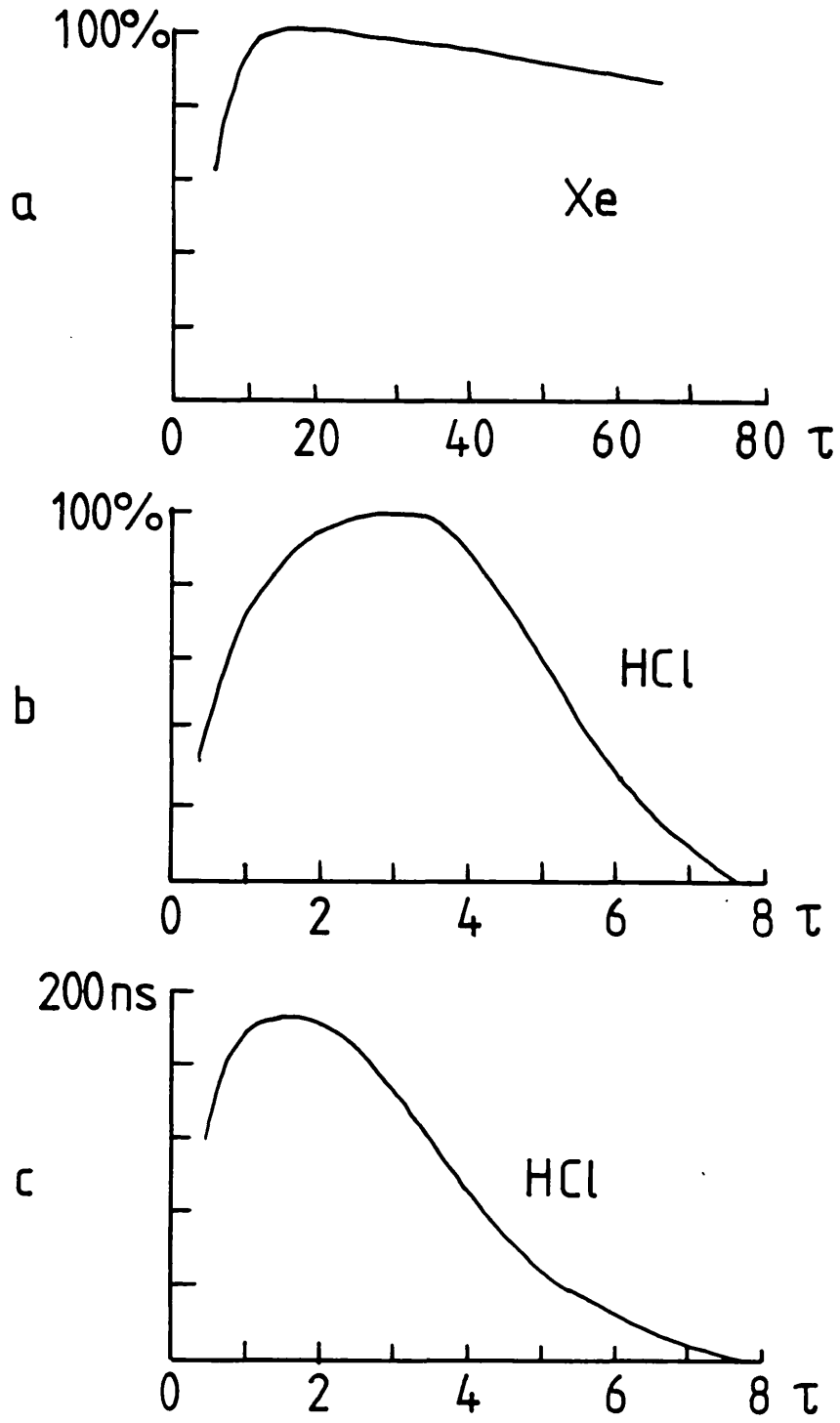

Figure 4.4 a), b) Normalised laser output energy as a function of partial pressure of a) Xenon and b) HCl.
c) Laser output pulse duration as a function of HCl partial pressure for a fixed electrical excitation rate.

produce a significantly (~50%) higher output energy than later shots. Replacing the argon buffer gas with neon removed this problem, there being no signs of any tracking up to the maximum laser chamber pressure of 3.5 atmospheres. At this gas pressure, and using a mixture of 3 τ HCl and 30 τ Xe, the laser produced up to 3.1J in a ~100 ns F.W.H.M. output pulse. However, at these output energy densities visible damage to the uncoated aluminium reflector occurred in a single shot, producing 'pin-prick' holes in the aluminium which would grow in size on subsequent shots. Coating the aluminium with a layer of MgF_2 improved the lifetime to a few tens of shots, and such reflectors were used until a large (3") multilayer dielectric reflector (> 97% at 308 nm, Technical Optics) was obtained.

Introducing some argon into the neon buffer gas produced a slight (< 15%) decline in laser output energy for partial pressures of argon less than one atmosphere in the total pressure of 3.5 atmospheres. However, for argon partial pressures above 1.2 atmospheres there was a rapid decline in laser output. Replacing the neon with helium buffer gas, laser output was again obtained for gas pressures up to 3.5 atmospheres with no sign of electrical tracking. However, the laser output duration tended to be some 20-30 ns shorter, and the output energy only two thirds of that produced using neon. This is in agreement with the results obtained by other workers[4.12,4.13].

A series of experiments where the partial pressures of the constituent gases in a neon buffered gas mixture of 3.5 atmospheres total pressure were carried out, and the results are represented in figure 4.4. There was no observed coupling

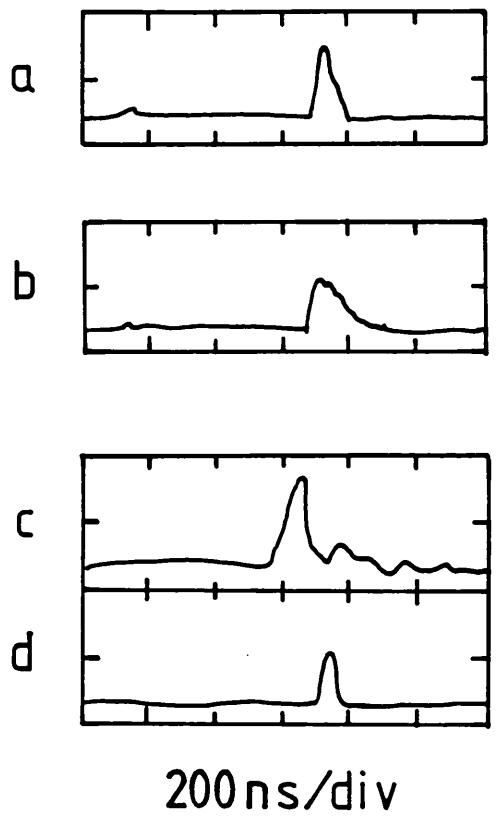

Figure 4.5 Laser output from a gas mixture containing, a) 3 τ of HCl and b) 2 τ of HCl. d) Laser output synchronised with, c) voltage appearing between discharge electrodes.

between the concentrations of the various gases, the same concentration of HCl, for example, being optimum for all partial pressures of xenon, and vice versa. Furthermore, the curves of figure 4.4a and b are insensitive to the electrical excitation rate, although that in figure 4.4c is not.

Figure 4.4a shows the normalised laser output energy as a function of partial pressure of xenon, showing a rapid fall in energy for pressures less than 10τ, but only a very slow decline for pressures much higher than this. In contrast, the laser output energy is strongly dependent on the partial pressure of HCl (figure 4.4b), the range to 50% output energy being only $\sim 5\tau$, and the laser output falling to zero for a pressure of $\sim 8\tau$. From curves 4.4a and b an 'optimum' laser gas mixture of 3τ HCl and 15τ Xe was chosen, and this was used in many of the remaining experiments described in this work.

The temporal pulse shape of the laser output was measured using a vacuum photodiode (I.T.L. T.F.I. 850 U.V.) with wire gauze attenuators where necessary, and was found to be strongly dependent on the partial pressure of HCl. In particular, the pulse duration was noticeably affected, and figure 4.4c shows the base width of the output pulse as a function of the partial pressure of HCl for a fixed electrical excitation rate. Figure 4.4c is, unlike figures 4.4a and b, quite strongly dependent on electrical excitation rate, as will be described in section 4.5 and Chapter 6. It can be seen that in moving from a mixture containing 3τ of HCl to one containing 2τ, the pulse energy will decline very slightly, while the pulse duration increases by $\sim$50%, implying a lower peak power. This effect is demonstrated in figure 4.5, where 4.5a shows the laser output from a gas mixture with 3τ of HCl, and 4.5b the output

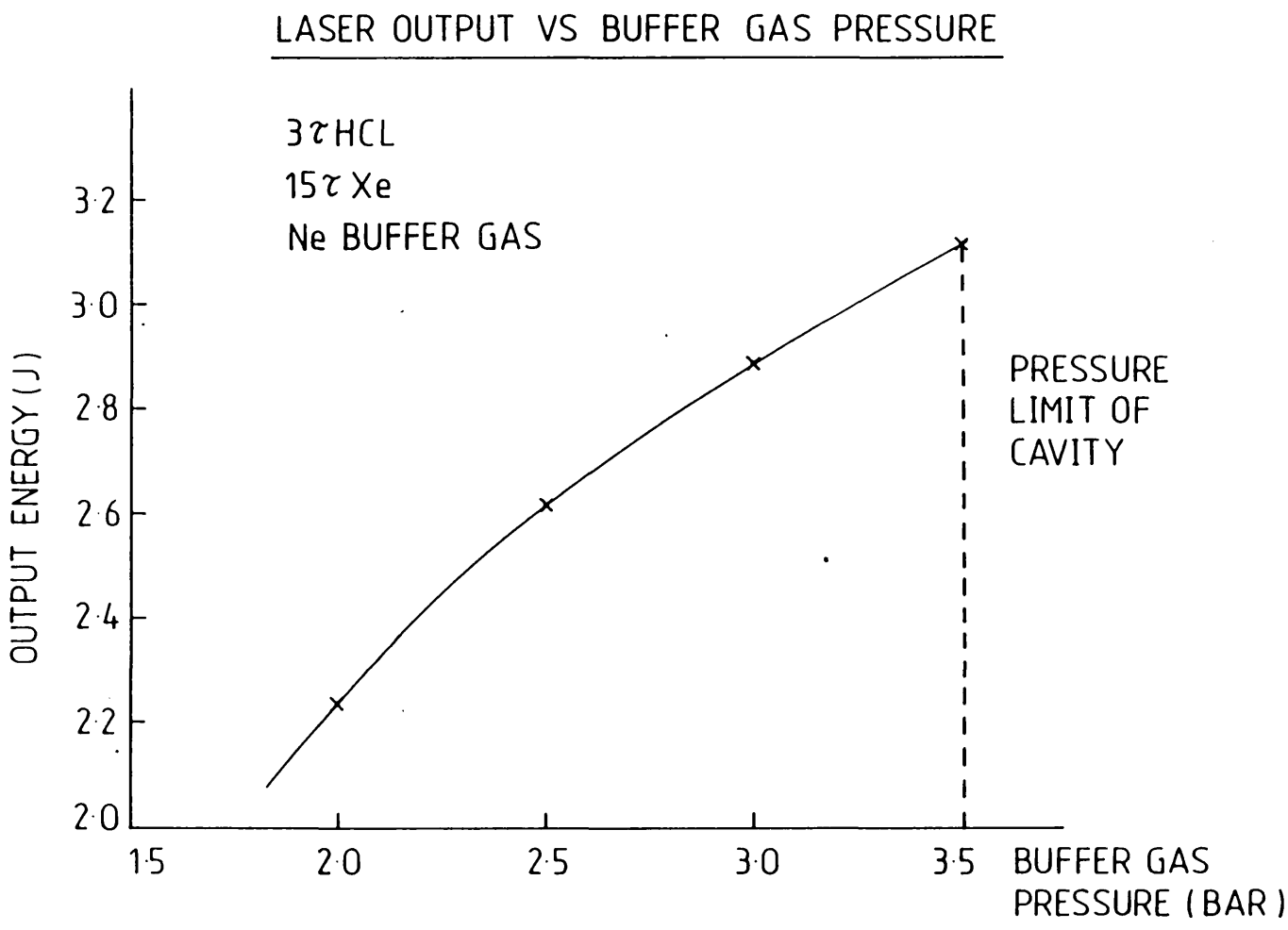

Figure 4.6 Laser output energy as a function of total laser gas pressure for constant electrical excitation.

from a 2 τ mixture. As can be seen, the peak power in the latter case is lower, and the pulse duration longer, mainly due to a more slowly decaying tail.

Figure 4.5d shows the laser output synchronised with the voltage appearing between the laser discharge electrodes, 4.5c. The delay of $\sim$40 ns between the discharge formation, as indicated by the voltage collapse, and the start of the laser output, is explained by the very low 'Q' optical cavity of 1.6m length with only an 8% reflectivity output coupler. Using this cavity, and a gas mixture containing 3 τ of HCl and 15 τ of Xe, the laser output energy was plotted as a function of the neon buffer gas pressure, again under conditions of constant stored electrical energy. The results are shown in figure 4.6 for a stored energy of 225J (30 kV) on the Marx. The monotonic increase in output with total pressure continues up to the maximum pressure limit of the laser chamber of 3.5 atmospheres, indicating that higher energies would be possible at higher pressures. Indeed, Lin et al[4.12] have shown that this increase continues up to and beyond a pressure of five atmospheres.

In order to increase the maximum output energy above the $\sim$ 3.1J shown in figure 4.6, the active volume of the laser was increased. This was done by machining a 3 cm wide flat section on the brass anode, and blending the edges of this section into the original 'half-round' profile of the electrode. This electrode arrangement, which is shown in figure 4.1c, has an 'r' value of 110/42 $\simeq$ 2.6 and defines an active volume of 90 x 4.2 x 3.0 = 1130 cm^3. From this volume, using the now standard laser gas mixture of 3 τ HCl, 15 τ Xe and 3.5 atmospheres of neon buffer gas (and a recently coated aluminium

reflector) a pulse energy of 4.7 Joules was obtained from a stored energy of 270J (33 kV) in the Marx. At the time this was the largest pulse energy which had been produced from an avalance discharge pumped excimer laser, although an increase of more than an order of magnitude has since taken place[4.14]. The electrical efficiency of the production of the 100 ns F.W.H.M. pulse was, neglecting the energy stored in the X-ray generator, 1.7%, a very respectable figure, significantly higher than that typical of other discharge pumped excimer lasers of the time.

4.4 Beam Quality

The beam quality was assessed in two ways. Routinely, a burn mark on blackened polaroid film was used, this method being adequate to reveal many features. At low electrical excitation rates, the laser beam first appears close to the anode, producing a faint burn of $\sim$ 1 cm diameter. Increasing the electrical excitation expands the output beam until, at an output energy of $\sim$0.7J, it completely fills the inter-electrode gap, measuring 4.2 x $\sim$2.8 cm^2. At this point there is still some structure evident within the beam, but further increasing the electrical excitation rate reduces this and expands the beam in the direction parallel to the discharge electrode surfaces, producing a beam of 4.2 x 3.3 cm^2, with very little structure at output energy levels of over 1.5J. However, polaroid burn marks are subject to 'saturation' once all of the black surface has been removed, and are therefore liable to indicate a smoother beam profile than is actually the case. As a check of the beam quality, the mark produced on thermal paper was also used. This again had to be interpreted with

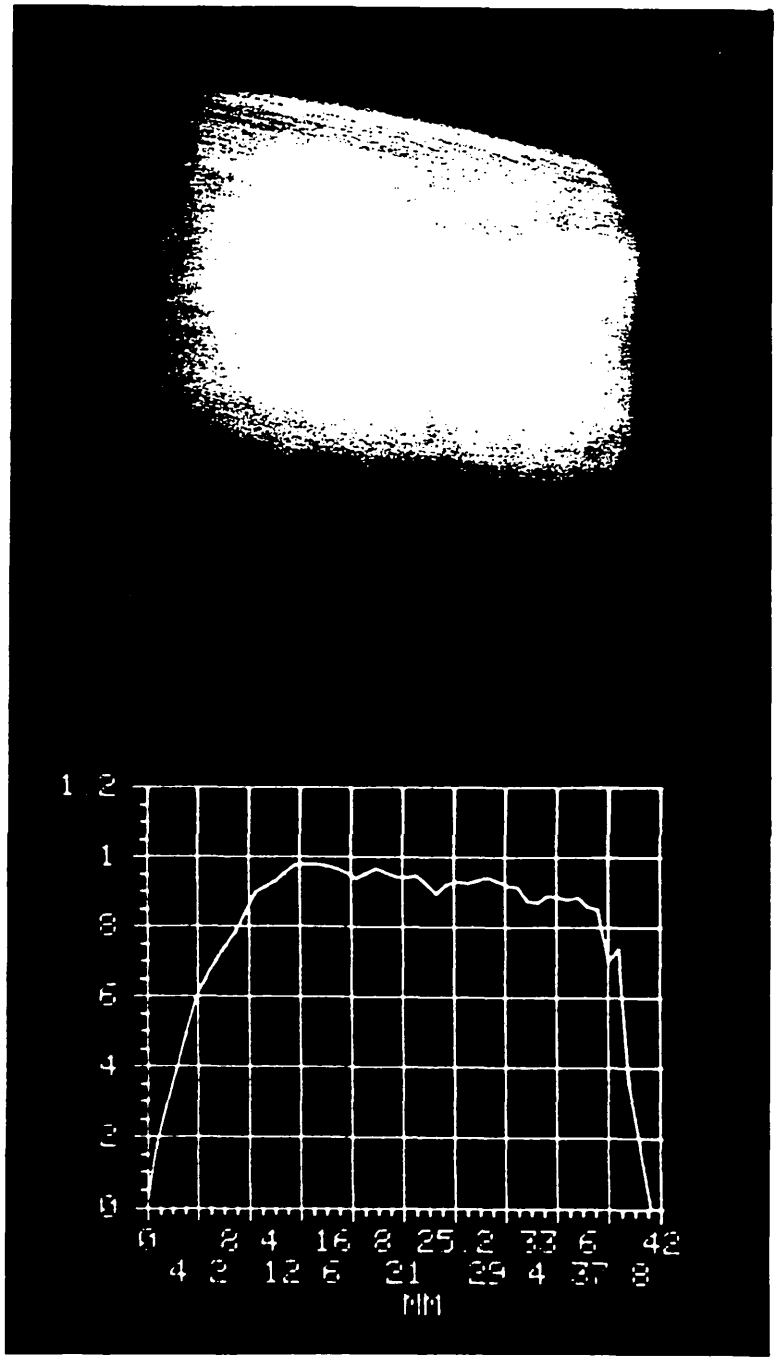

Figure 4.7 Polaroid burn mark, top, at laser output energy of 2.7J. Normalised horizontal intensity profile of beam.

care, saturation of the paper once more being possible, although intense features appear as a black burn on the otherwise blue image of the beam. Used in conjunction, the polaroid and thermal paper burn marks could give a reliable, and very rapid, indication of the quality of the output beam across its entire cross section.

However, as a more quantitative measure of the beam profile, which is not subject to the 'saturation' problems of the previous techniques, a small aperture photo-detector was scanned across the beam. This consisted of an I.T.L. vacuum photodoide with its aperture stopped down to 200 μm, using a mounted pin-hole. This was scanned across the beam in steps of 500 μm at a distance of 40 cm from the output coupler, and the peak height of the detected signal was recorded and stored on a floppy disk using a Tektronix 7912 A.D. digitiser and P.D.P. 11 minicomputer. The results were taken with the laser electrical excitation rate such that the total output energy was 2.7J, and three readings were taken at each point. The results are shown in figure 4.7, which shows a polaroid burn mark at the top, with the scanned beam profile drawn, to scale, underneath. The standard deviation of the three intensity readings at each point was $\sim$3%, comparable to the size of the structure recorded over the central region. The readings were taken in a random order to eliminate systematic errors due to any slow drift in laser output energy, and indeed the results show that the output energy remained constant to better than 3% over the 250 pulses required to acquire this data. Being a 'single-shot' prototype system, this represents the largest number of successive shots under identical operating conditions that have been recorded, and indicates that the laser gas lifetime and system reliability are at least adequate for the present system.

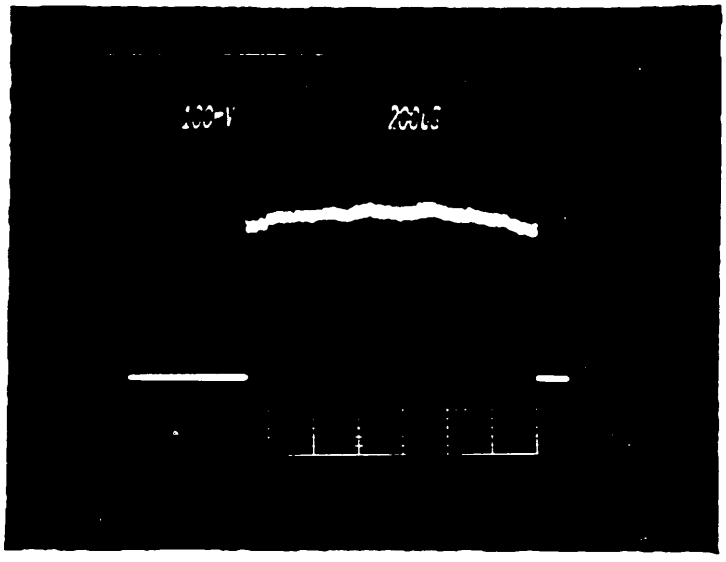

Figure 4.8 A 1" sample of far field laser output. The two lines result from the two interlocking arrays of photodiodes.

In figure 4.7 the discharge cathode is on the left, and the anode on the right. As can be seen from the beam profile, the central region is quite flat with little structure, although it is slightly 'tilted'. At the anode, the intensity drops quite sharply to zero, but near the cathode the decline is more gradual, being spread over almost one centimetre. The same effect can be seen on the burn mark where the anode edge is well defined (and clipped by the optics at the top right) while that at the cathode is more diffuse. Also near the cathode there is horizontal structure running towards the other electrode. This is similar to the structure which can also be observed in other avalanche discharge pumped excimer lasers, for example the Lumonics TE861M4 in an adjacent laboratory, and is probably caused by filamentation of the discharge within this region. This can be caused by the depletion of preionisation electrons near to the cathode when the discharge voltage is first applied[4.8], and has a strong link with the overall discharge stability, as will be further demonstrated and discussed in Chapter 6.

The far field beam profile was monitored using a diode array (Reticon) placed some 10m from the output coupler. At this point the beam had expanded to around 8 cm in the horizontal dimension which, from an original size of 4.2 cm, indicates a beam divergence of $\sim$3 mrad, comparable to commercial systems. Figure 4.8 shows the central 1" of the beam as measured with the Reticon, the two horizontal lines are a result of the electrical offset between the two arrays of 512 photodiodes in the Reticon. As expected, the beam is fairly flat in profile with little structure, and declining in intensity towards the edges of the sample.

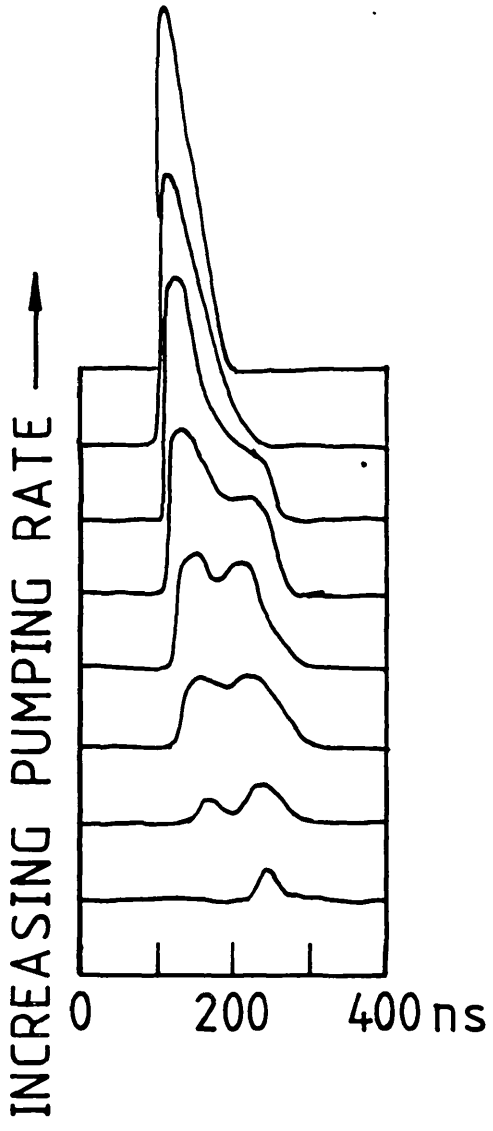

Figure 4.9 Evolution of the laser output pulse shape as the electrical excitation rate is increased.

4.5 Temporal Output

As mentioned in section 4.3, the laser output pulse duration is dependent, not only on the concentration of HCl in the laser gas mixture, but also on the electrical excitation rate. Obviously at very low excitation rates the laser does not reach threshold, there is no laser output and hence the output pulse duration is effectively zero. Increasing the excitation rate above threshold produces a relatively short output pulse, generally occurring late in the discharge. As the excitation rate is further increased the pulse shape evolves, as shown in figure 4.9, the leading edge moving forward initially, and then the trailing edge moving forward also. The increase in laser gain as the excitation rate is increased explains the increase in the amplitude of the pulse, and the decrease in the delay to the onset of laser action, but the forward movement of the falling edge, or the suppression of laser output at later times cannot be explained so easily. The reader is referred to Chapter 6 of this work for an investigation of the effect. However, at all moderate electrical excitation rates the laser output duration is $\sim$140 ns F.W.H.M., comparable to the electrical length of the P.F.L.

The optical gain of the laser was investigated using the single pass/double pass amplified spontaneous emission (A.S.E.) method[4.15,4.16], where the small signal gain, α, can be obtained from the peak single pass A.S.E. power, S_1, and double pass, S_2, by means of the formula

$$\alpha = \frac{1}{l} \ln \left[\frac{(p+1)p}{(d+1)d} \cdot \frac{(S_2/S_1) - 1}{R} \right]$$

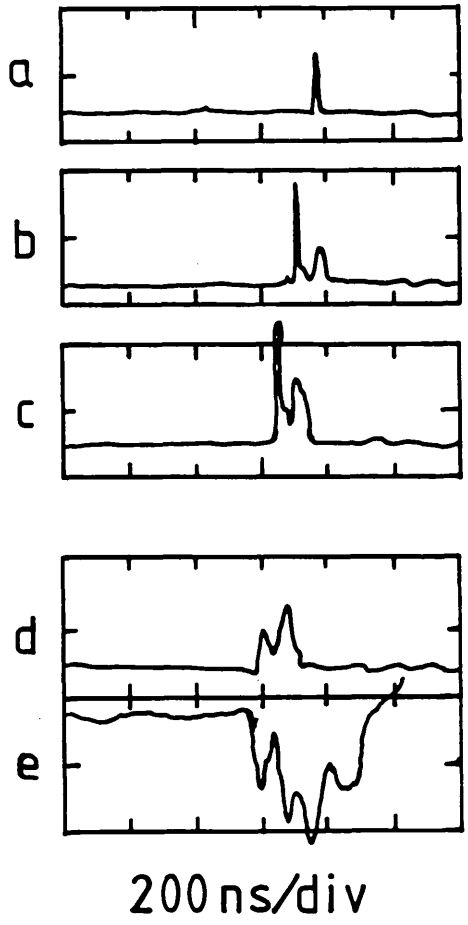

Figure 4.10. a), b), c). Single pass A.S.E. signal as laser discharge current is increased. Laser discharge current, e), shown synchronised with typical single pass A.S.E. signal, d).

where 'l' is the gain length, 'd' is the distance to the detector, 'p' is equal to the sum of l, d and twice the distance from the gain medium to the reflector, and 'R' is the reflectivity of that reflector (see Appendix IV). The single pass signal S_1 was obtained by removing the reflector and misaligning the end windows so that there was no feedback into the gain medium. The double pass signal was then obtained by replacing the reflector so that the maximum possible transit of the gain medium was two complete passes, one in each direction.

The small signal gain of the laser was expected to be high, comparable to the 12%/cm found by Taylor et al[4.17] using a frequency doubled dye laser probe beam. If the gain were to be as high as this, then, on a double pass, we would have

$$e^{\alpha l} = e^{0.12 \times 2 \times 90} > e^{21}$$

indicating that gain saturation would occur. To try and avoid this the measurements were made with the laser being excited from the 0.13Ω impedance P.F.L., where the output energies, and presumably gain, were lower than in the case of the frequently used 0.28Ω P.F.L. Using the 0.13Ω P.F.L., the current through the laser discharge is as shown in figure 4.10e, and 4.10d shows the synchronous single pass A.S.E. measured with this excitation. As can be seen, the peaks in the gain correspond closely to the peaks in the current. On first reaching laser threshold, only the second of these two peaks occurs (4.10a), the magnitude of the current being greater at this time. Increasing the electrical excitation rate, and hence the overall

magnitude of the current, leads to another pulse appearing at a time corresponding to the smaller, first current peak. However, further increasing the excitation rate causes this earlier A.S.E. peak to grow at the expense of the later peak, 4.10 b,c. Very similar behaviour to this is obtained in Chapter 6, where an explanation of the effect, based on the results of a series of experiments, is given.

Therefore it can be concluded that it is the temporal peaks in the discharge current, leading to similar peaks in the laser gain, that give rise to the 'double pulse' nature of the laser output observed in figure 4.9.

The value of the small signal gain obtained from the single pass/double pass A.S.E. results varied from 6%/cm at low electrical excitation rates to as low as 3%/cm at higher excitation rates. This shows that there certainly is gain saturation at the higher excitation rates. Furthermore, the relatively low value of the gain at low electrical excitation rates indicates that saturation is taking place here also. Attempts to measure the small signal gain by partitioning off a shorter length of gain medium have proved difficult due to the electrical problems associated with inserting a 'beam-block' between the discharge electrodes.

Further efforts to measure reliably the small signal gain have not been undertaken, partly due to the practical difficulties involved, but mainly due to the fact that the laser discharge was suspected to be inhomogenous, and, therefore, likely to produce a spatially non-uniform gain. Hence, any gross measurement would lead to only an average value, which would be of limited usefulness.

a

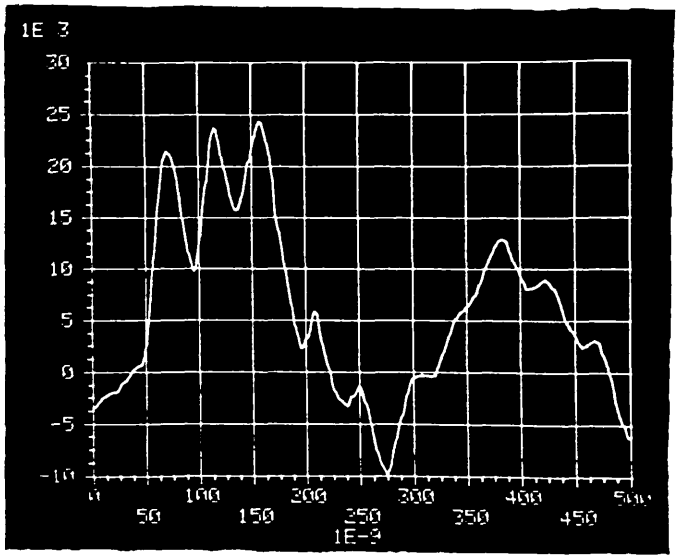

b

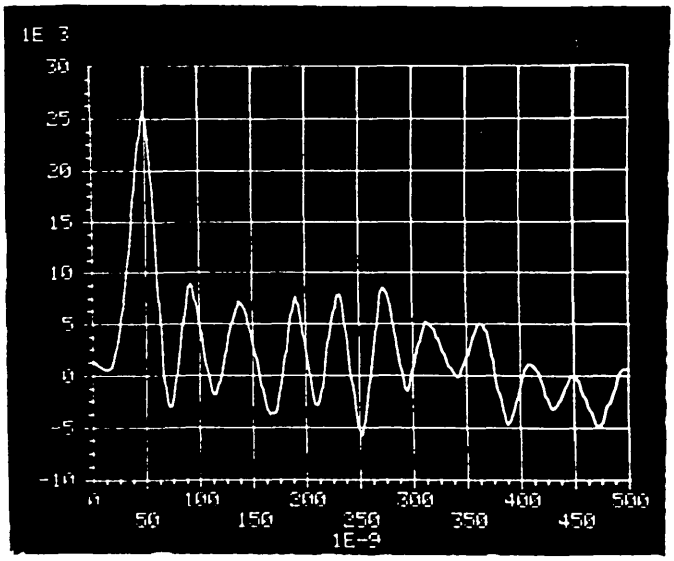

Figure 4.11 a) Discharge current

b) Discharge voltage

4.6 Current and Voltage Measurements

As mentioned towards the end of Chapter 3, the discharge current was measured using both a Rogowski coil current transformer (EEV type MA459) around part of one of the earth return plates, and a low resistance foil (0.2Ω) current viewing resistor in one of the earth returns. The results obtained were qualitatively similar, although both suffered from a degree of calibration uncertainty, the Rogowski coil due to the fact that only part of the total current was passed through it, and the foil resistance due to the uncertainty in its absolute resistance value. Therefore, the calibration of the current displayed in figure 4.11a could be in error by up to 25%, although the waveform is quite accurate. The bandwidth of the detection system is ~100 MHz, and so risetimes of less than ~5 ns will be distorted, but current risetimes as short as this are unlikely due to the inductance of the laser head. As can be seen, the current pulse is of some 300 ns duration, and there is significant ringing after this time. This indicates both a mismatch between the impedances of discharge plasma and P.F.L., and a significant inductive component to the load. This topic, together with the variations in current waveform with other circuit and laser parameters, will be dealt with in the next chapter.

While the measurement of current using both the Rogowski coil and viewing resistor were considered reliable, the measurement of discharge voltage using the resistive divider was thought less secure. The resistive divider consists of nominal 15 kΩ and 50Ω resistances in series fabricated from plastic tubing with ammonium chloride solution as the conducting medium. The 50Ω output is made by supporting a stainless steel disc, with a hole in the centre, some ~8 mm above a flat

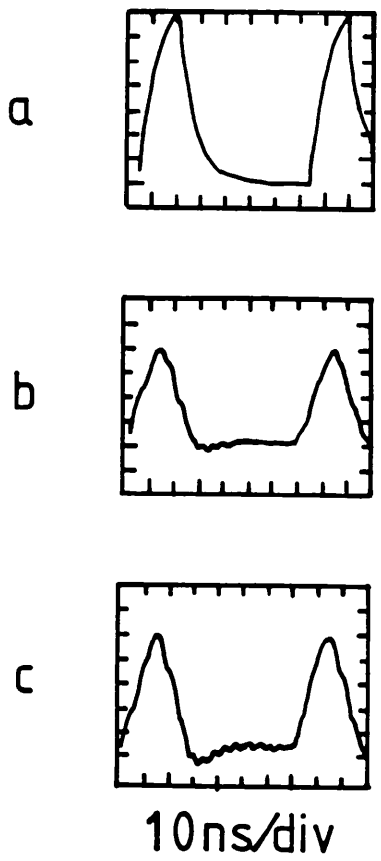

Figure 4.12 a) Voltage from pulse generator, b) as measured through Tektronix P6015 probe, c) as measured through 'home-made' probe.

stainless steel earth plate, using perspex spacers. In order to prevent surface electrical breakdown when measuring high peak voltages, the physical length of the probe from high voltage connector to earth plate, is 35 cm. The inductance inherent in this relatively long length led to fears of a slow risetime, so as a test the probe was compared with a commercial probe and used to measure voltage risetimes comparable to those in the laser produced by a signal generator. Figure 4.12a shows the output of the signal generator as displayed on a Tektronix 7904 oscilloscope (bandwidth 1 GHz), having voltage rise and fall times of ~10 ns. Figure 4.12b shows the same voltage as measured through a Tektronix P6015 X1000 100 MΩ probe of bandwidth 75 MHz. As can be seen, the waveform is clearly distorted, and there is overshoot and ringing on the falling edge. The 'home made' 50Ω X300 probe gives a similar result to the P6015, producing slightly more overshoot and ringing. It is therefore to be concluded that the home made probe has a bandwidth comparable to the 75 MHz of the P6015, and that voltage rise and fall times of less than ~20 ns will not be recorded accurately. With this in mind, both the P6015 and the home made probes were used to measure the voltage between the discharge electrodes of the laser.

The high impedance Tektronix probe, together with the 1MΩ input impedance oscilloscope required, proved to be very susceptible to electromagnetic noise. This was in the form of short spikes (< 5ns) of sufficient amplitude (> 100V) to strongly suggest that its use should be discontinued in the interests of preserving the oscilloscope plug-in amplifier.

The much lower impedance home-made probe and 50Ω oscilloscope is much less susceptible to electrical noise. However, the measured voltage between the discharge electrodes

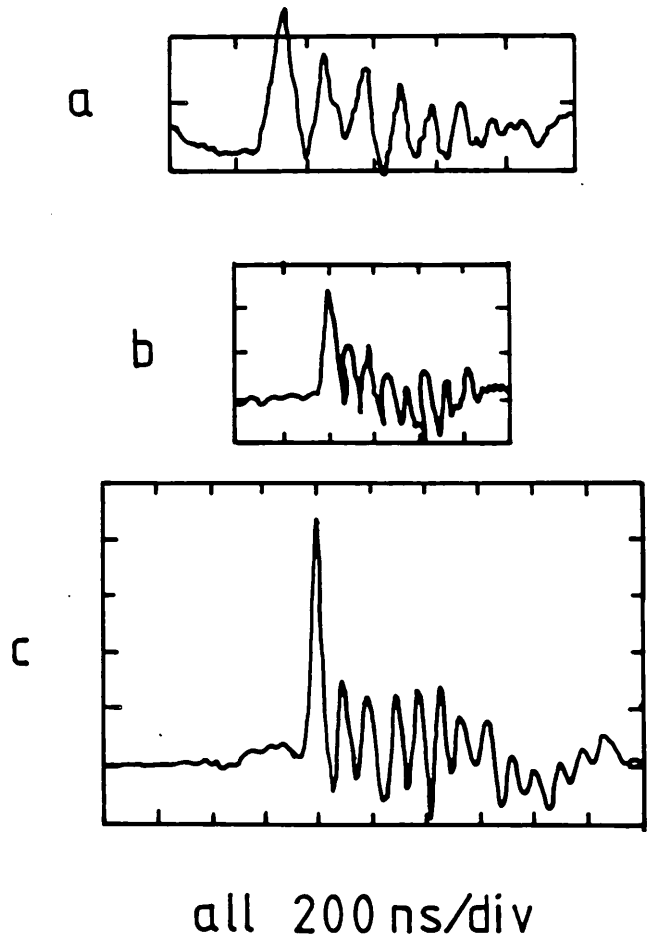

Figure 4.13 Voltage between discharge electrodes as measured with 'home-made' voltage probe and displayed on a) Tektronix 519 oscilloscope, b) Tektronix 7834 storage oscilloscope, c) Tektronix 7912 A.D. digitiser.

when using a normal laser gas mixture was not of the expected form. Figure 4.13a shows the measured voltage as recorded on a Tektronix 519 oscilloscope. As can be seen, after the initial voltage collapse occurring as the discharge plasma is initiated, the voltage is of an oscillatory nature. This is in contrast to the expected behaviour in which the voltage should attain a steady value, corresponding to a stable discharge, for the duration of the pulse from the P.F.L. The same waveform recorded on a Tektronix 7834 storage oscilloscope, is shown in figure 4.13b, giving a voltage waveform which is even more strongly modulated, and in some sections appears to suffer from 'time-reversal'. This effect of time running from right to left has occasionally been observed when using the 519, but never to the extent shown in figure 4.13b. The greater susceptibility of the 7834 to electrical noise is undoubtedly due to the solid state, low voltage, high gain plug-in amplifier used as opposed to the 519's medium voltage ($\sim$ 20V) direct access to the cathode ray deflection plates. Also, the higher voltages and better screening of the valve based time-base of the 519 is better suited to noisy electrical environments than the solid state, 7834 version. The voltage waveform of figure 4.13c is that recorded on a Tektronix 7912 A.D. digitiser in an adjacent laboratory. The signal was transferred between laboratories at a level of about 100V using low loss, high voltage, coaxial cable (U.R.M 67) shielded with copper tubing. This shielding, together with the greater distance between recording instrument and any sources of electrical interference, leads to a smooth recorded signal containing no obvious electrical noise.

However, even though the waveforms of figure 4.13a,c appear to be substantially free of 'noise', they do not show the

expected voltage behaviour. This is due to the inductance of the voltage measuring loop. When there is a rapid change in current in the electrical circuit, such as when the rail gap switches, or when the laser gas breaks down, giving rates of change of current of $dI/dt \simeq 10^{12} A\ s^{-1}$, a spurious voltage, V_L, will be induced in the voltage measuring loop given by

$$V_L = L_m \frac{dI}{dt}$$

where L_m is the mutual inductance between the voltage measuring loop and the circuit where the change of current occurs. This induced voltage will appear together with that produced by the resistive divider, and gives rise, for example, to the negative excursion of the measured voltage immediately after the initial voltage fall in figures 4.13a and c. Obviously, a reduction in the value of L_m will reduce these effects, but as the mutual inductance is governed by geometrical factors, and as the physical size of the voltage probe is limited by electrical breakdown considerations, there is a limit to how small L_m can be made whilst still maintaining a reasonable peak voltage handling capability.

In theory, the inductive component of the measured voltage may be calculated and removed, but this requires an accurate, synchronised measurement of the currents in all components close to the voltage measuring loop, together with a calculation of the mutual inductance between each part of the circuit and the measuring loop. This is clearly not possible, although the close temporal correspondence between the peaks and troughs of the current waveform (figure 4.11a) and those of the voltage waveform (figure 4.11b) invites a 'handwaving' correction to be made. However, numerical differentiation of the digitised

current waveform using a P.D.P.11 minicomputer, and subtraction of this waveform from the measured voltage proved inadequate to produce a sensible voltage waveform, showing that a single current measurement is not enough and/or that the fidelity of that measurement is not sufficient for the required data processing. This also indicates that the 'handwaving' method is of dubious validity.

Rather than pursue this line of attack further, relying on ever more accurate current measurements and more data processing, a different method of voltage measurement was employed, where the effects of induced voltage are negligible.

4.7 Electro-Optic Voltage Measurements

As described in the previous section, the inductance inherent in any electrically conducting voltage monitor leads to both a limited bandwidth and risetime, and to a susceptibility to electromagnetic pick-up. These problems may be avoided by using an electrically insulating voltage monitor, which can, in principle, be placed directly on the points between which the voltage is to be measured, in this case the discharge electrodes, without the need for any further electrical connections or circuitry. Such an arrangement would have effectively zero inductance and, due to being an insulator, place a negligible load on the discharge circuit.

The electro-optic effect in a non-linear crystal may be used as a non-conducting voltage monitor as an optical output signal can be generated which is dependent on the voltage applied to it. Furthermore, the technology associated with such a voltage monitor has been well tried and tested in optical modulators such as Pockels' cells, where a voltage is applied specifically to affect the transmission of incident light.

Because of this readily available technology, a Pockels' cell arrangement was used in the electro-optic voltage monitor. Although the ideal electrical geometry would use a transverse cell contacting the two electrodes this is ruled out, due to the exposure of the crystal to corrosive gases (HCl) and to its blocking of the excimer laser beam. Therefore the cell was mounted external to the laser chamber on top of the P.V.D.F. laser body, and in electrical contact with the discharge electrode mounting plates. Also, due to the physical size, and hence expense, of a crystal required to give an acceptable half wave voltage when mounted transversely, a longitudinal geometry was chosen. This necessitated some 3 cm of electrical connection from the discharge anode and cathode mounting plates to the Pockels' cell, but allowed the use of a readily available commercial cell.

On applying a voltage V to the electrodes of the longitudinal Pockels' cell, a phase difference, $\Delta\phi$, is introduced between light rays orthogonally polarised at 45° to the crystal axes given by[4.18]

$$\Delta\phi = \frac{2\pi}{\lambda} n_o^3 r_{63} V \qquad (4.1)$$

where λ is the wavelength of the light, n_o is the 'normal' refractive index of the crystal and r_{63} is the relevant component of the electro-optic tensor. This phase difference can be used to change the polarisation state of light originally polarised along one of the crystal axes, and this may be converted into an amplitude modulation by introducing a polariser after the crystal which is crossed with reference to the original input light beam. This gives an intensity transmission of the

form[4.18]

$$I = I_o \sin^2 \left[\frac{\pi}{2} \cdot \frac{V}{V_\pi} \right] \qquad (4.2)$$

where $V_\pi = \lambda / (2n_o^3 r_{63})$

The region of maximum sensitivity (max. dI/dV) of this non-linear response is where $V = V_\pi / 2$. As V_π is of the order of a few kilovolts for many electro-optic crystals, the region of maximum sensitivity may be chosen to lie close to the sustaining voltage of the laser discharge which was predicted to be $\simeq 7$ kV. Therefore an A.D.P. Pockels' cell (Electro Optic Design 12XK), with a measured V_π of approximately 15 kV at HeNe wavelength was used. The breakdown voltage of the Pockels' cell, and hence peak voltage measuring capability, was not known exactly, but was estimated by the manufacturer[4.19] to be >70 kV for pulses of less than 100 ns in duration, and therefore quite capable of handling the initial voltage spike between the discharge electrodes before the laser plasma forms.

The optical system used in the electro-optic voltage monitor consisted of a small, 0.5 mW HeNe laser (Hughes Aircraft Company), fitted with a polaroid polariser, the output beam of which passed through the Pockels' cell and through a second 'crossed' polaroid polariser before being focused into the end of 20m of multimode optical fibre (R.S. Polymer). Light emerging from the fibre was detected using a photomultiplier (R.C.A. 7265), and the signal displayed on either a Tektronix 7834 storage oscilloscope or Tektronix 7912 A.D. digitiser.

The half wave voltage, V_π, of the Pockels' cell, was measured

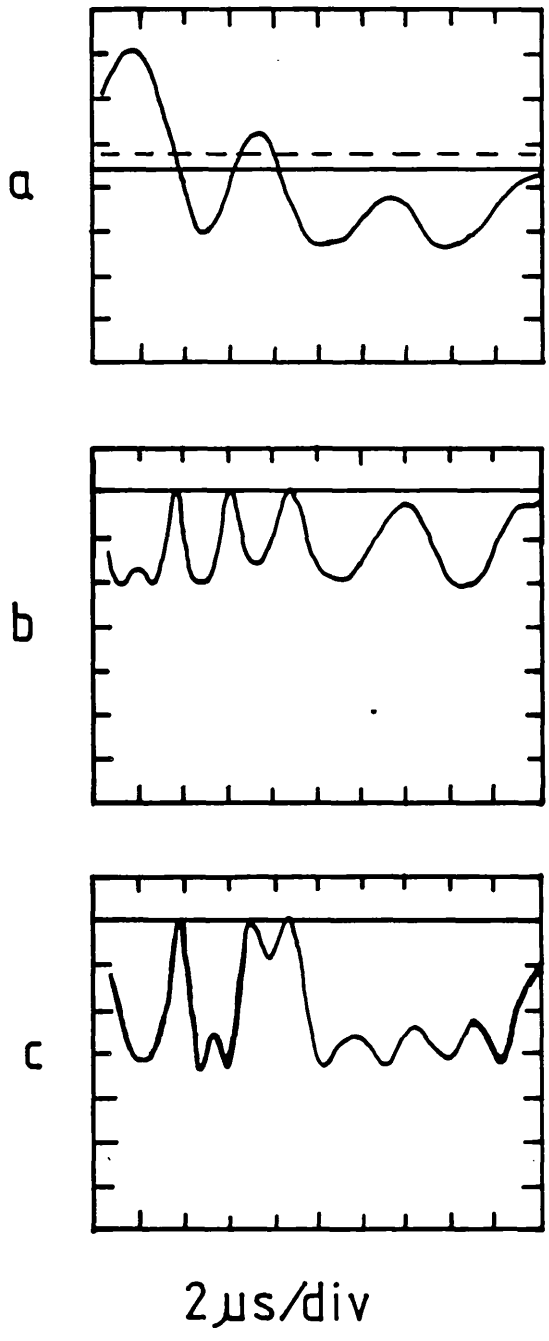

Figure 4.14 a) Voltage from trigger generator, 7 kV/vertical division. b) Signal from Pockels' cell voltage monitor, c) Signal from Pockels' cell voltage monitor with added birefringence.

both with D.C. and pulsed signals. The simpler method, using a constantly applied voltage to the Pockels' cell, indicated a value of V_π = 15.1 ± 0.2 kV. The pulsed half wave voltage was measured using the output voltage of a small signal generator, and this is shown in figure 4.14a, where the vertical scale is approximately 7 kV/div. and zero volts is marked by the solid line. The signal recorded on the Tektronix 7834 storage oscilloscope from the photomultiplier is shown in figure 4.14b, the solid line again representing zero. It can be seen that the signal, which is negative in polarity, falls to zero when the applied voltage is zero. The half wave voltage can be measured from the first voltage peak, which is clearly seen to exceed V_π , causing a 'turn-over' of the output signal. Using this technique, V_π is measured as 14 ± 1 kV, somewhat lower than the D.C. value.

The fact that the transmitted intensity, given by Eqn. 4.2, is not a single valued function of the applied voltage gives rise to a certain ambiguity of interpretation of the recorded signal. The waveform of figure 4.14a cannot be reconstructed purely from the signal recorded in figure 4.14b, as both positive and negative voltage excursions produce output signals of the same polarity. Furthermore, the 'dip' in the first recorded peak corresponding to the voltage rising above V_π could equally well result from a real 'dip' in the voltage at this point.

These ambiguities can be resolved by introducing a small degree of birefringence between the Pockels' cell and polariser. This adds a further phase shift, δ , to that produced by the cell, modifying the system response to

$$I = I_0 \sin^2 \left[\frac{\pi}{2} \cdot \frac{V}{V_\pi} - \delta \right] \qquad (4.3)$$

This provides a zero offset by allowing some light to be transmitted at V=0, but none when $V = 2V_\pi \delta / \pi$. The voltage for which no light is now transmitted is shown dashed in figure 4.14a, and the recorded signal from the photomultiplier in figure 4.14c. This shift of zero has reduced the effective signal from the first positive peak below the new 'half wave' value, and shows it to be smooth, containing no 'dips'. Also, the signals from the negative going voltage peaks have been increased above the new 'half-wave' value, thus giving a clear differentiation between signal peaks occurring from voltages of opposite polarity. The absolute value of the polarity can be inferred if the orientation of the birefringence is known with respect to the 'fast' and 'slow' axes of the Pockels' cell, but for the present application the voltage to be measured is known sufficiently well from previous measurements and theoretical predictions to allow the absolute polarity to be determined by inspection.

In inserting the birefringence, care must be taken to ensure that the phase shift, δ, produced, is small enough for the continuous transmission of light at zero applied voltage to be insufficient to saturate the photomultiplier, otherwise the signal will be strongly modulated by the gain recovery and depletion of this component.

The bandwidth of the voltage monitor is limited by the photomultiplier, which has a specified risetime of 2.7 ns. The response of the detection system as a whole was assessed by injecting an unpolarised, 10 ns F.W.H.M. duration, pulse

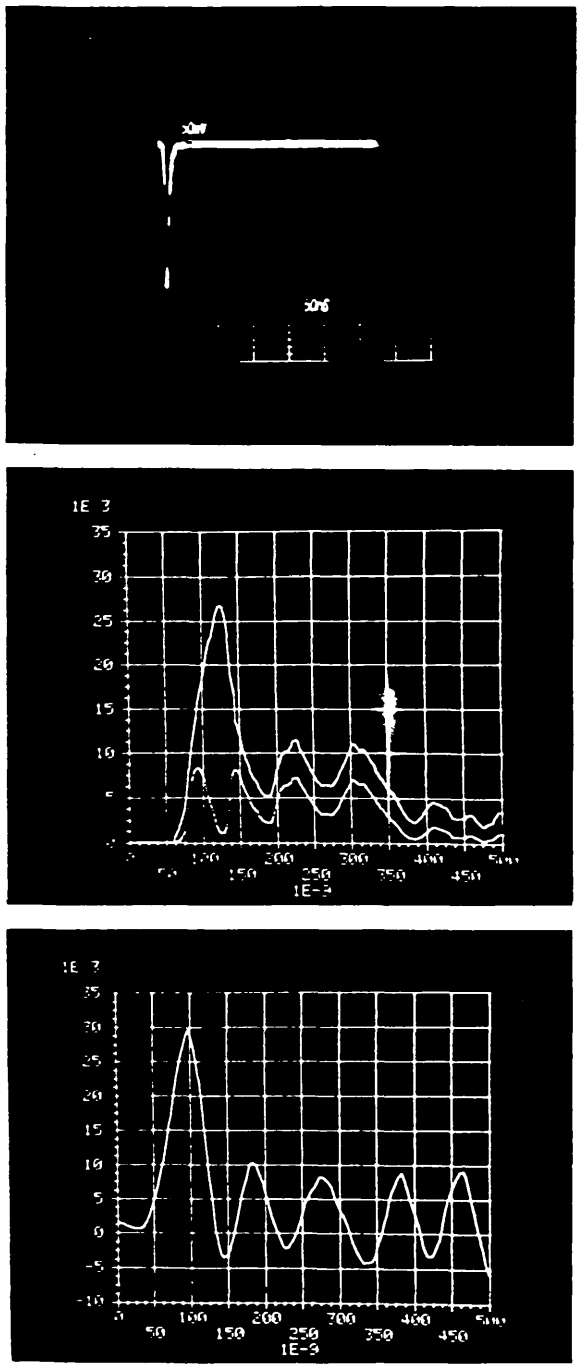

Figure 4.15 a) 10ns pulse from dye laser injected into electro-optic voltage monitor detection system.

b) Signal recorded as electro-optic measurement of voltage between discharge electrodes, lower trace, and numerically reconstructed voltage, upper trace.

c) Voltage as measured with resistive divider.

of light derived from a Nitrogen laser pumped R6G dye laser through the Pockels' cell and into the fibre. The signal recorded by the photomultiplier on the storage oscilloscope or digitiser was not measurably different from that produced using a photodiode (risetime 100 ps) close to the dye laser. This is in agreement with a bandwidth of >100 MHz. The electrical response time of the Pockels' cell is in the region of one nanosecond, and so this should not further limit the bandwidth of the voltage monitor.

The short duration dye laser pulse was also used to check the optical system for reflections as it was suspected that these may occur, particularly from the ends of the fibre. However, as figure 4.15a shows, no reflections were observed. Furthermore, the dye laser pulse was used to assess the magnitude of the signal which could be drawn from the photomultiplier without inducing saturation. It was found that for this 10 ns signal it was necessary to limit the output to <700 mV into 50Ω to maintain pulse fidelity. Therefore, in measuring the rather longer duration signals from the voltage monitor the voltage was kept at the 2-300 mV level.

A typical signal from the electro-optic voltage monitor is shown in the lower trace of figure 4.15b, recorded on the Tektronix 7912 A.D. digitiser. In this trace the initial voltage spike appears as a trough as the voltage is greater than V_{π} . This fact is taken into account in numerically extracting the voltage between the discharge electrodes from the recorded signal, and this voltage is shown as the upper trace of figure 4.15b. This curve shows the voltage plateau, albeit with some modulation, after the initial voltage collapse, unlike the trace recorded using the resistive divider voltage monitor, 4.15c.

Due to the nature of equation 4.2, the voltage waveform extracted from the recorded signal is critically dependent on that signal when V = 0, V_{π}, $2V_{\pi}$, etc. Hence the very slight difference in height of the signal peaks at t ≃ 90 ns, 140 ns, corresponding to V = V_{π} and hence maximum transmission through the Pockels' cell/polariser arrangement, is shown as a noticeable mismatch on the deconvolved voltage trace at t ≃ 140 ns. For this reason, the peak voltage is somewhat in doubt (± 2 kV), but, for reasons which will be described in Chapter 5, it is the value of the voltage after the initial fall which is of most interest, and the form of this voltage is accurately recorded up to t = 350 ns. After this time the recorded signal becomes too small for accurate calculation of the voltage. As described earlier, a small added birefringence was used to check the validity of the assumption that the voltage continues to rise immediately after t = 90 ns. The absolute polarity of the waveform is assumed positive by comparison with figure 4.15c, and by virtue of the polarity of the charged P.F.L.

In operation, electrical noise on the voltage monitor was unmeasurable (<2 mV), reflecting the advantages of using the Pockels' cell as voltage sensor and optical fibre for signal transmission. Optical noise was reduced from a high level to < 5 mV by carefully screening the Pockels' cell, polarisers, lens and fibre end with black card and black cloth. Enclosing the HeNe beam incident on the Pockels' cell in cardboard tube further reduced the noise to a level of approximately one hundredth of the signal level.

In summary, the electro-optic voltage monitor provides reliable measurements of high voltages (<30 kV) with rapid

risetimes (<10 ns) and, due to the optical nature of the output signal, with almost complete independence from electromagnetic noise. The non-linear response may be used to advantage to place the region of maximum sensitivity close to the voltages of interest and, although the output signal requires processing to extract the true value of the voltage, this is a relatively simple operation.

CHAPTER 5

HIGH EFFICIENCY OPERATION

5.1 Introduction

A factor of major concern in the performance of excimer lasers, both large and small, is the efficiency of their operation, defined as the optical output energy as a fraction of the electrical input energy. In large laser systems, such as may be used as laser fusion drivers, where output energies of the order of kilojoules are required, the cost of the electricity supplied becomes significant and greatly influences the economics of the entire process as an energy generation scheme. In smaller, 'table-top' excimer lasers, the electricity bill is not so significant, but a more efficient laser can reduce the capital cost of the discharge circuit and energy storage capacitors by allowing lower rated components to be used. Alternatively, the same electrical components may be operated below their rated values, giving benefits in longevity.

At the time of the design of the present laser system the efficiency of discharge excited excimer lasers was typically below 1%. This is significantly lower than the intrinsic efficiencies expected. Discharge excited lasers should be at least as efficient as e-beam pumped lasers[5.4], where intrinsic efficiencies betwen 5 and 10% are common[5.1,5.2]. The overall, 'wall-plug', efficiency of e-beam pumped lasers is, however, much lower than this due to the inefficiency of the e-beam generation process, foil losses and incomplete or non-uniform absorption of the e-beam in the laser gas. Similarly, the poor efficiency of discharge pumped excimer lasers is due, at least in part, to incomplete deposition of the stored energy

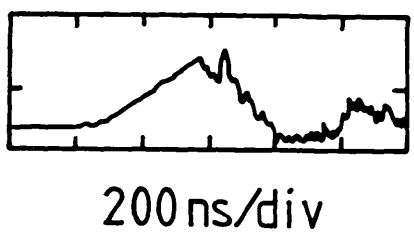

Figure 5.1 The P.F.L. voltage during the charging of the P.F.L. and the laser discharge.

in the laser gas mixture. This is obviously the case in most commercial excimer lasers, where capacative charge transfer circuits are used to provide voltage gain at the expense of 'wasted', reflected energy[5.3]. The fact that such circuits are employed may be traced back to the highly non-linear behaviour of the discharge plasma.

As described in Chapter 3, the laser discharge plasma presents a time varying resistance contained within a necessarily inductive laser chamber. Furthermore, the voltage required to initiate the discharge is much higher than that required to sustain it. Added to these problems is the need to form the discharge plasma quickly before the preionisation electrons are lost or swept away from the discharge cathode. Chapter 3 describes the discharge circuit designed in the present work to overcome these problems, whilst allowing a high efficiency of energy transfer. Using this circuit, the efficiency of energy transfer from the P.F.L. into the laser plasma in a time corresponding to the double electrical transit time of the P.F.L. (2τ) is given by equation 3.25, which is rewritten here as equation 5.1

$$\eta = 1 - \left(\frac{R - Z}{R + Z}\right)^2 \qquad (5.1)$$

where the efficiency, η, is shown to depend on the impedances of the P.F.L., Z, and of the load, R. Clearly, in order to obtain maximum efficiency, the two impedances must be matched. However, while the impedance of the P.F.L., Z, is a parameter which can be adjusted at will, the impedance of the discharge plasma, R, is a function of both the discharge circuit and the impedance of the electrical driving circuit. As R is dependent

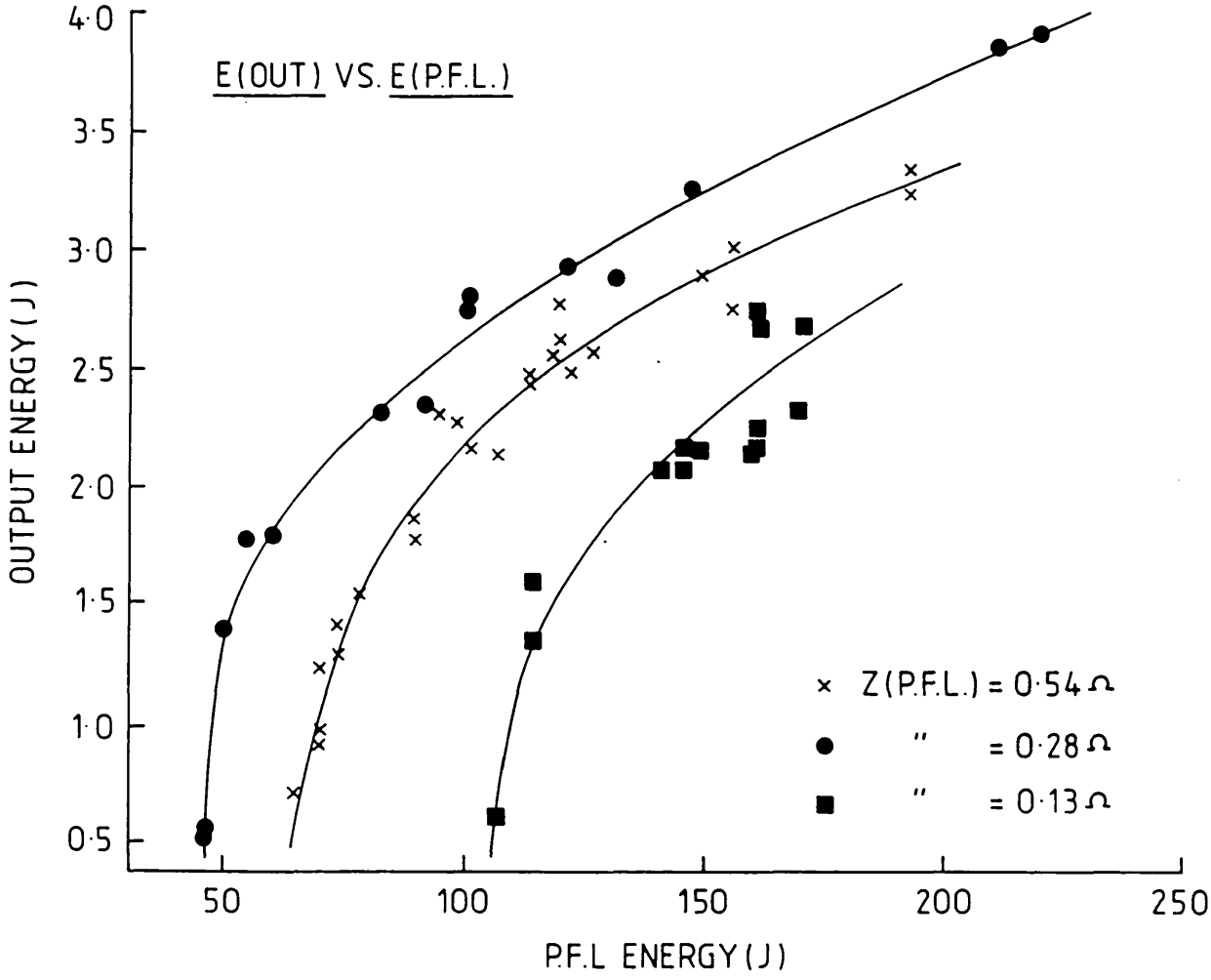

Figure 5.2 The laser output energy in Joules as a function of the energy stored on the P.F.L. for three impedances of P.F.L.

on many parameters through a complex relation, it is not possible to 'select' a value of R in the same way as one can select a value of Z. It is therefore necessary to perform a series of experiments covering a wide range of parameters for the impedance matching condition to be identified. It is this series of experiments which is described in this chapter.

5.2 High Efficiency - Experimental

The experiments described in this section were carried out using the discharge electrode configuration used towards the end of the laser optimisation describred in Chapter 4 (figure 4.1c), and the optimised laser gas mixture of 3 τ HCl, 15 τ Xe and neon buffer gas up to a total pressure of 3.5 atmospheres. The output energy of the laser was measured as a function of the electrical energy stored on the P.F.L. for three different impedances of P.F.L. The stored energy was calculated from the voltage on the P.F.L., as measured using an ammonium chloride resistive potential divider, just prior to the breakdown of the rail-gap switch. Such a voltage waveform is shown in figure 5.1, where the voltage on the P.F.L. is seen to rise up to the time when the rail-gap switches. There then follows a small fall in voltage for the time taken to charge the short section of line between rail-gap and laser head. Once this is charged, the voltage rises again until the laser discharge plasma is formed, after which it falls to zero. The pressure of dry air in the rail-gap was adjusted for differing P.F.L. charging voltages to ensure that the rail-gap always switched at a similar point close to the peak of the charging waveform. The P.F.L. impedance was adjusted by changing the spacing between the plates (Eqn. 3.28), and the change in P.F.L. voltage risetime thus produced from the

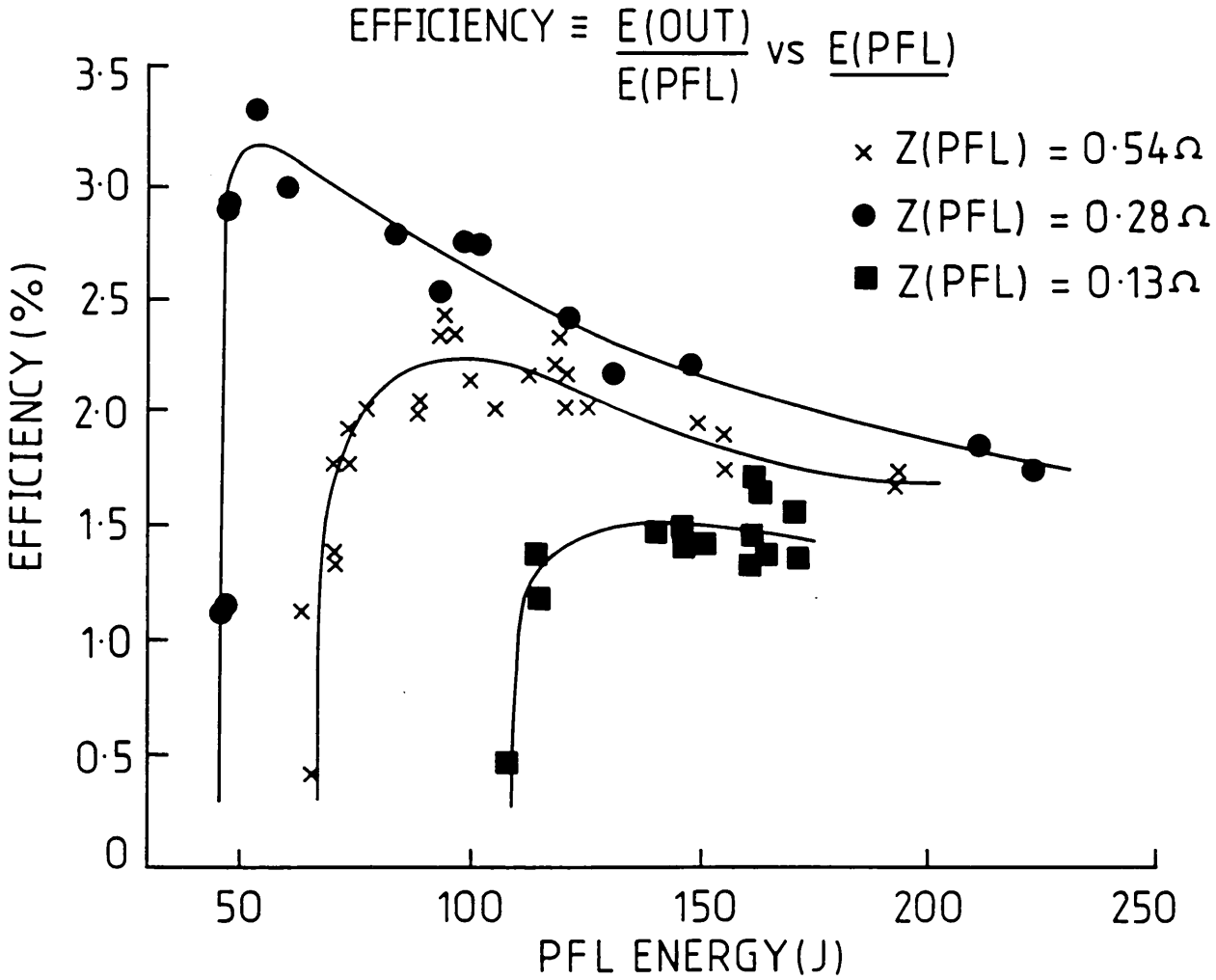

Figure 5.3 The laser efficiency as a function of energy stored on the P.F.L.

change in the P.F.L. capacitance (Eqn. 5.3) was allowed for by altering the delay in the X-ray preionisation circuit to ensure that the discharge voltage between the electrodes was always in good synchronisation with the preionisation.

The results obtained are shown in figure 5.2, where the laser output energy is plotted as a function of the energy stored on the P.F.L. for three impedances of P.F.L., namely 0.54, 0.28 and 0.13Ω. All three curves show the output energy increasing as the P.F.L. energy is increased, the 0.28Ω line giving the best results. It is more informative to plot the data of figure 5.2 with laser efficiency, defined as the output energy as a fraction of the energy stored on the P.F.L., as the ordinate. This is done in figure 5.3, showing that the highest efficiency obtained is some 3.2%. This is significantly higher than those achieved in conventional excimer lasers and, as will be described later, compares favourably with other 'high-efficiency' lasers using more complicated discharge circuitry.

The very rapid fall in efficiency at low P.F.L. energies for each of the P.F.L. impedances occurs where the voltages being employed are insufficient to ensure proper operation of the rail-gap. This statement is substantiated by a series of time integrated photographs of the rail-gap during operation. These photographs show clearly the number of spark channels present within the rail-gap under the various operating conditions. At the same time, measurements of the current through the discharge were made. As mentioned previously, the presence of significant inductance in the load fed from the P.F.L. will destroy the 'classical' P.F.L. behaviour of figure 3.6, giving rise to an oscillatory, LC, component in the current and voltage waveforms. This component is clearly

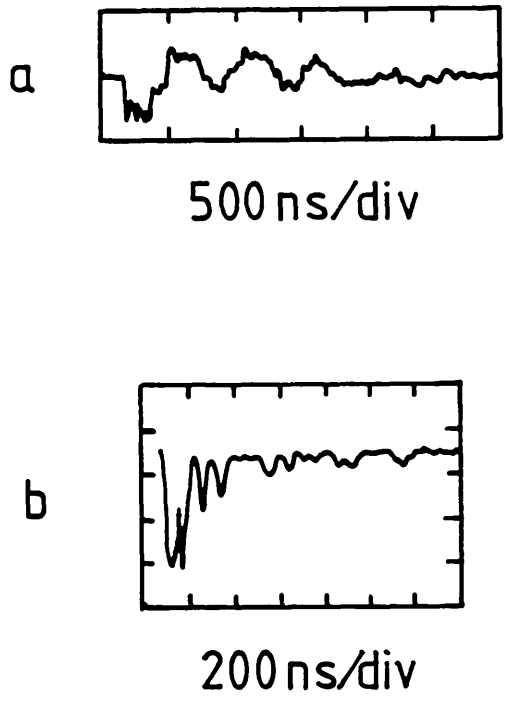

Figure 5.4 a) Discharge current passing through the laser head b) Unprocessed signal from electro-optic voltage monitor representing voltage between discharge electrodes.

visible in the measured current waveform shown in figure 5.4a, and may be used to calculate the series inductance, L, through the simple formula

$$\tau = 2\pi (LC)^{\frac{1}{2}} \qquad (5.2)$$

where τ is the period of the current oscillation and C is the capacitance of the P.F.L. The inductance calculated in this way is shown in figure 5.5, where it is plotted against the energy stored on the P.F.L. for purposes of comparison with figures 5.2 and 5.3. The inductance values calculated from the period of the current oscillation using other, more complex, LC approximations to the discharge circuit, do not differ from those shown here by more than 15%.

The inductance thus calculated is that of the load seen by the P.F.L., and consists of the inductances of the rail-gap, the short transmission line section, the laser head and the discharge plasma. The numbers shown close to the data points in figure 5.5 refer to the number of spark channels within the rail-gap detected photographically. It can be seen that where the number of spark channels becomes small, the measured inductance increases, and that this occurs at precisely the P.F.L. energy at which the efficiency shown in figure 5.3 falls dramatically.

The decrease in the number of spark channels, and hence the increase in inductance, in the rail-gap at low P.F.L. energies occurs because of the dependence of the channel formation on the rate of rise of voltage (dV/dt) across the gap[5.5]. When the P.F.L. is being charged to a lower voltage, and hence lower stored energy, dV/dt is lower, resulting in fewer spark channels, and hence a higher inductance. This explains why all

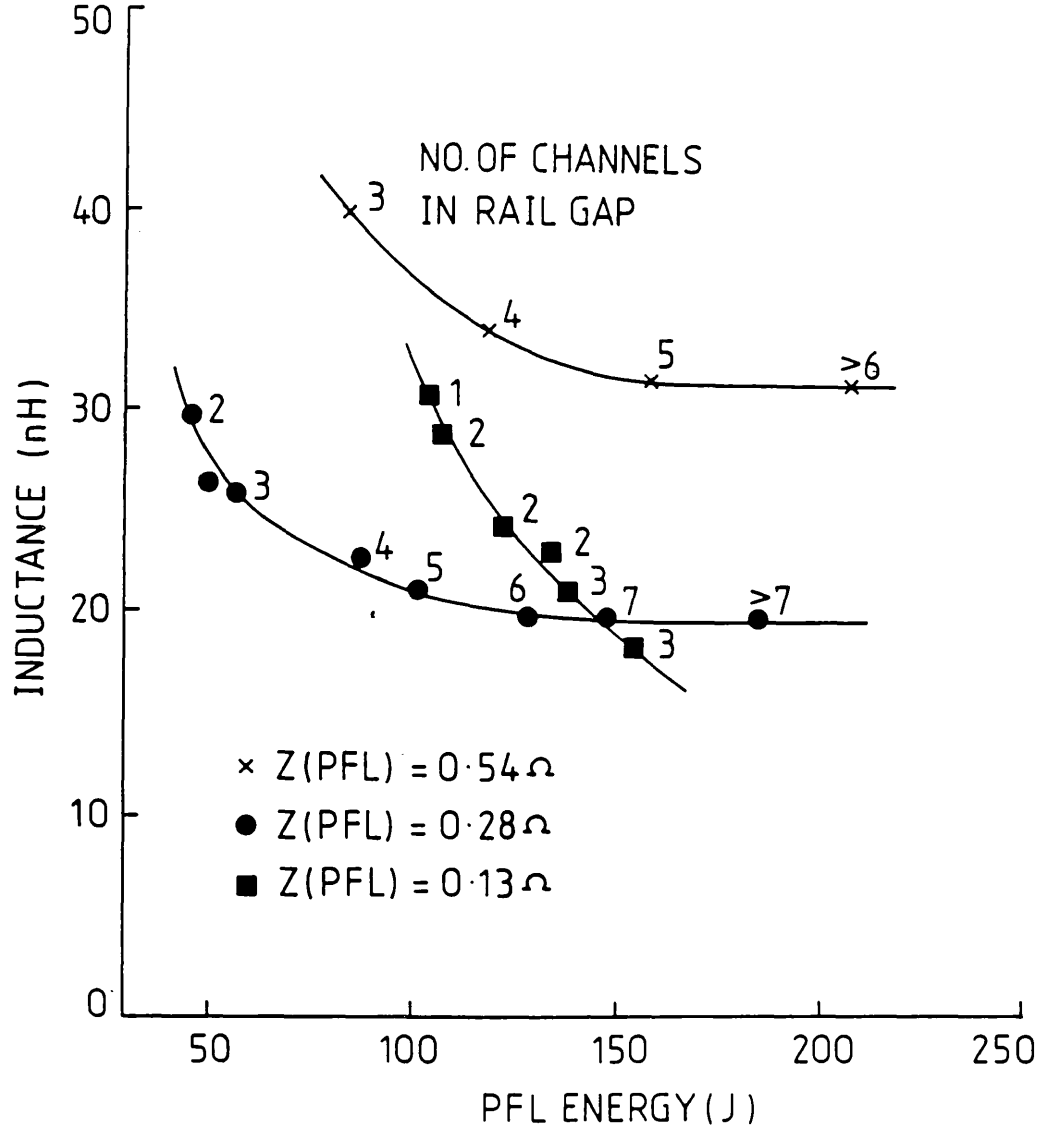

Figure 5.5 Measured inductance of load placed on P.F.L. The figures close to the data points represent the number of spark channels within the rail-gap. Experimental conditions are identical to figures 5.2 and 5.3.

three inductance curves in figure 5.5 rise at low P.F.L. energies. However, dV/dt is also affected by the risetime of the voltage on the P.F.L., and this is given by (see Appendix II)

$$t_r = \pi \sqrt{L_m \frac{C_m C_{PFL}}{C_m + C_{PFL}}} \qquad (5.3)$$

where C_m and C_{PFL} are the capacitances of the erected Marx bank and P.F.L. respectively, and L_m is the series inductance of the Marx and the associated electrical feeds to the P.F.L. Therefore, when using a lower impedance P.F.L., where the plates are closer together, the capacitance is increased and hence the voltage risetime slowed, thereby reducing dV/dt. This factor, together with the fact that a given voltage corresponds to a higher stored energy for a line of lower impedance, explains why the decrease in the number of spark channels as the P.F.L. energy is decreased occurs earlier for the line of lowest impedance.

In the limiting case of having many spark channels within the rail-gap, this component presents a small and constant inductance, no longer dominating the total inductance of the load. Under these circumstances the inductance curves of figure 5.5 'level-off' to a value determined by the geometry of the short transmission line section and laser head. The difference between the limiting values shown for the 0.54Ω and 0.28Ω P.F.L.s is due to the difference in the inductance of the short transmission line section caused by the change in the line spacing between the two impedances, and agrees well with the change in inductance calculated from equation 3.27. On this basis, the inductance of the 0.13Ω P.F.L. would be expected to level-off at a value of ~14 nH, and the inductance of the

laser head alone is estimated at between 6 and 7 nH, in close agreement with the value calculated from first principles.

While the measurements of the inductance and number of spark channels of the rail-gap give a clear indication of the conditions under which it works satisfactorily, and hence define an operating 'window' within which the laser may be expected to work well, they offer no explanation of the form or order of the efficiency curves in figure 5.3 other than predicting the rapid fall in efficiency at low P.F.L. energies. To explain the more gradual decline in efficiencies when moving to higher P.F.L. energies, and why the 0.28 Ω P.F.L. gives better results than the 0.54 Ω , it is necessary to examine the efficiency of energy transfer from the P.F.L. to the load. This is given by equation 5.1

$$\eta = 1 - \left(\frac{R - Z}{R + Z}\right)^2 \qquad (5.1)$$

This equation may be recast by noting that the voltage developed across a stable discharge - the discharge sustaining voltage, V_s - will be related to the discharge impedance, R, via the discharge current, I, thus

$$V_s = I R \qquad (5.4)$$

In the initial time period 2τ , corresponding to the double transit time of the P.F.L., the current, I, must be drawn from the P.F.L. Hence a voltage, V_{PFL}, will be developed across the impedance, Z, of the P.F.L. given by

$$V_{PFL} = I Z \qquad (5.5)$$

However, this voltage, V_{PFL}, must be the difference between the voltage to which the P.F.L. was initially charged, V_c, and the voltage dropped across the discharge plasma, V_s. Therefore we have from equations 5.4 and 5.5,

$$Z = \frac{V_{PFL}}{I} = \frac{V_c - V_s}{I}$$

and

$$R = \frac{V_s}{I}$$

Substituting these values for R and Z into equation 5.1 gives

$$\eta = 1 - \left(\frac{2V_s - V_c}{V_c} \right)^2 \qquad (5.6)$$

This is our main result and shows that the energy transfer efficiency is maximal and equal to unity when the voltage to which the P.F.L. is charged is equal to twice the discharge sustaining voltage,

$$\text{i.e.} \quad V_c = 2 V_s \qquad (5.7)$$

The condition expressed by equation 5.7 has been obtained independently by Taylor et al[5.6] by equating the energy stored in the P.F.L., S, where

$$S = \tfrac{1}{2} C V_c^2 = \tfrac{1}{2} Q V_c$$

to that deposited in the load, D, where

$$D = V_s \, I \, 2\tau = Q \, V_s$$

and also by Long et al[5.7], by equating the voltage drop across the P.F.L., V_{PFL}, where

$$V_{PFL} = V_c - V_s = I \, Z$$

to that across the discharge plasma, V_s, where

$$V_s = I \, R$$

However, unlike equation 5.6 derived in the present work, neither of these authors provides any indication of the efficiency of operation away from the impedance matched condition.

The fact that the condition for optimum efficiency, equation 5.7, contains no reference to either P.F.L. or discharge impedance has caused some workers in the field to believe that the idea of impedance matching has been replaced with this new, mystical formula. This is not the case. Equation 5.7 is merely an easily measurable consequence of reaching the impedance matched condition. The way that this is achieved is by choosing a certain P.F.L. impedance, Z, and then, using the fact that the discharge impedance, R, is a function of the discharge current, varying the electrical excitation rate such that a plasma of the desired impedance is formed between the discharge electrodes. The most simple way of detecting this is by monitoring the voltages V_c and V_s until equation 5.7 is satisfied. However, the impedances of the P.F.L. and discharge plasma are still being matched, and, importantly, at the value chosen for the P.F.L. impedance. It is therefore necessary to use a P.F.L. of a similar impedance to the discharge plasma likely to be formed between the given electrode configuration

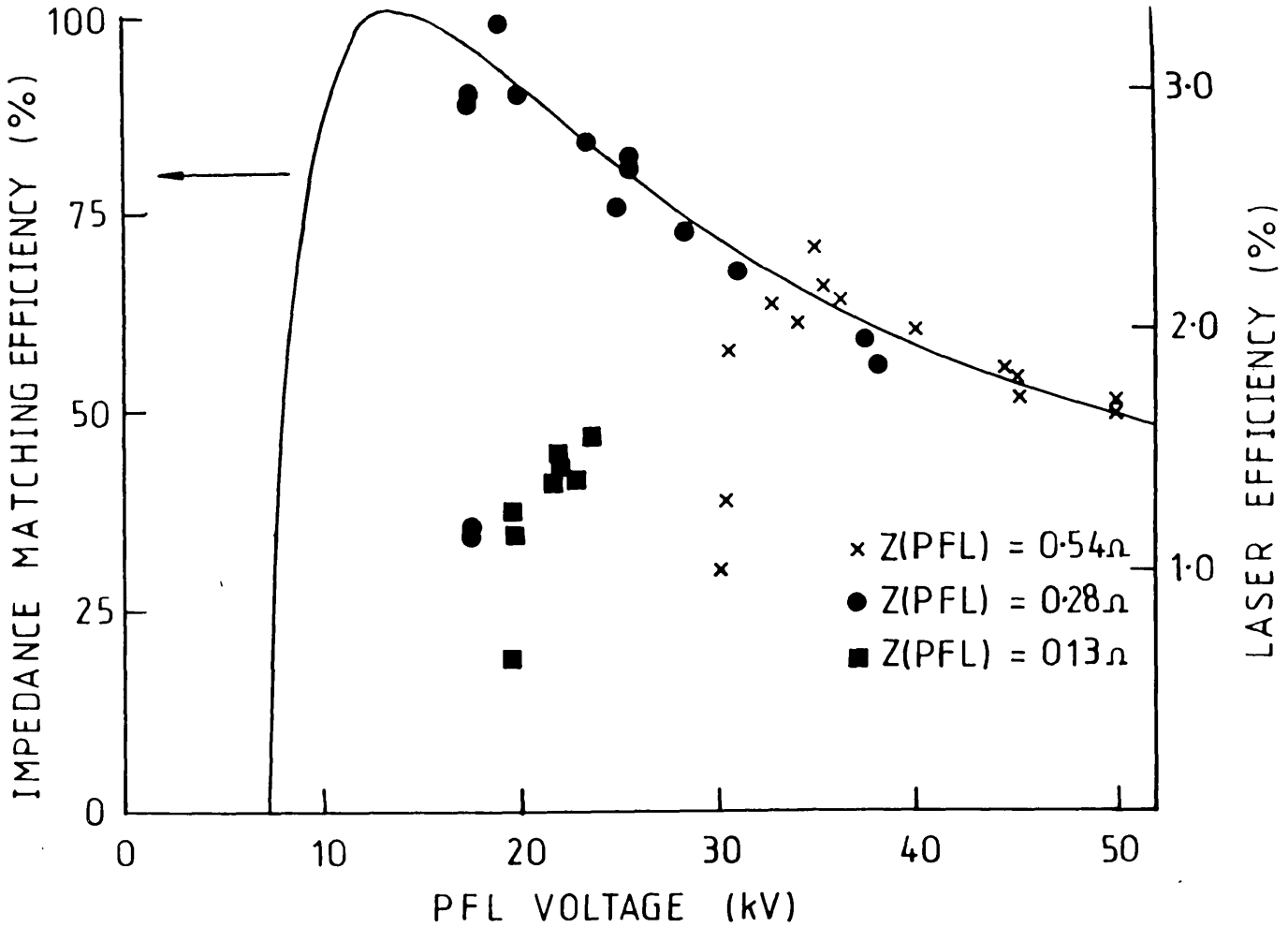

Figure 5.6 Theoretical impedance matching efficiency curve (equation 5.6) for V_s = 7 kV (left scale) and experimental laser efficiency data (right scale).

at the given gas composition, pressure, geometry and reasonable excitation rate.

Taylor et al[5.6] have shown that the discharge sustaining voltage, V_s, is essentially independent of the discharge current density in the range 40-200 A/cm^2.

Other authors have noted a similar effect, the discharge plasma acting as an almost constant voltage load. In the present work the discharge sustaining voltage was found to vary slightly, and does, in fact, show some variation throughout the duration of the discharge (figure 4.15b). It is possible that this variation is observed only due to the superior, electro-optic, voltage measurement technique used in the present work - it could easily be dismissed as inductive pick-up if an electrical monitor were used. However, the dependence of V_s on the magnitude of the discharge current is still found to be small, an increase of $\sim$15% in V_s resulting from a doubling of the discharge current.

It is therefore not unreasonable to make the assumption that V_s is constant over the values of discharge current of interest. Making such an assumption, it is possible to plot the impedance matching efficiency, η, against the P.F.L. charging voltage, V_c, by using equation 5.6, and such a plot is shown in figure 5.6 for V_s = 7 kV. As expected, the efficiency is equal to unity for V_c = 14 kV, but above this value it falls only relatively slowly. For $V_c < 2V_s$ there is no direct evidence that V_s remains essentially constant, and it seems likely that V_s will, in fact, decrease somewhat. However, even allowing that this may be the case, the efficiency of energy transfer still drops quite rapidly in this region, becoming equal to zero when $V_c = V_s$.

Also shown in figure 5.6 is the laser efficiency data from figure 5.3, but this time plotted against the P.F.L. charging voltage, V_c, rather than the stored energy. As can be seen, if the points where the rail-gap ceases to operate properly are ignored, the data for the 0.54 and 0.28Ω P.F.L.s fit the theoretical curve quite closely. The best fit occurs for $V_s = 7 \pm 0.5$ kV, in good agreement with the measured value (figure 4.15b). This graph also shows that, using the 0.28Ω P.F.L., operation at a charging voltage as low as 2.6 V_s is possible, due to the transient voltage gain produced by the short transmission line section. At this voltage, the energy transfer efficiency is 90%. Certainly in the case of the 0.54Ω P.F.L., and probably in the case of the other two impedances, the low voltage performance is limited by the rail-gap and laser head inductance.

If an external electrical 'spiker' circuit were used to replace the short transmission line section in producing break down of the laser gas and rail-gap, the additional 10% of impedance matching efficiency could be obtained. However, the added complication of providing an extra, synchronised, high voltage circuit is hardly justified. Moreover, the efficiency of 3.2% obtained from the present self-synchronised, 'passive', system from a laser gas mixture of 3.5 atmospheres total pressure, compares very favourably with the 4.2% efficiency obtained by Long et al[5.7], using such a spiker circuit, from laser gas at 5 atmospheres pressure.

5.3 High Efficiency - Discussion

The efficiencies quoted in the previous section refer to the laser output energy as a fraction of the energy stored on the P.F.L. They do not include energy losses in the high voltage

generation, or the Marx bank, or the energy used in the pre-ionisation circuit. However, they do include losses in the rail-gap, and for this reason the intrinsic efficiency of the laser, defined as the output energy as a fraction of the energy deposited in the laser plasma, will be somewhat higher than the 3.2% quoted. Direct measurement of the energy deposited in the laser plasma, and hence intrinsic efficiency, proved to be impossible due to the poor calibration of the discharge current waveform. However, the discharge voltage, as represented by the unprocessed signal from the electro-optic voltage monitor shown in figure 5.4b, falls to a very low value after the initial discharge sustaining period, indicating very little energy deposition after this time. Because of this, and using an estimate of the energy lost in the rail gap, it seems likely that the intrinsic efficiency of the present laser is of the order of 4%. This is comparable to the value estimated by Levatter et al[5.8] for a laser working at a similar overall pressure, and somewhat lower than that obtained by Long et al[5.7] from a higher total pressure of laser gas. This, together with the almost linear increase in laser output energy with gas pressure found in Chapter 4, indicates that the intrinsic laser efficiency increases with gas pressure, and hence that more efficient operation could be obtained using a mechanically stronger laser chamber.

The fall of the discharge voltage to a very low value while the current remains quite high, as shown in figure 5.4, shows that at late times there is a very low impedance between the discharge electrodes. Also, the rate of decay of the current waveform, $\gtrsim 1\ \mu s$, is comparable to that predicted from energy losses due to the finite resistivity of the P.F.L. water dielectric, indicating very little energy deposition in the

laser gas. These results are commensurate with the existence of arc-like channels between the discharge electrodes, rather than a true glow discharge. More evidence to support this observation is given in the next chapter.

In the present laser system, the need to use relatively low P.F.L. charging voltages to produce high efficiency operation restricts the output energy available at these high efficiencies. The energy output may be raised by storing more energy at the lower charging voltage, necessitating a higher capacitance P.F.L. The most simple way to increase the P.F.L. capacitance in the present system is to place the P.F.L. plates closer together, thereby also decreasing the impedance. However, as figures 5.2, 5.3 and 5.6 show, this does not have the desired effect, producing a serious degradation of the laser performance. Furthermore, the results no longer fit equation 5.6 as figure 5.6 shows. The inductance inherent in the low impedance circuit, figure 5.5, is no higher than that in the other two circuits and so it is not merely the magnitude of the inductance which is responsible for the poor performance. However, this inductance will give rise to a reactive component of the total impedance which is similar for all three P.F.L.s. Therefore, when attempting to operate at lower total impedances, this reactive component will form a larger fraction of the total impedance. This will result in reduced energy deposition in the load during the time of interest. Furthermore, the LC component of the discharge current will be slowed according to equation 5.2, with respect to the other P.F.L.s, further reducing the energy deposition rate.

Therefore, it is the inductance in the discharge circuit, originating predominantly from the rail-gap, which reduces the

energy deposition rate in the discharge plasma. This may be understood either in terms of the P.F.L. feeding and inductive load, or in terms of the simple L.C. circuit equivalent. The true situation lies between these two extremes.

Clearly, then, it is the rail-gap which limits the performance of the present laser system. Under conditions where the rail-gap operates satisfactorily, the laser performance is comparable to the best yet achieved for an XeCl laser. However, it would be useful if the range of conditions under which this standard of operation is possible could be extended. One way of doing this is to use the technique employed by Long et al[5.7] and subsequently, in various forms, by others[5.9, 5.10, 5.11], in which a separate high-voltage, but relatively low energy, circuit is used to both produce the voltage spike necessary to attain fast and uniform breakdown of the laser gas, and to facilitate commutation of the P.F.L. switch. Using this technique in conjunction with a conventional rail-gap switch, Long et al demonstrated a significantly wider operating range. This technique also removes the need to use the short transmission line section between the rail-gap and laser head, thereby reducing the total inductance. As mentioned earlier, the gain in system versatility is greater than that in absolute performance compared to the present system.

Moving away from rail-gaps altogether - something which may prove essential if high repetition-rate lasers are to have reasonable lifetimes - other low inductance switching techniques have been employed. Ewing[5.9] et al have used a combination of external spiker circuit and saturable magnetic switching, and Taylor et al[5.11] have used a novel method of magnetic switching producing its own 'spike'. To date magnetic switching techniques

have proved somewhat less efficient than rail-gaps, due to the energy expended in saturating the magnetic cores. However, the lifetime of the cores is expected to be much greater than that of a spark-gap, assuming adequate, and uniform, core cooling can be provided.

Falling short of full magnetic switching is magnetically assisted switching. In this technique, the laser is switched in a conventional manner, but one or more stages of magnetic compression are used after the switch[5.3,5.13,5.14]. This greatly reduces the strain on the switch as the total energy may be transferred through the switch relatively slowly at low powers and then temporally compressed to give the required power for laser operation. Such techniques may soon allow solid state switching devices to replace the previously used spark-gaps and thyratrons[5.12,5.13].

While the use of magnetic materials either as switches themselves, or in conjunction with other forms of switching, has been shown to produce good results and shows potential for further development, the search for other methods of high-power, low inductance, low jitter switching continues, not just for excimer lasers but for pulsed power supplies in general.

CHAPTER 6

LONG PULSE OPERATION

6.1 Introduction

Conventional avalanche discharge pumped excimer lasers have relatively short gain durations (<20 ns) and this severely limits their usefulness in many applications. With such a short gain time only a few round trips of a typical optical cavity are possible, and this leads to output beams of poor spatial quality and high divergence, many times the diffraction limit. Furthermore, techniques such as spectral filtering and passive mode-locking which require the laser light to traverse a frequency selective or absorbing medium many times, are very difficult to apply. The short gain time also places a limit on the energy per unit volume which can be extracted from the laser. These factors have, to date, limited the use of excimer lasers very largely to pumping other lasers such as dyes. The many other potential applications such as photolithography, where the combination of high power and short wavelength make the excimer laser an excellent candidate, have not yet been commercially realised due to the poor beam quality. Even in the realm of dye laser pumping, the Nd:YAG laser, despite its unfavourable wavelength, is often to be preferred over the excimer due to its superior beam quality. Added to the improved beam quality, the possibilities of producing narrow-bandwidth and/or short pulse (sub-picosecond) output from a long gain duration excimer laser make its investigation important.

The short gain time of excimer lasers has been a feature of their operation since the earliest days of their construction. The first discharge pumped excimer lasers used no preionisation,

and hence their operation was limited to the short period of time before the formation of arcs or streamers within the discharge. This can be as much as 30ns at low total gas pressures[6.1], but is significantly shorter than this at pressures approaching atmospheric[6.2]. The electrical circuits developed to supply energy to the discharge over this very short timescale were necessarily fast, and generally relied on charge transfer, L-C inversion or P.F.L. techniques. However, the combination of low total laser gas pressure and short excitation time led to output pulses of very limited energy. In order to allow a more favourable combination of gas pressure and pulse duration, it is necessary to preionise the laser gas. This is done by introducing free electrons before the discharge is initiated, thereby reducing the number of orders of magnitude through which the electron density must be avalanched to reach the density present in the discharge plasma. This leads to the formation of a more uniform discharge which will persist for longer than one initiated without preionisation. Using U.V. preionisation to delay the onset of arcs, commercial excimer lasers can operate at pressures of up to ~ 4 atmospheres, producing output pulses of relatively high energy (~ 0.5J) in durations of ~ 30 ns. Whilst representing a major advance in the non preionised lasers, this performance is still far from what can be obtained if a stable discharge can be initiated. The instability of the discharge is due partly to the poor uniformity of preionisation offered by the U.V. light, and partly due to the discharge circuit which has changed very little since the earliest, non-preionised lasers.

By using a more suitably designed P.F.L. based discharge circuit, and by paying particular attention to the uniformity of the U.V. preionisation, pulses of up to 70 ns have been

generated[6.4,6.5]. This is the longest pulse duration yet reported from a high energy U.V. preionised, avalanche discharge pumped excimer laser. Longer pulses have been achieved using a resistively ballasted electrode[6.6,6.7,6.8]. The work of Taylor[6.5], Watanabe[6.4] and others has shown that the uniformity of the preionisation plays a crucial role in determining the pulse duration which can be obtained. However, since the U.V. light used for preionisation is generally produced from localised sources, sparks, and only penetrates a few centimetres through a typical excimer laser gas mixture, good uniformity is very difficult to achieve.

In this respect, X-rays provide a much more attractive form of preionisation as they can be produced from an extended source with good spatial uniformity, and the much greater penetration of X-rays in the laser gas ensures little depletion of the dose far from the X-ray source. The potential for long pulse operation using the greater preionisation uniformity offered by X-rays was quickly realised by Levatter et al, who first[6.9] produced pulses of almost 100 ns F.W.H.M. and later[6.10] extended them to nearly twice this value. In both of these cases the laser output duration was, with a carefully chosen gas mixture, comparable to the duration of the electrical excitation. As described in Chapter 3, the present laser system was initially designed with a discharge circuit capable of providing electrical excitation over a time of $\sim$160 ns, comparable to that of Levatter.

6.2 Long Pulse Operation - Experimental

The variation of the laser output pulse shape and duration was first noted early in the development of the laser system.

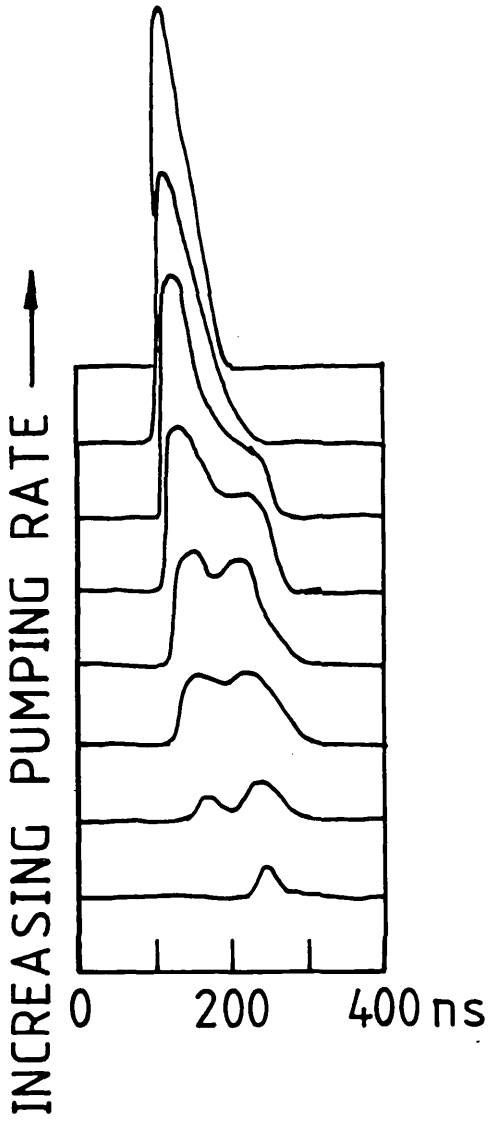

Figure 6.1 Laser output pulse for various electrical excitation (pumping) rates.

The duration is strongly dependent on the concentration of HCl in the gas mixture, as indicated by figure 4.4c, and also on the electrical excitation rate, as is shown in figure 4.9, which is repeated here as figure 6.1. These results were obtained with the gas mixture optimised for energy output, i.e. 3 τ HCl, 15 τ Xe with 3.5 atmospheres of neon buffer gas. The 'double-hump' nature of the output is explained in Chapter 4 to originate from modulation of the laser gain caused by changes in the discharge current. Figure 6.1 shows that as the excitation rate is increased from below threshold the laser output grows in both magnitude and duration until it extends over the full pumping period. However, increasing the pumping rate further results in the pulse becoming peaked early in the discharge, and the output at later times declining. Eventually, the laser ceases to lase for the full duration of the electrical excitation, terminating somewhat before the end. As mentioned in Chapter 4, this premature termination was not expected and requires explanation. However, it can be seen that with the electrical excitation of 160nsused in figure 6.1 the laser output duration is similar to this over a wide range of electrical excitation rates; figure 6.1 shows a variation in discharge current of a factor of approximately six.

The partial pressure of HCl does not affect the form of the evolution of the output pulse shown in figure 6.1. However, HCl pressures somewhat lower than 3 τ result in slightly longer pulses and delay the onset of pulse shortening to higher pumping rates, although at comparable output energies. Slightly higher pressures of HCl have the reverse effect, bringing forward the pulse shortening.

Despite the fact that the output pulse durations achieved

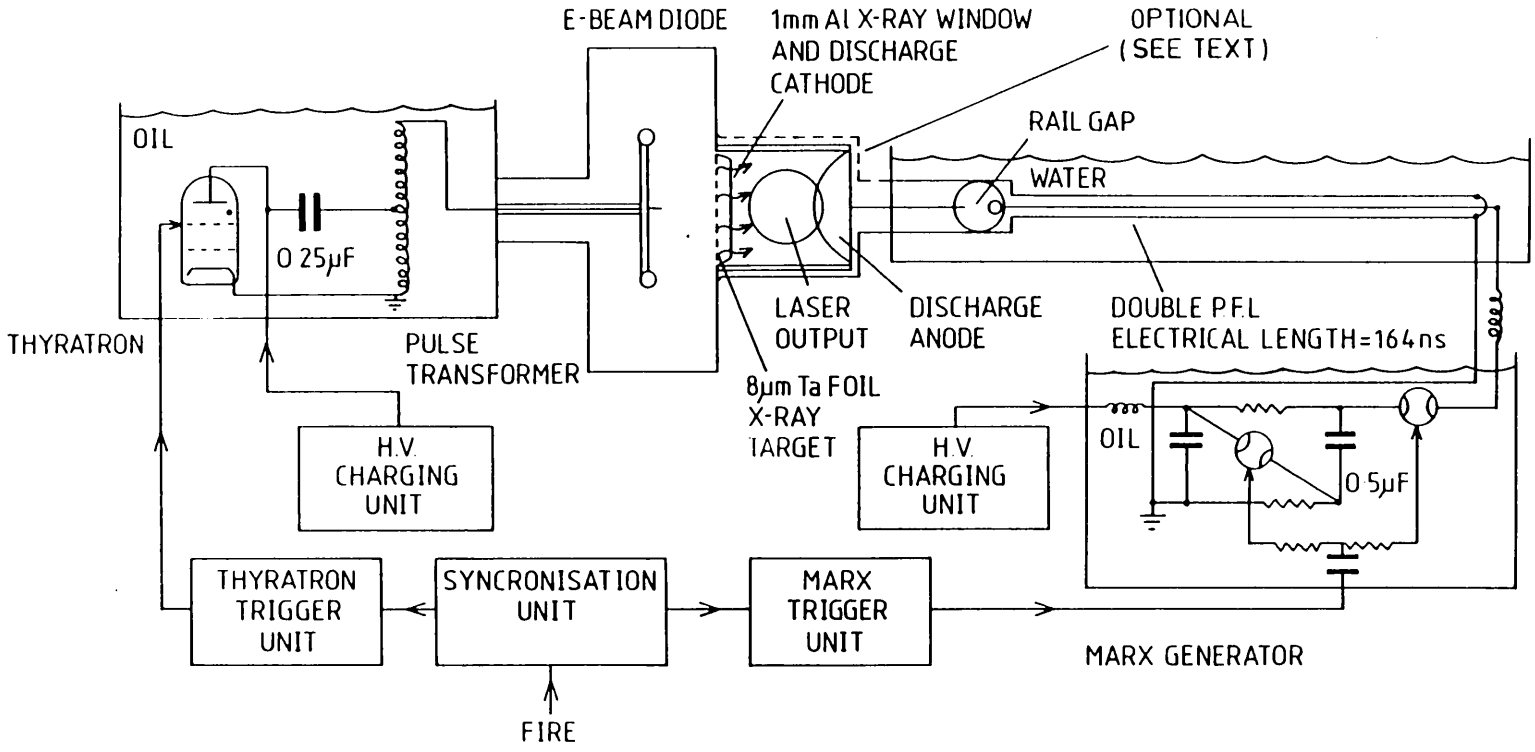

Figure 6.2 Schematic diagram of laser system, showing earth return plate (dotted) which is removed to convert double P.F.L. into single P.F.L. of twice the electrical length.

here are many times that of typical U.V. preionised lasers, and comparable to the best achieved at the time, it is clear that there is a pulse terminating mechanism at work, particularly at high electrical excitation rates. In order to investigate more thoroughly this mechanism, and to extend further the laser pulse, it is necessary to provide electrical excitation over a longer period of time. There are several ways in which this can be done. The most obvious, and in many ways the best, is to physically extend the aluminium plates of the P.F.L. However, laboratory space considerations dictated that if this were to be done, a folded geometry would have to be adopted. This would greatly reduce the versatility of the P.F.L. in terms of varying its impedance, as well as involving some constructional work. Due to these considerations it was decided, at least as an initial measure, to reconfigure the double P.F.L. into a single P.F.L. of twice the electrical length. This can be done relatively simply by removing one of the earth return feeds such as that shown dotted in figure 6.2, although this has several disadvantages. Firstly, and most importantly, the inductance of the laser head is effectively doubled as half of the earth return part of the discharge circuit has been removed. This increased inductance is particularly detrimental to laser performance, as mentioned in the previous chapter, and raises the value of the lowest impedance P.F.L. which will give satisfactory operation. Secondly, the P.F.L. impedance is doubled for a given spacing between the plates. This changes the P.F.L. impedances at which the rail-gap operates best, as its operation is governed largely by the rate of charge of the P.F.L. and hence the total P.F.L. capacitance. As the single P.F.L. of a given capacitance has twice the impedance of the double P.F.L. of the same

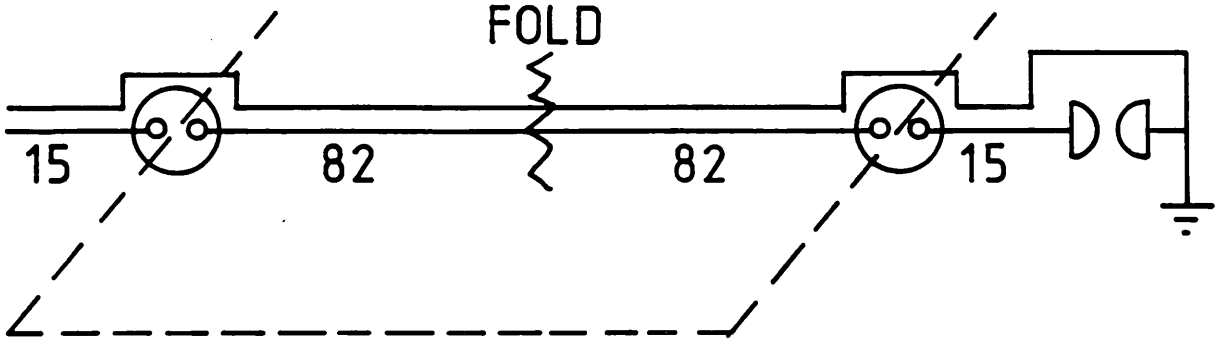

Figure 6.3 Equivalent arrangement for single P.F.L. configuration. Only central section is initially charged. The two rail-gaps shown are one and the same. The numbers below the line refer to the electrical single transit time in nanoseconds.

capacitance, the rail-gap operating characteristics may be transferred with little alteration from the 0.13 Ω double to the 0.26 Ω single P.F.L., and from the 0.28 Ω double to the 0.56 Ω single etc. It would therefore be expected that it would operate better with the 0.56 Ω single P.F.L. than the 0.26 Ω , and this is indeed the case. This fact, together with the increased inductance of the load, leads to the optimum performance being attained at a P.F.L. impedance of 0.56 Ω , higher than the optimum value using the double P.F.L.

A third point is that the single P.F.L. is not a straightforward P.F.L. arrangement, but is a folded version of the line shown in figure 6.3. Initially only the central section is charged. This is then switched, by the rail-gap, onto both the feeds to the laser head and also an open ended section of line. It should be noted that there is only one rail-gap, but that this effectively switches two sections as shown in figure 6.3. As might be expected, this arrangement does not lead to the classical P.F.L. voltage and current waveforms of figure 3.6, but gives rise to the current waveform shown in figure 6.4. This displays a 'plateau' for a time of ~ 300 ns corresponding to the double transit time of the single P.F.L. The series of dips occurring at times t = ~200, ~400, ~600 ns are caused by the initially uncharged sections of line at either end of figure 6.3. The large current peak at t ≃ 500 ns occurs as a result of the voltage reflected back from the laser head before the discharge plasma forms, returning back to the laser head some 390 ns later (~ 2 x (15 + 82 + 82 + 15) ns). The shape of the current waveform is largely independent of its magnitude and hence laser excitation rates. Clearly this is not an ideal waveform for very long pulse operation of the laser, but it does

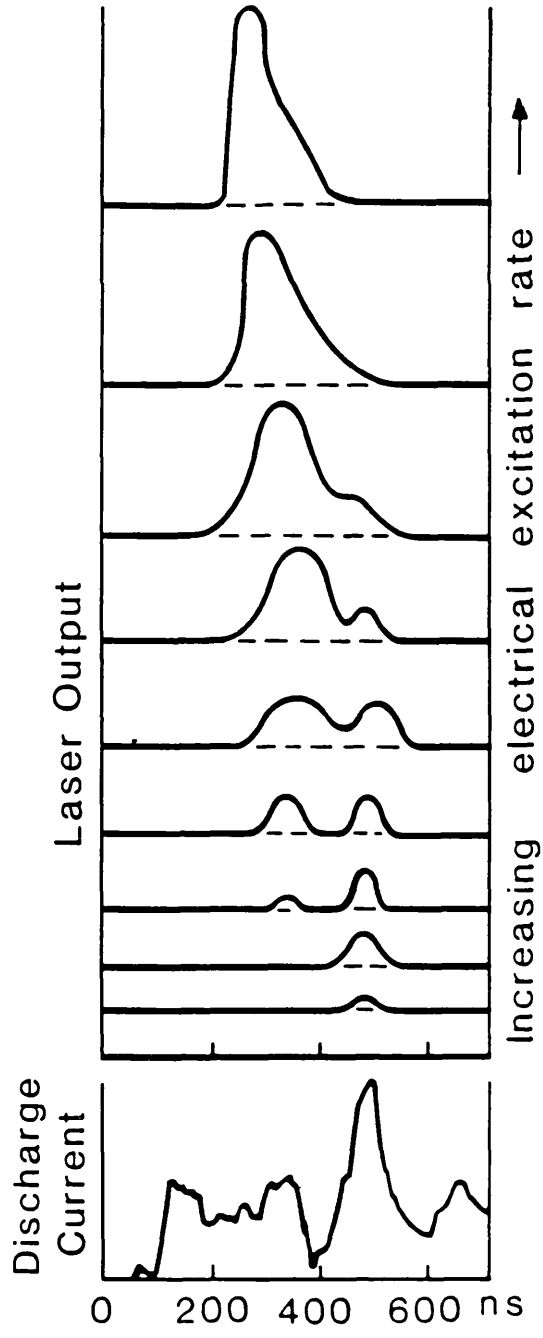

Figure 6.4 Laser discharge current, bottom, produced by single P.F.L. arrangement and laser output pulses, above, for various electrical excitation rates.

produce some very interesting and informative laser output pulse shapes. These are shown in figure 6.4, synchronised with the current waveform for various electrical excitation rates.

At very low excitation rates optical output occurs only at the point of highest current, even though this is very late in the discharge. As the excitation rate is increased, the output at this time increases until another output pulse appears, preceding the original and occurring at the time of the end of the current 'plateau'. On further increasing the excitation rate it is this pulse which grows in magnitude, eventually dominating the original. It is in this regime where the two pulses have merged together that the longest output pulses are obtained. Further increasing the electrical excitation rate advances the start of the pulse only slightly, and the pulse becomes strongly peaked at an early time, leading to a reduction in the F.W.H.M., although the base width remains constant. However, if the excitation rate is increased still further, the output at later times in the pulse actually begins to fall. Eventually no laser output is produced at later times, such as the time corresponding to the current spike at which the output pulse first appeared at low excitation rates. Throughout these changes in output pulse shape and duration as the excitation rate is increased the output energy increases smoothly and monotonically.

These results provide a dramatic demonstration of the suppression of lasing at late times, or the premature termination of the laser output, and show that electrical excitation rate is a major factor in the terminating mechanism. This phenomenon is discussed further in the next section.

The concentration of HCl within the laser gas mixture again has an influence on the output pulse duration. As before, it does not substantially alter the output pulse shapes of figure 6.4, but changes the electrical excitation rate to which the various shapes apply. The longest laser output pulses have been obtained with HCl partial pressures of $\sim 1.5\,\tau$ where energies of 0.7J in pulses of up to 250 ns. F.W.H.M. and 315 ns base width at 10% level have been produced. This represents the longest pulse duration yet produced from a high power avalanche discharge pumped excimer laser[6.11]. Comparable and longer pulses have been produced using a resistively ballasted laser[6.7] and also recently by Taylor et al[6.12], but in both cases the output energy was orders of magnitude less than in the present system. The long pulse output energy of between 0.6 and 1.0J obtained in the present work is significantly lower than the energies attainable using the shorter electrical excitation as provided from the double P.F.L. This is due partly to the increased inductance of the laser head, and partly to the lower than optimum energy concentration of HCl. Increasing the amount of HCl results in higher energies, but from somewhat shorter pulse durations, the pulse shortening at higher excitation rates occurring earlier. Lower concentrations of HCl reduce the energy still further and with no increase in pulse duration, presumably due to the lower laser gain.

The concentration of xenon in the laser gas mixture does not affect the pulse duration any more than would be expected from the very weak variation of output energy with xenon pressure shown in figure 4.4a. The pressure of the buffer gas, neon, has more effect. It works in conjunction with the pressure

of HCl to set the gain of the laser. For example, using the low HCl pressure of 1τ and only one atmosphere of neon, the gain is too low for the production of long output pulses. However, adding more neon increases the gain sufficiently for the laser output duration to increase. This process continues up to the maximum pressure capability of the laser chamber of 3.5 atmospheres, and therefore, by extrapolation, it seems likely that if higher total gas pressures could be used, then the partial pressure of HCl could be further reduced, and longer output pulses may be possible.

6.3 Laser Termination Mechanisms

There are several possible explanations for the premature termination of the optical output of the laser whilst still apparently under strong electrical excitation. A mechanism suggested several years ago is the depletion of the halogen donor molecule, usually HCl. The recombination of the neutral chlorine atom, produced from the radiative decay of the XeCl*, and hydrogen to reconstitute the HCl occurs efficiently, but on a slow, millisecond, timescale. This reaction may therefore be neglected during the duration of the laser pulse, and hence each HCl molecule can give rise to no more than one laser photon. Once all the HCl molecules have been used, the laser will stop. This mechanism has been put forward to explain the termination of lasers with pulse durations of 20 ns, 50 ns, 200 ns, as advances have been made. To calculate whether this mechanism is applicable, it is necessary to have a comprehensive model of the discharge kinetics in order to determine what fraction of the chlorine atoms liberated from the HCl do indeed produce XeCl* molecules. With the present degree of understanding

of the discharge kinetics, the concensus of opinion is that the HCl population is not significantly depleted throughout the entire discharge volume during a laser pulse of a few hundred nanoseconds[6.7,6.10]. However, one of the most recent publications[6.13] indicates depletions of between 50 and 85% in a 200 ns pulse. It is clear, therefore, that the kinetics are still not sufficiently well understood to be able to predict, with confidence, the timescale over which such depletion becomes significant. However, experimental evidence to be presented here, together with that found by other authors[6.7], indicates that global HCl depletion is not the major cause of laser termination.

A second possible explanation of the premature termination is the production, in the discharge, of species which absorb radiation at the laser wavelength. If these species are long lived, the absorption may increase throughout the discharge as their number grows. This absorption could be sufficient to offset the laser gain, and hence produce termination. Again, a very detailed model of the kinetics is required to calculate exactly what absorption should occur, but certainly species such as Ne_2^+, Ne^{**}, Ne_2^*, Xe_2^+ and Xe_2^* all show absorption near the laser wavelength, and may be expected to be produced within the laser discharge[6.14]. The calculation of the concentrations of these species is beyond the scope of present models of discharge kinetics, but fortunately the magnitude of the absorption is relatively simple to assess by experimental means.

If an increase in absorption were responsible for the laser termination, then increasing the 'Q' of the laser cavity, and thereby lowering the lasing threshold, would result in the laser output starting earlier in the discharge and finishing

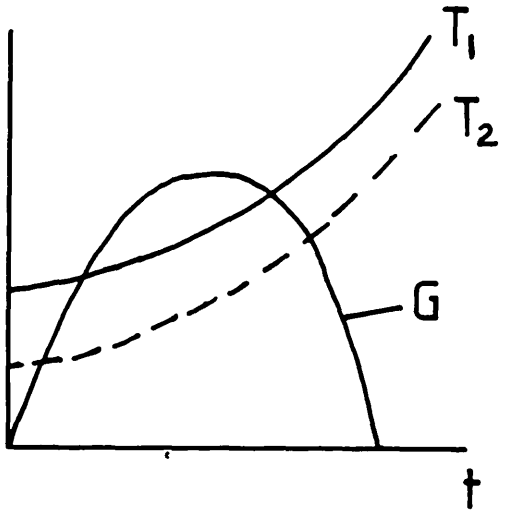

Figure 6.5 Laser threshold, T_1, shown increasing with time due to build-up of absorbing species. Threshold lowered, T_2, by increasing cavity 'Q'. Laser gain, G, shown to exceed the lowered threshold at both earlier and later times.

later. This is demonstrated schematically in figure 6.5, which shows the laser threshold, T_1, increasing with time as the losses due to absorption build-up. As can be seen, for any reasonable gain curve, G, a lowering of the threshold by a fixed amount to T_2 increases the time for which the gain exceeds threshold at both early and late times, and hence the laser pulse should be similarly extended. However, experimentally, this is not found. Increasing the cavity 'Q' by replacing the uncoated quartz flat output coupler with a 80% reflectivity plane dielectric mirror in the present system advances the start of the output pulse by up to 15 ns, but does not alter the time of the pulse termination. This remains identical within experimental error ($\pm$ 1ns) to that obtained using the normal cavity over the full range of operating parameters. This cannot be simply explained in terms of the build-up of absorbing species. It is just possible that the increase in cavity flux produced with the higher 'Q' cavity is responsible for an increase in the production of absorbing species which is just sufficient to counterbalance the lowered laser threshold, but it is highly unlikely that this should occur so precisely over a wide range of operational conditions.

It is therefore to be concluded that absorption is not the terminating mechanism, and indeed, the measured value of the absorption obtained in a similar XeCl* laser system by Taylor et al[6.14] is too small to produce any significant decline in laser output. Hence, the increase in cavity, 'Q', while allowing somewhat longer laser pulses to be produced, 265 ns F.W.H.M., but at lower energies, $\sim$ 0.3J, has no discernable effect on the laser termination. This, therefore, turns attention towards possible mechanisms which are independent of the laser optics.

Throughout the development of discharge pumped rare gas halide excimer lasers, the stability of the discharge has been a constant source of concern. It is therefore quite possible that, despite the gains made using X-ray preionisation and carefully designed low impedance discharge circuits, instability of the discharge may still be a problem. Prior to the publication of the present work[6.15] the most convincing identification of discharge instability as a laser termination mechanism was that performed by Hogan et al[6.7,6.8]. In this work a resistively ballasted laser was used in which one of the electrodes consisted of an array of bolts resistively isolated from each other. While the resistive ballasting provides some stabilisation against arc formation, the segmented electrode construction is sure to produce non-uniformities within the discharge. It is therefore not certain that the mechanisms identified in Hogan's U.V. preionised 5mJ output energy, resistively ballasted laser should be applicable to a non-ballasted, multi-joule, X-ray preionised laser. Hence, it is with an investigation of the stability of the discharge that the remainder of this chapter is concerned.

6.4 Discharge Stability

The uniformity and stability of the laser discharge are important subjects for investigation, not only as a possible laser termination mechanism, but also as a vital precursor to measurements of gross quantities such as gain and absorption.

The discharge uniformity and stability were monitored in several ways. The first, and most direct technique, involved taking both time integrated and time resolved photographs of the discharge as viewed perpendicular to the laser axis and

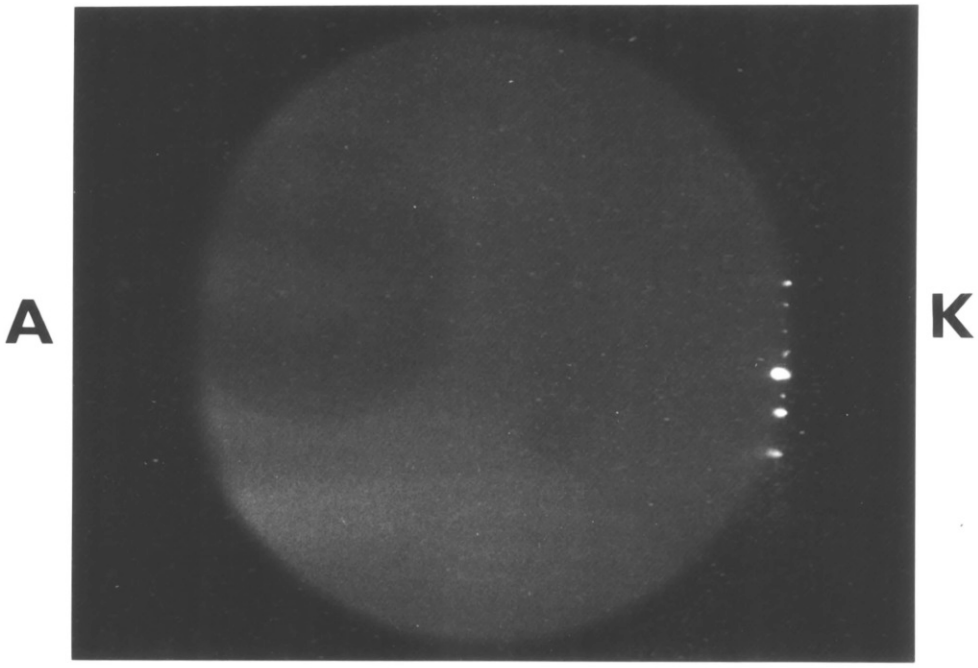

Figure 6.6 Time integrated photograph of discharge transverse to laser axis. Discharge cathode, K, is at the right-hand edge of photograph. Anode, A, is out of the field of view. Circular pattern is due to spurious reflections.

parallel to the faces of the discharge electrodes. A viewing port was machined in the P.V.D.F. laser chamber approximately 10 cm from one end of the discharge electrodes. The 25 mm clear aperture was covered with a perspex window, and hence only visible, rather than ultraviolet, light was observed. The discharge cathode, where structure within the discharge may well be expected to originate due to loss of preionisation electrons, is on one edge of the field of view.

Time integrated photographs, figure 6.6, taken using a close focus glass lens and standard 35mm camera body, did not reveal any structure within the body of the discharge. However, close to the cathode, marked 'K' in figure 6.6, small 'hot-spots' were recorded. These varied in number and brightness from shot to shot, figure 6.6 showing the maximum observed. The origin of these bright spots is not known, although it is expected that the rough surface of the aluminium cathode, acquired during passivation, enhances their formation. It is not known if similar spots appear close to the anode as this is not in the field of view. Other than in the region close to the cathode no structure is seen within the discharge. The faint circular pattern shown originates from reflections between the camera lens and viewing port. The lack of observed structure within the discharge is not surprising as, even if structure were to form at a late stage, it would be recorded against the background of the previous $\sim$200 ns of uniform discharge, and hence may well be rendered invisible.

To avoid this possibility it was necessary to take time resolved photographs of the discharge. This was done using a fast electro-optic framing camera (Hadland Imacon HE 701) capable of taking 10 ns exposures separated by 47 ns. The

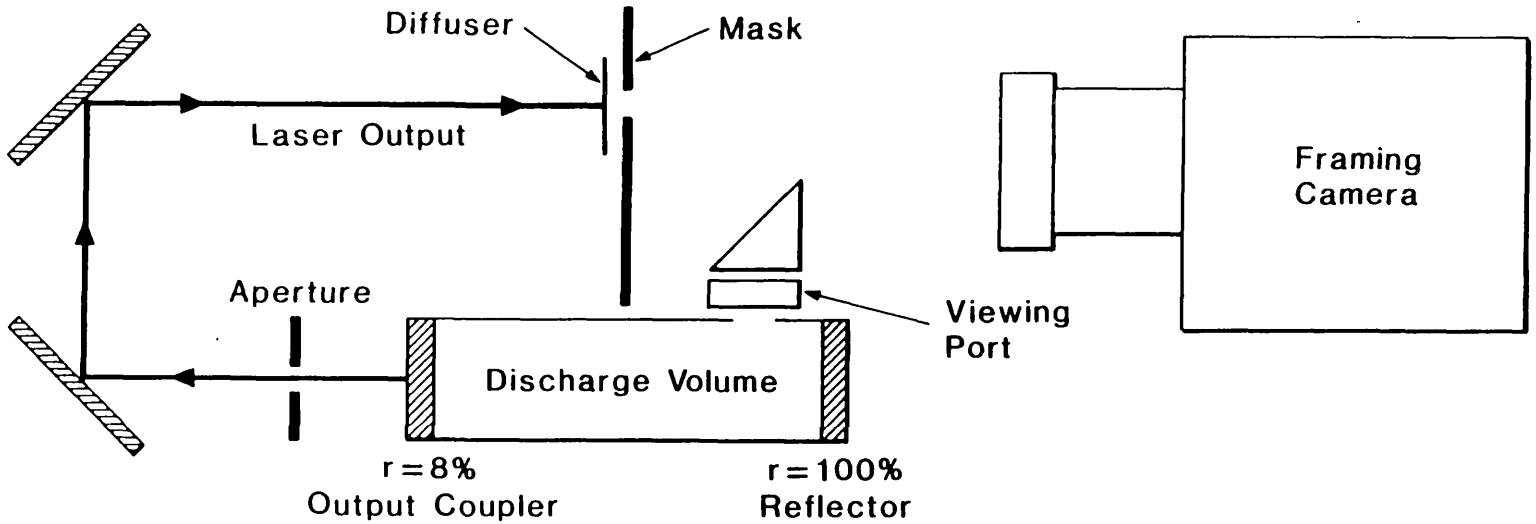

Figure 6.7 Experimental arrangement for framing photographs of laser discharge. Note reflection of laser output beam brought onto diffusing screen with field of view of camera.

experimental arrangement is shown in figure 6.7. A partial reflection of the laser output beam is brought onto a diffusing screen within the field of view of the camera and is used both as a time marker and as a monitor of the laser output intensity. A typical set of exposures is shown in figure 6.8A. They are taken in the order indicated by the white numbers and continue to both left and right of the recorded images corresponding to the relative darkness before the discharge is initiated and after it has finished. The larger of each pair of images is that of the discharge, and the smaller spot beneath it is the laser output marker at that time. The diffuse dark spot towards the bottom of the image of the discharge is due to a camera photocathode defect. Frequent movement of the image on the photocathode ascertained that this concealed no information.

Under all normal operating conditions, using the usual X-ray exposure and laser gas mixture, images similar to those in figure 6.8A were obtained. The discharge precedes the laser output, as expected, and continues to emit some visible radiation after the laser has ceased. Structure of any kind was never seen within the discharge. However, by reducing the X-ray exposure, and hence preionisation electron density, and by increasing the concentration of HCl within the laser gas mixture, structure can be induced.

Using the normal laser gas mixture containing 3 τ of HCl but reducing the X-ray exposure to $\sim$9 mR, slightly below the lasing threshold noted in Chapter 2, the discharge appears as shown in figure 6.8C. Structure within the discharge is clearly visible, and no laser output is observed. However, the non-uniform discharge is sustained for the duration of the electrical excitation without degenerating into arcs or

Figure 6.8 10 ns exposure framing camera photographs of laser discharge taken at 47 ns intervals in the sequence shown in A. The discharge cathode is at the left of the 1" field of view, and the anode off to the right. The smaller spot beneath the discharge is a reflection of the laser output beam, and the diffuse dark spot towards the bottom of the image of the discharge is a photocathode defect. All results shown originate from the double P.F.L. with :-

A - normal gas mixture, (3τ HCl), usual preionisation ($\sim$100 mR).

B - high HCl gas mixture (6 τ HCl), reduced preionisation ($\sim$15 mR).

C - normal gas mixture (3 τ HCl), reduced preionisation ($\sim$9 mR).

D - deliberately induced arc, normal gas mixture (3 τ HCl), no preionisation ($\sim$0 mR).

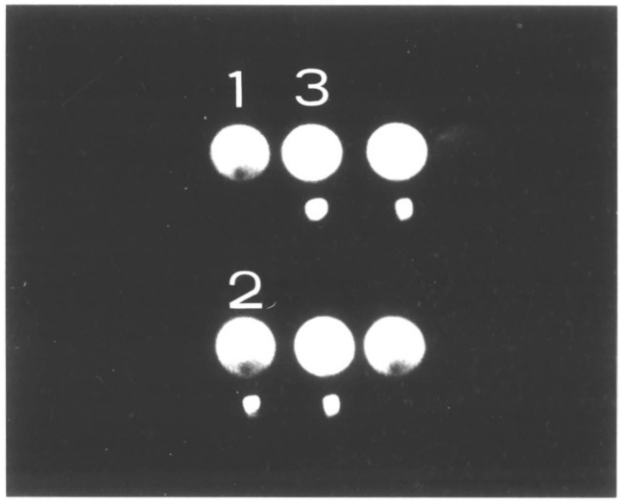

A

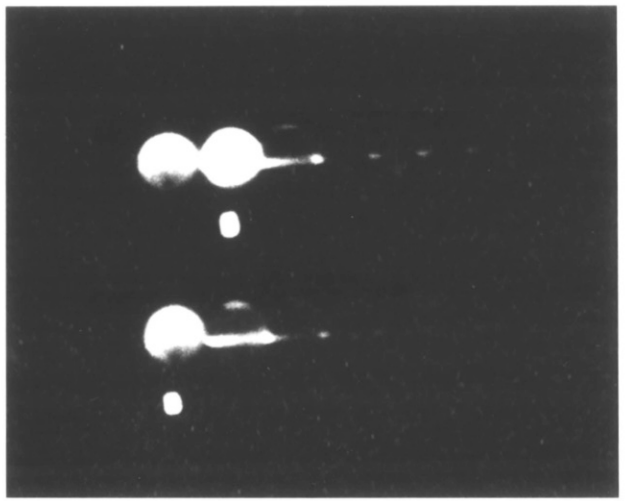

B

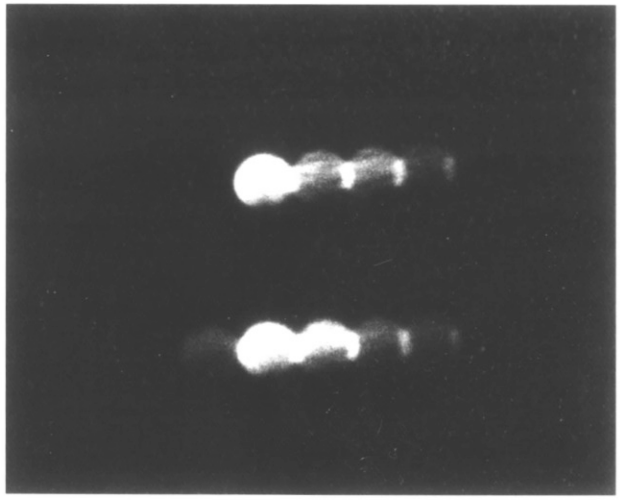

C

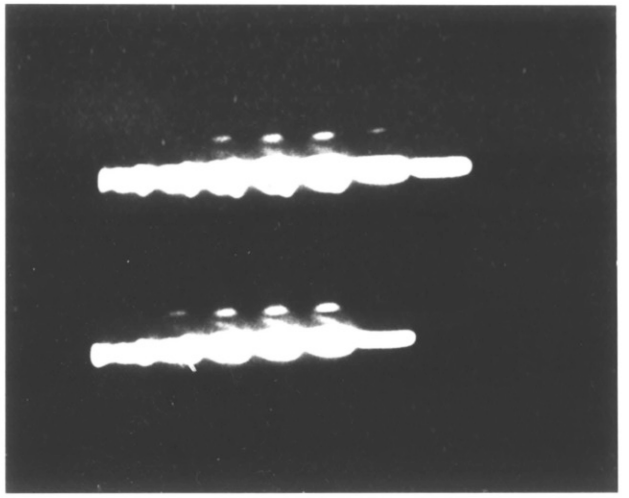

D

very narrow discharge channels.

Using the high partial pressure of HCl of 6 τ and an X-ray exposure of 15 mR, a different discharge is formed, as is shown in figure 6.8B. In this case the discharge initially appears to be uniform, and strong laser output is produced, but, within the 47 ns inter-frame spacing, the discharge dramatically collapses into narrow channels, immediately terminating the laser output. The slight overlap of adjacent images in figure 6.8B doubles the photographic exposures at that point, revealing features too faint to be recorded with a single exposure. This shows that the columnar discharges, which run in the direction between the discharge electrodes, persist for some considerable time. Indeed, both the non-uniform discharge of figure 6.8C and the channel discharge of 6.8B last for a longer period of time than the normal discharge of 6.8A. This indicates a possible difference in energy deposition rate within the discharge plasma. The extreme case is shown in figure 6.8D, where the laser was fired with no preionisation. The resulting arcs continue for a long period of time, greater than the recording time of the framing camera, demonstrating the very low energy deposition and impedance mismatching between the P.F.L. and the low impedance arc channels. The arcs of figure 6.8D were photographed through an attenuation of a factor of approximately one hundred, with respect to the other parts of figure 6.8. This large discrepancy in brightness, in the visible region of the spectrum, between the arcs of figure 6.8D and the channel discharges of figure 6.8B suggests that the two may be essentially different in nature, even though their dimensions are comparable. Further evidence to support this theory is

presented later in this chapter.

While the results of direct observation of the discharge using the framing camera showed that structure and non-uniformities could exist and develop, no such features were observed under normal operating conditions, even when the laser output did terminate prematurely. Indeed, the premature termination could be observed in photographs such as 6.8A, where the laser would extinguish well before the end of an apparently uniform discharge.

Using a fine wire gauze, the spatial resolving power of the framing camera was determined to be better than 200 μm within the discharge region. However, in operation, it necessarily averages over the depth of discharge which is being viewed, in this case ~3 cm. Thus, if features such as those produced in figure 6.8B were to be more closely packed together, it is possible that spatial overlap over the 3 cm depth could render them invisible. Using the framing camera, the unavoidable spatial averaging reduces the sensitivity of the detection system; however, using the following technique, the spatial averaging is used to enhance the detection efficiency.

The second technique used to monitor discharge uniformity employs a dye laser probe beam which is passed through the length of the discharge, slightly off-axis, and is then recorded on film. Any structure or non-uniformities in the discharge will scatter the dye laser beam, and hence any change in the spatial distribution of the beam will provide a measure of such structure. The experimental arrangement is shown in figure 6.9, and consists of a commercial N_2 laser (A.V.C.O. Everett C950) pumping a dye laser made from a R6G dye cell, aperture, and aluminium reflectors. The output from the dye laser is

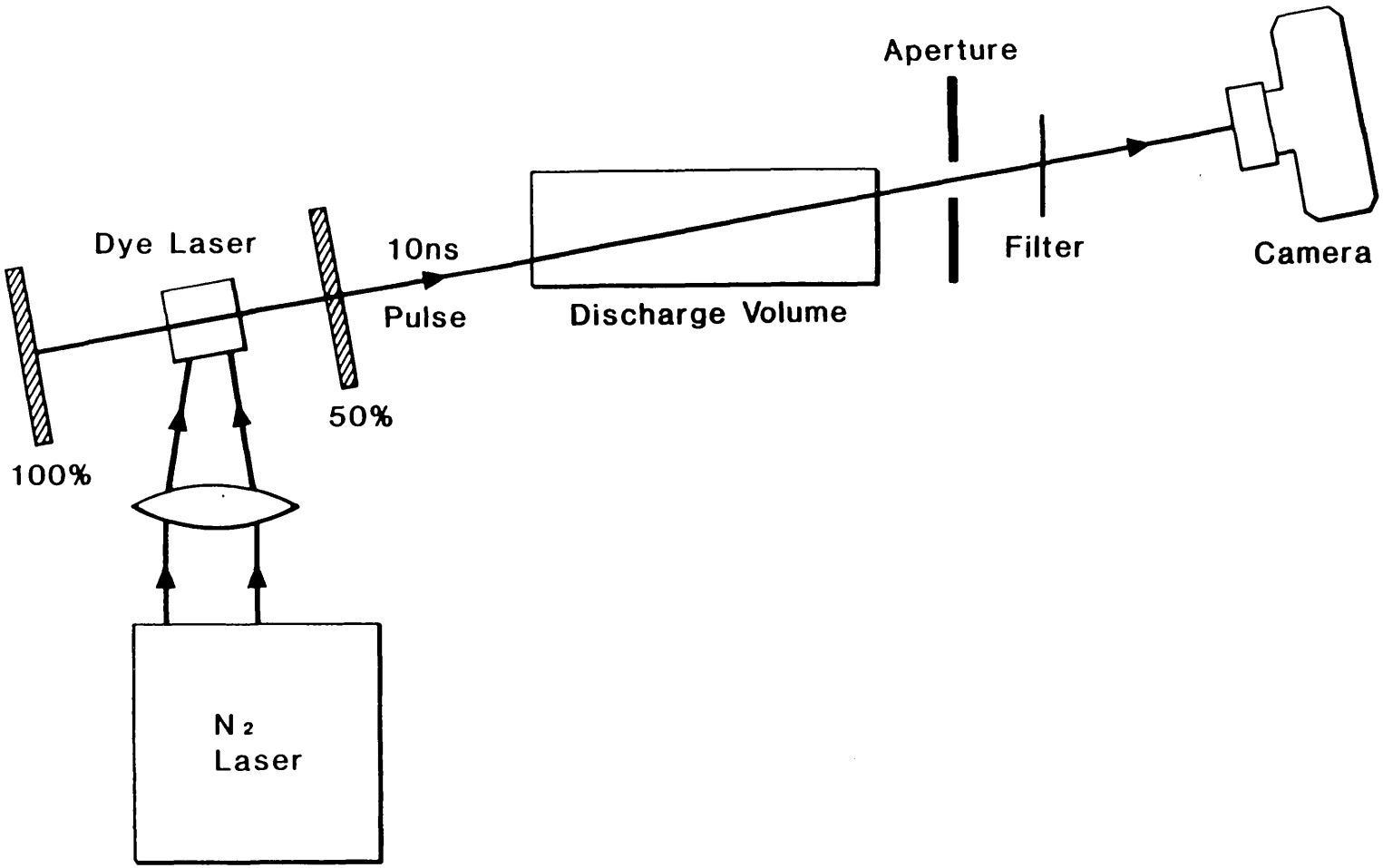

Figure 6.9 Experimental arrangement for dye laser probe beam scattering experiments.

estimated to be of the order of a millijoule, and occurs in a clean, 10 ns F.W.H.M. pulse, very short compared to the excimer laser discharge duration. The beam passes through a 1.5 mm aperture immediately prior to entering the laser discharge volume and emerges as a 2 mm spot. This is recorded directly on monochromatic (Ilford HP5) film placed several metres away, and giving a distribution of $\sim$1 cm on the film. A glass spectral filter is used to attenuate the background light from the laser discharge. It is advantageous to have a highly modulated spatial beam profile from the dye laser as a beam containing much fine structure will be changed more noticably by small angle scatter than will a pure Gaussian beam. The photograph at the top left of figure 6.10 shows the beam profile after passing through the laser chamber containing static laser gas, and the fine structure is clearly visible. With respect to this photograph, the discharge anode is on the left, and the cathode on the right.

If the dye laser passes through the laser gas a few tens of nanoseconds after the discharge has been started, the recorded image is similar to that shown at the top right of figure 6.10. The contrast between the dye laser and the background is somewhat reduced, but the original structure of the dye laser beam remains intact. The time, 35 ns, shown under the photograph, refers to the length of time between the start of the laser output and the passage of the dye laser beam. It was necessary to measure this for every shot as the jitter of the N_2 laser was high ($\pm$ 30 ns). The delay between the discharge initiation and the appearance of the laser output remains constant for a given set of operating conditions, and has a value of $\sim$50 ns for the results shown in figure 6.10, which were obtained from a normal laser gas mixture,

Figure 6.10 Dye laser beam profiles through static excimer laser gas mixture (top left), and through excimer laser discharge at various times after the start of the excimer laser output.

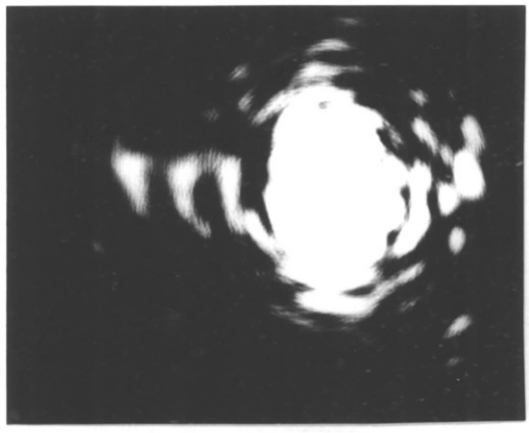

DYE LASER

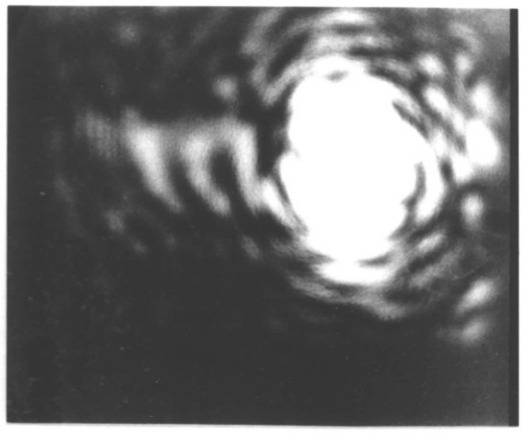

35ns

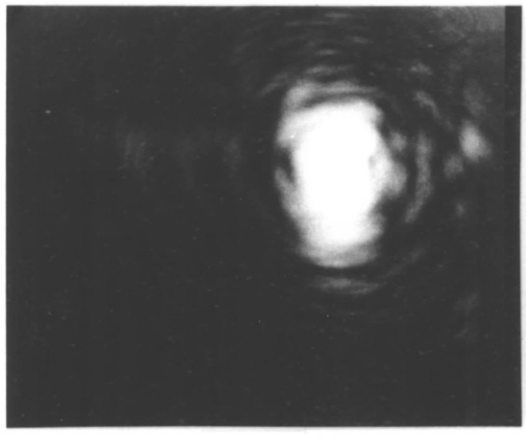

140ns

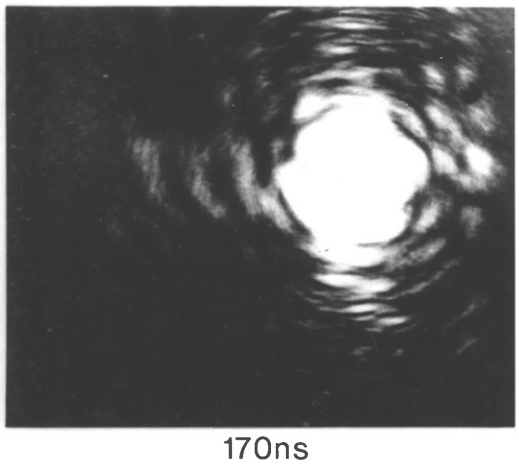

170ns

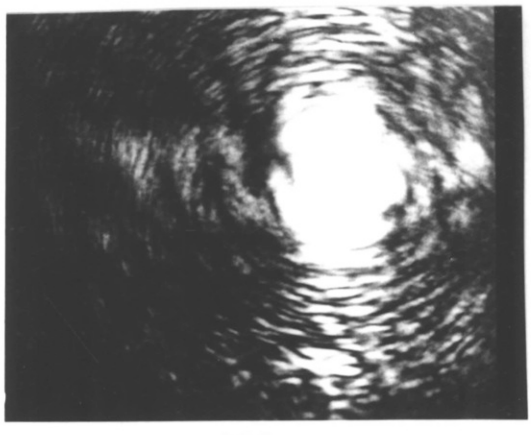

270ns

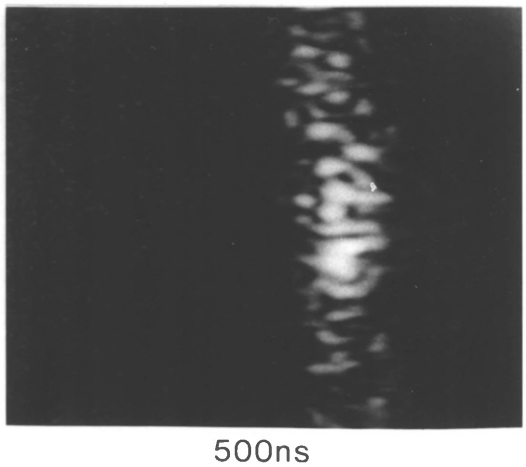

500ns

using the standard degree of preionisation and a 0.28Ω P.F.L. charging voltage of 25 kV. However, if the dye laser beam is delayed by more than 100 ns from the start of the laser output, some change in its structure becomes visible. This is more clearly seen on the negative than on the prints in figure 6.10, but by 170 ns delay the change is quite noticable. The scatter of the dye laser beam becomes greater as the time delay is increased, and by ~500 ns all of its original structure is lost. The light is scattered predominantly in the vertical plane, as would be expected from structure within the discharge running horizontally between the electrodes. These results show that such structure does exist within the discharge, and from a time not later than 100 ns after the start of lasing, even under conditions where the framing camera photographs indicate a completely uniform discharge. Under conditions where structure is visible with the framing camera, the scatter of the dye laser beam occurs earlier, and to a greater extent than shown here. This demonstrates the greater sensitivity of the probe beam scattering technique.

The structure found in the above experiment will scatter the excimer laser beam in the same way as it scatters the probe dye laser beam, and so constitute a loss which increases with time. This will certainly contribute to the termination of the laser, but may not be the major cause. If the observed structure is electrical in origin, it may well also adversely affect the discharge kinetics of XeCl* formation and quenching. The following experiment was designed to detect any change in kinetics between the uniform discharge and the structured discharge.

The third discharge monitoring technique employed

involves measuring the time varying emissions from various species within the laser plasma. In particular, the XeI ($7p\left[5/2\right]_3 \rightarrow 6s\left[3/2\right]_2$ transition at 467.123 nm and the XeII ($6p\,^4D^o_{7/2} \rightarrow 6s\,^4P_{5/2}$) at 484.433 nm. The emissions from these lines have been used previously as an indicator of discharge kinetics, and the reader is referred to the original work for a detailed discussion of the technique[6.7,6.16] as only an outline of the theory will be presented here. Briefly, the population of the upper level of the neutral xenon XeI transition has been found to be approximately proportional to the electron density in the discharge at the current densities used in the present laser system ($\sim$100 A/cm^2). This is commensurate with a single step excitation of this low lying level, although at higher current densities saturation of the population occurs. Therefore, if the cross-sectional area through which the total discharge current flows were to be reduced, at a constant discharge sustaining voltage, the increased electron density within this region will offset the smaller discharge volume and hence there will be little change in the total XeI, 476 nm emission.

In contrast, the upper level of the XeII, 484 nm transition lies some $\sim$ 26 eV above the neutral xenon ground state, and its excitation proceeds, therefore, by a step-wise reaction involving many electrons.* Because of this, the upper state population, and hence emission, is proportional to a high power of the electron density. Therefore, if the discharge cross-section were to decrease as before, the increase in emission from the smaller region of higher electron density would be more than sufficient to offset the smaller discharge volume,

---

* For a full justification of this statement the reader is referred to reference 6.7.

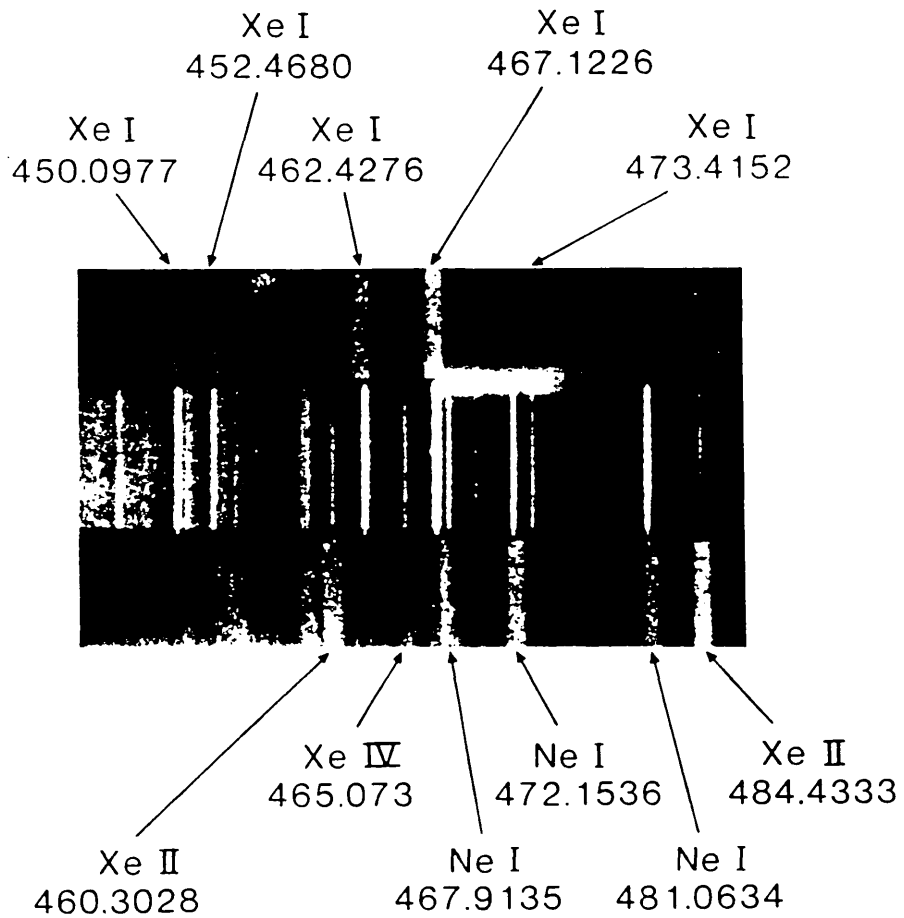

Figure 6.11 Laser fluorescence spectra.

Centre - end-light when excited from long, single P.F.L. where premature termination is apparent.

Top - side-light when excited from shorter, double P.F.L. where no premature termination is observed.

Bottom - as top, but with reduced preionisation.

resulting in an increase in the total XeII, 484 nm emission.

This argument, whilst strictly only justified for the two transitions in question, may be generally, but loosely, applied to all similar transitions originating from either high or low lying excited levels. Thus the XeII line may be typical of many other XeII lines, and likewise for the XeI. Experimental justification for this is given in figure 6.11, which shows three spectra. The central spectrum is that of the end-light emissions from the laser when excited from the long, single, P.F.L. where the laser terminates well before the end of the electrical excitation. The spectrum above this shows the side-light emission from the laser discharge when pumped from the shorter, double P.F.L. under conditions of full preionisation where premature laser termination is not observed. As can be seen, only the low-lying XeI lines are present in this spectrum. The lower spectrum shows the emission observed under similar conditions to the upper, except that the preionisation is reduced to a level corresponding to that in figure 6.8B, where the discharge is visibly unstable. Under these conditions the emission from the XeII lines, and other species with high excitation energies, such as NeI and XeIV, are clearly visible, even on a shorter exposure than the upper spectrum. This shows that the XeI, 476 nm and XeII, 484 nm emissions in particular, and similar lines in general, do indeed give an indication of the discharge character. Furthermore, the central spectrum under conditions of hitherto unexplained premature laser termination, is shown to exhibit features which are not observed in the 'stable' upper spectrum, but which are strongly apparent in the 'unstable' lower spectrum.

The upper and lower spectra of figure 6.11, taken through

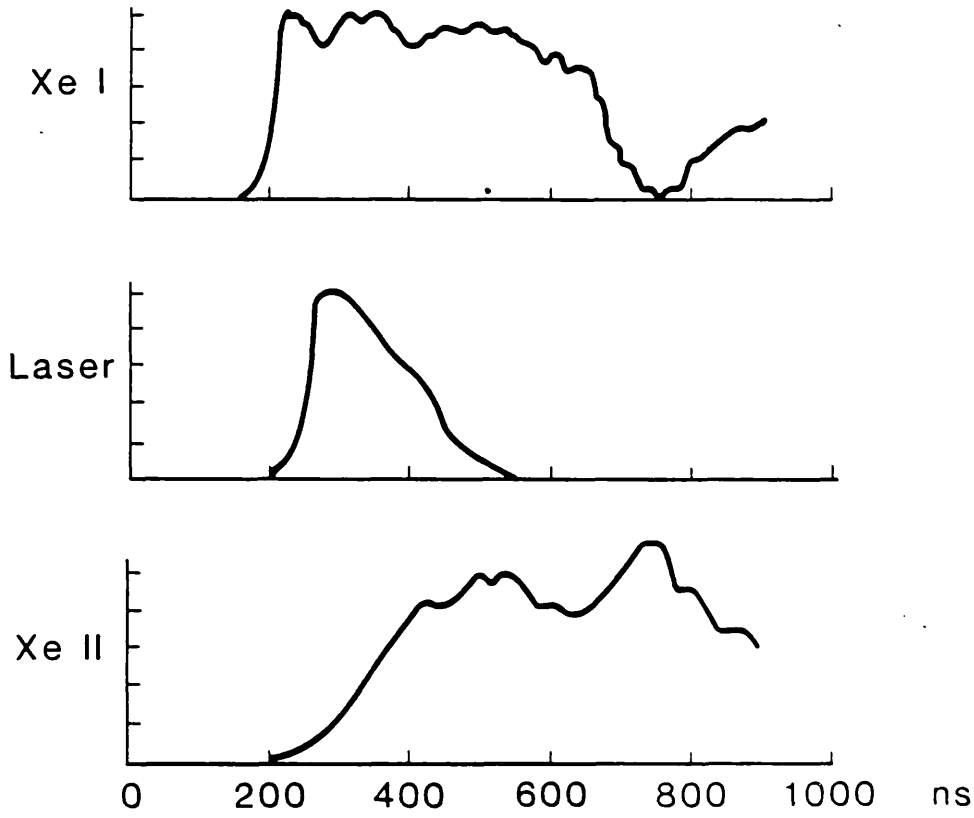

Figure 6.12 The laser output (centre) synchronised with the XeI, 476 nm emission (top) and XeII, 484 nm emission (bottom).

the perspex side-light viewing port, show the same spectral lines as the central end-light spectrum, taken through the quartz output coupler. This shows that fluorescence from the perspex is negligible, and provides a useful check on the reliability of the framing camera observations made through this port.

The time histories of the XeI, 476 nm and XeII, 484 nm emissions were recorded using a Monospek 600 monochromator, EMI TUVP56 photomultiplier and Tektronix 519 oscilloscope. The measurements were taken in end-light, and are displayed in figure 6.12, synchronised with the laser output shown in the centre. These results were taken with the laser pumped from the long, single P.F.L. The XeI emissions follow the electrical excitation quite closely, starting before the laser output and remaining at a fairly constant level until the end of the electrical excitation, long after the end of the laser pulse. In contrast, the XeII emissions increase gradually throughout the duration of the laser pulse, and show some variation at a later stage.

This gradual increase in XeII emissions is unlike the rapid rise observed by Hogan et al[6.7] which was associated with the sudden formation of discrete discharge channels within their resistively ballasted laser, but is commensurate with the relatively slow growth of discharge non-uniformities indicated in the present work by the probe beam scattering experiments. Together these results provide strong evidence of the formation of narrow, columnar, structure within the discharge. Whether this structure corresponds to arcs is, however, doubtful. The greater luminosity of deliberately generated arcs has already been mentioned. Furthermore, it was found in the course of these experiments that the spectrum

of an arc is entirely different from any of those obtained from the laser discharge, whether stable or not. Indeed, over the spectral region covered in figure 6.11, there are no common spectral lines. It is therefore to be concluded that the channel discharges produced in the laser discharge do not constitute what is normally considered as an arc.

6.5 Conclusions and Discussion

The direct observation of the discharge plasma using the framing camera has shown that structured and non-uniform discharges can be produced, and, furthermore, that they can be sustained for some time. Although providing no evidence that such structure is present under normal operating conditions with the usual amounts of preionisation and gas mixture, the results give a strong indication of the form any non-uniformities or instabilities would take.

The results of the dye laser probe beam scattering experiments, however, show that structure does develop under normal operating conditions, from a time not later than 100 ns after the start of the laser output, and that this structure then develops in a relatively slow and gradual manner. Furthermore, the scattering is indicative of horizontal structure between the discharge electrodes in agreement with the previous direct observations of the discharge.

The emissions from the transitions in xenon show that the effective discharge cross-section is collapsing with time at a similar gradual rate to the increase in dye laser scatter.

Taken together, these results provide conclusive proof that the effective cross-section of the laser discharge decreases with time in a non-uniform way. This action reduces the volume of gas being pumped, scatters the resulting laser

radiation, and changes the kinetics of the regions still under electrical excitation. It is a combination of these factors which results in the termination of the laser output.

The cause of the discharge collapse has not been identified, but the strong experimental dependence on HCl concentration indicates that this molecule plays a major role. Removal of the 'hot-spots' on the discharge cathode shown in figure 6.6 would be expected to increase the maximum pulse lengths possible, as would the use of a more suitable very long pulse discharge circuit. Also, the use of higher total gas pressures, and hence lower concentrations of HCl, would be expected to afford some improvement. However, these modifications would not appear to offer the hope of large, order of magnitude, extensions in pulse length. Before this can be achieved, a detailed understanding of the factors governing the stability of the laser discharge is required. The studies published in the literature[6.17,6.18] to date are at odds with many of the experimentally observed facts, and so must be treated with some scepticism. However, a recently developed theory[6.19] may go some way to explaining the discharge behaviour. In simple terms, the theory states that, assuming dissociative attachment to HCl to be the dominant electron loss mechanism, if a region of higher than ambient electron density should occur, then the local HCl population would become locally depleted due to electron dissociative attachment. This would reduce the rate of loss of electrons leading to a still greater local excess of electrons. Hence, a positive feedback loop is established in which increasing electron density and decreasing HCl concentration go hand in hand. Making several approximations, the equation

$$\frac{1}{\tau^2} \sim \tfrac{1}{2} k^2 n [HCl]_0 \qquad (6.1)$$

is obtained where k is the rate coefficient for electron dissociative attachment to HCl, n is the initial electron density in the discharge, $[HCl]_o$ is the initial HCl concentration, and τ is the time taken for the global electron density to double. The authors of this work[6.19] have found a strong correlation between this time, τ , and the time taken for catastrophic instabilities to occur in the resistively ballasted discharge laser of Hogan et al[6.7]. This strong correlation is, at present, justified only by qualitative arguments, and the closeness of the fit of the experimental data presented in reference 6.19 to equation 6.1 is not convincing. Hence, further work is required to test the applicability of this theory. At this stage it is possible to comment that the laser output pulse duration shows a dependence on the partial pressure of HCl, $[HCl]_o$, and electrical excitation rate, n , similar to that predicted by equation 6.1. Furthermore, the commonly observed shorter output pulses from, say, KrF lasers, may be explained by the increased value of the electron attachment rate to the halogen donor, k.

If the above theory is essentially correct, then it places an upper bound on the time for which a stable discharge may be sustained, which may be very difficult to avoid.

CHAPTER 7

CONCLUSIONS AND DISCUSSION

7.1 Introduction

This chapter presents a brief review of the work detailed in this thesis, with the emphasis placed on the results, their relevance, and the conclusions to be drawn from them. The areas worthy of further investigation or development are indicated, together with tentative plans for such work. Various potential applications for excimer lasers are described in section 7.5, and the specifications of the lasers required are outlined. Finally, a summary of the achievements of the present work is given in section 7.6.

The review is divided into three sections, the first dealing with the design and development of the laser system, and the subsequent optimisation of the laser performance. The second summarises the advances made in the area of high electrical efficiency operation, and the third is devoted to the production of extended duration laser output pulses.

7.2 Design and Development

In the design of the X-ray preionisation source, Chapter 2, and discharge circuit, Chapter 3, the careful application of existing technologies has produced a laser system of commendable performance. This performance, together with many laser parameters, is summarised in figure 7.1. It should be noted that several of the maxima shown are not attainable simultaneously.

The X-ray source used to preionise the $\sim$1000 cm^3 active volume was found to produce an average exposure of $\sim$100 mR in a pulse of $\sim$300 ns duration. Studies with the present

Laser Parameters

Active Volume	$< 1150\ cm^3$
Gas Mixture/Pressure	$3\ \tau$ HCl, $15\ \tau$ Xe
	3.5 atm Ne buffer
X-ray exposure	$\sim$100 mR

Laser Performance

Max. Output Energy (1)	4.7J
Max. Pulse Duration (2)(3)	250 ns F.W.H.M.
Max. Electrical Efficiency (4)	3.2%
Peak Power Output (1)	>50 MW
Peak Power Density (1)	$3.7\ MW/cm^2$
Beam Cross-Section (5)	$4.2 \times <3.3\ cm^2$
Beam Uniformity (5)	$\pm$ 3%
Beam Divergence (5)	$\sim$3 mr
Shot to shot variation	<5%
Jitter	<5 ns

Conditions

(1) Pulse Duration 100 ns F.W.H.M., Elec. Eff. 1.9%

(2) Extended P.F.L., low HCl gas mixture, energy $\lesssim$ 1J

(3) 265 ns F.W.H.M. attainable at lower output energies

(4) Output Energy 1.6J

(5) At Output Energies > 1.5J

Figure 7.1

Summary of Laser Performance

laser system have shown that an exposure of only ~ 5 mR in a pulse of ~100 ns would be sufficient to give adequate preionisation for the laser. This would allow a large reduction in the energy stored in the X-ray source, reducing the capital cost and improving the overall system efficiency. The minimum average X-ray exposure giving stable laser action in the present system was found to be ~ 11 mR, somewhat higher than that found by other authors[7.1]. This is probably due, at least in part, to the poorer uniformity of exposure in the present work.

Nevertheless, the X-ray source is capable of providing adequate preionisation over a much larger volume than that used at present and, with the addition of a peaking capacitor or short P.F.L. to the circuit as described in Chapter 2, should be suitable for volumes of up to 50 litres at currently used gas pressures.

For lasers of more modest volume, $\lesssim 1$ litre, a smaller X-ray source is required, and it seems likely that the expense and complication of an e-beam based source will be difficult to justify in this case. For such applications other forms of X-ray generators such as W.I.P. sources[7.2] or B.R.V. sources[7.3] may be more suitable. High efficiency of X-ray generation need not be an important factor if the X-ray source can be incorporated into the discharge circuit in much the same way as the spark array of many commercial U.V. preionised lasers is incorporated into their discharge circuits.

The discharge circuit of the present system has proved capable of supplying sufficient excitation to produce strong laser action throughout the large active volume over prolonged periods of time. The electrical triggering of the Marx bank and X-ray source, and careful design of the 'self-breaking'

rail-gap have produced a system of low-jitter and high reliability which is capable of high efficiency operation.

The maximum laser output energy obtained of 4.7J from a laser gas mixture containing 3 τ HCl, 15 τ Xe and neon buffer to a total pressure of 3.5 atmospheres, was, at the time, the largest produced from an X-ray preionised excimer laser and represents a specific output energy of 4.2 J/l or 1.2 J/l atm. The results presented in chapter 4 show that significantly higher total output energies are to be expected from higher pressures of laser gas. The output beam uniformity is good at $\pm$ 3% over the 4.2 x 3 cm^2 cross-section, and the divergence estimated at ~3 mr.

7.3 High Efficiency Operation

Due to careful design of the discharge circuit, the detrimental effects of the large difference between the discharge initiation voltage and the discharge sustaining voltage have been minimised, allowing highly efficient laser operation to be obtained. We have demonstrated the operation of a simple, passive, 'peaking' line to produce transient voltage gain between the discharge electrodes before the plasma forms without reflecting the stored electrical energy. This system has been shown to produce very good results, although its operating range is rather restricted due to the characteristics of the rail-gap switch. The maximum efficiency obtained of 3.2% compares very favourably with the highest yet achieved of 4.2% from a higher pressure (5 bar) of laser gas[7.4]. The intrinsic efficiency of the laser has been estimated at ~ 4%, and this too may be expected to increase with increasing laser gas pressure. However, due to the operating characteristics of the rail-gap and the inductance

of the laser head, this high-efficiency operation has been possible only at relatively low output energies (<2J). Triggering the rail-gap switch either electrically or using a laser should improve the operating range. The use of an external 'spiker' circuit to produce rapid laser discharge initiation and commutation of the rail-gap has already been demonstrated by other workers[7.4] to lead to a large extension of the switch operating parameters, allowing high efficiencies to be obtained at higher output energies. Such techniques represent the 'state of the art' in laser switching technology and, despite their relative complexity, may become commonplace unless an alternative high-power transfer, low inductance, low-jitter switch can be found. At present, the rail-gap is unparallelled in its simplicity, high voltage and current capability and potentially low inductance. These properties make it the automatic choice for large, 'single-shot', laser systems. However, for smaller systems, the rapidly developing technology of magnetic switching using saturable inductors [7.5,7.6] has advantages in terms of longevity and repetition rate while delivering an adequate performance in other respects, although at a greater capital cost than the rail-gap. It is too early to predict whether magnetic switching will eventually replace the thyratrons and spark-gaps of conventional lasers. Magnetic pulse compression, however, seems assured of a place in lasers of the future. By temporally compressing the energy which is to be fed to the laser discharge, it is possible to attain the required input power whilst performing the primary switching at much reduced power levels[7.7]. Such switching is now within the capabilities of semiconductor devices, and all solid-state laser power supplies have already been demonstrated on a small scale[7.7]. It is likely that further

development of both the magnetic compression stage and of the semiconductors themselves will soon provide sufficient power to run excimer lasers of a few hundred millijoules output energy.

Used in conjunction with conventional rail-gap switching techniques, magnetic pulse compression may possibly be used to provide the very high electrical excitation rates which today are only possible using an electron beam. This offers the possibility of discharge pumped lasers of higher power and shorter wavelength than are possible at present.

7.4 Long Pulse Operation

Using a simple modification to the discharge circuit, laser output pulses of up to 250 ns F.W.H.M. and 315 ns base width (@ 10% points) have been produced at energies of the order of one Joule. This represents the longest pulse duration yet achieved from a high power avalanche discharge pumped excimer laser. Extension of these pulses to 265 ns F.W.H.M. has been demonstrated using a higher 'Q' optical cavity, but at the expense of output energy. Once again, the evidence presented in chapter 6 indicates that longer duration output pulses should be possible using a higher total pressure of laser gas, but with a reduced partial pressure of HCl.

Although the modified discharge circuit produces current and voltage waveforms which are less than ideal for the production of long duration output pulses, they are sufficient to reveal some interesting and informative behaviour, demonstrating the premature termination of the laser output pulse. The output pulse shape, duration and position in time have been shown to be strongly dependent on the partial pressure

of the halogen donor molecule, HCl, and on the electrical excitation rate.

The observed premature termination of the laser output has been investigated using the following techniques:

1. Time integrated and time resolved photography of the laser discharge.
2. Probe beam scattering within the discharge.
3. Time integrated and time resolved observation of the emissions from various atomic and ionic species within the laser gas mixture.

and has been found to be caused by the gradual collapse of the uniform laser discharge into a series of narrow columnar discharges running between the electrodes. These lead to scatter of the laser radiation and to non-uniform, and possibly inefficient, formation of the excimer species.

The cause of the collapse of the discharge has not yet been identified, although its dependence on several parameters has been noted. Until the mechanism is understood it is difficult to predict whether significant advances in laser output pulse duration will be made.

A mechanism has been suggested recently[7.8] which links the local depletion of the halogen donor molecule with the local increase in electron density and indicates that a positive feedback loop between these two factors could lead to discharge instability. Work is under way to test the predictions of this model.

7.5 Applications

The high power and short wavelength of excimer lasers has led to their application in several areas, notably in the pumping of dye lasers. However, in many other areas of their

potential application they are let down by their other properties, either their broad bandwidth or their poor beam quality. The present laser system offers the possibility of improvements in both of these areas.

The broad bandwidth of excimer lasers is inherent in the structure of the excimers, as described in chapter 1, and therefore very strong spectral filtering is required if narrow linewidth operation is to be achieved. This has proved difficult in the past, due to the short laser gain duration, and hence limited number of cavity round trips. However, with the longer gain time of the present, and other recently developed systems, the increased number of cavity round trips has allowed single longitudinal mode operation to be achieved[7.9], although this has involved a great deal of effort and produced an output energy much less than that obtained in broadband emission.

It is debatable whether the narrow-bandwidth excimer laser with all its inherent complication is more attractive than a simple narrow-bandwidth frequency double dye laser amplified in the excimer[7.10]. The latter technique, however, has the disadvantage that the gain of the excimer is usually so high that frequency selective components are still required to suppress lasing at other wavelengths. Work is planned at present to demonstrate narrow bandwidth operation using a frequency doubled dye laser injected into an excimer laser cavity employing a phase conjugating, narrow-bandwidth S.B.S. reflector. This should also have the advantage of improving the spatial quality of the output beam.

The extended gain duration of the present system also offers possibilities of passive modelocking, and hence short pulse production. Pulses as short as $\gtrsim 300$ ps have been

generated by this technique[7.11], but this is still much greater than the bandwidth limit, and the rapid shortening of subsequent pulses which is indicative of modelocking has seldom been observed. It is possible that the relative failure of passive modelocking attempts has been due to the poor matching of the absorber and laser gain dynamics, and that a more suitable combination may give drastically improved results. However, once again, the mode-locked excimer laser must be compared both in performance and complication with the excimer-amplified, frequency-doubled dye laser counterpart.

The relatively poor beam quality of excimer lasers is due to both the low 'Q' of the optical cavities employed and to the restricted number of cavity round-trips possible in the short laser gain time. The extended gain duration of the present system offers the possibility of more round-trips and hence improved beam quality. Alternatively, the beam divergence may be decreased by using unstable optics[7.12], or by amplifying a high quality injected beam. This could be derived from a separate laser, perhaps a frequency doubled dye, or from a low power, high Q cavity oscillator arrangement around part of the excimer laser active volume.

Improving the beam quality in these ways should lead to the application of excimer lasers in one of their most promising areas, namely that of photo-lithography and material ablation.

The use of a form of photo-lithography to replace the tortuous process of e-beam writing of semiconductor chips is becoming more common. However, the form of photolithography used involves the exposure of photoresist to ultra-violet light projected through a mask, and the subsequent etching of both the photo-resist and the material beneath it. Thus, this

method of 'wet' processing involves several steps, and is time consuming. However, if a higher power U.V. source is used, such as an excimer laser, the use of photoresist and etching can be avoided as the radiation itself will be sufficient to directly remove layers of material. Excimer lasers are ideally suited to this application for several reasons. Firstly, their relatively short output pulse duration means that the 'dry' processing is carried out in a few hundred nanoseconds, thereby easing problems of target stability and, indeed, allowing the wafer to be processed whilst moving past the laser on a 'conveyor-belt'. Furthermore, the short wavelength of the excimer laser radiation allows greater resolution with line widths of < 1μm being possible. In this application, the relatively broad-bandwidth of the excimer laser is an advantage, as it reduces the unwanted coherence effects produced by other lasers. For optimum resolution the shortest wavelength should be used, and for this reason excimers such as ArF (193 nm) are to be favoured over XeCl (308 nm). To date, however, the great advances in XeCl laser performance produced by X-ray preionisation have not been matched by similar advances in the performance of the rare gas fluoride excimer lasers. This may be a result of the larger electron attachment coefficient to F_2, which could lead to a less stable discharge. Further work into the stability of F_2 containing discharges is required before any prediction of the likely improvements in ArF, KrF and XeF laser performance can be made. A further point of concern for photolithography is the positioning of the mask. This can be placed close to the semiconductor itself[7.13], but is then subject to the full laser power, and hence is liable to damage. Alternatively, it may be placed in a region of low laser flux, and the beam

subsequently amplified, taking care to preserve the spatial quality, possibly by the use of phase conjugating optics, before being directed onto the target via an imaging system. This 'projection photo-etching' has recently been demonstrated in a simple non-amplifying system[7.14,7.15]. The energies required to achieve single shot processing of an entire semiconductor wafer are, at present, only attainable at the XeCl wavelength, but similar energies at shorter wavelengths will probably become possible in the near future. However, the single shot annealing of an entire wafer which is not so wavelength sensitive, is already possible using the largest XeCl lasers.

The third major advantage of using excimer lasers for photolithography concerns the way in which the target material is removed, and is also of significant interest for the medical applications of the lasers.

When using conventional visible or infra-red lasers to remove material, the incident radiation is absorbed by the target and causes local heating. This eventually 'boils away' material in the immediate vicinity but, being a thermal process, and hence relatively slow, seriously overheats the surrounding area. This creates a damaged region, extending several microns from the centre of the laser beam, and has severe consequences, both for semiconductor manufacture and delicate human surgery. Using radiation of a sufficiently short wavelength, however, the material can be removed in a different way. Each photon of the incident radiation has sufficient energy to break the molecular bonds of the target material, and to impart a significant amount of kinetic energy to the constituent parts of the molecule. Thus the material is removed by a chemical rather than thermal process, producing

much less damage to the surrounding material or tissue. Such techniques have been used to demonstrate incisions of sub-micron dimensions in the cornea of the eye with much less damage to the surrounding area than that caused by a visible laser, or a traditional steel or diamond scalpel[7.16]. With the development of optical fibres capable of transmitting the high peak power ultra-violet radiation many other areas of internal surgery, in particular laser angioplasty, are now possible, using excimer lasers[7.17, 7.18]. However, concern still exists over the possible carcenogenic effects of the ultra-violet radiation, although it is expected that this may be restricted to certain wavelength regions only[7.19].

While lasers of sufficient power for the foregoing applications either exist at present or are expected to be built within the next few years, the often cited application of excimer lasers to laser fusion[7.20] and laser isotope separation[7.21] require powers far in excess of that which is currently available in a discharge pumped system. However, X-ray preionisation has been shown to offer great scaling potential, and lasers of $\sim$1 kJ output pulse energy are currently planned[7.22].

7.6 Summary

In short, the aims of the present work have been the following:

i) To demonstrate the efficacy of using X-rays to preionise an XeCl laser.

ii) To preionise a larger volume than can be achieved using U.V. preionisation, and hence extract larger energies.

iii) To achieve good uniformity of preionisation, leading to good beam quality, improved discharge stability and hence longer duration laser output pulses.

iv) To improve the overall electrical efficiency compared to conventional excimer lasers.

All of these goals have been accomplished, and the studies undertaken have led to confident predictions of further improvements in all areas. Advances of orders of magnitude in output pulse energy are possible at electrical efficiencies of perhaps 5%. However, while methods of further extending the laser output pulse duration have been indicated, it does not seem likely that these will result in extensions to more than $\sim$400 ns F.W.H.M. at the present specific output powers.

REFERENCES

1.1 W.N. Hartley, H. Ramage, R. Dublin Soc. Trans., 7, 339 (1901)

1.2 S. Mrozowski, Z. Phys., 76, 38 (1932)

1.3 F.G. Houtermans, Helv. Phys. Acta., 33, 933 (1960)

1.4 N.G. Basov, V.A. Danilychev, Yu. M. Popov, Sov. J. Quant. Elec., 1, 18 (1971)

1.5 C.A. Brau, J.J. Ewing.
Appl. Phys. Lett., 27, 350 (1975)
Appl. Phys. Lett., 27, 435 (1975)

1.6 M.G. Golde, B.A. Thrush. Chem. Phys. Lett., 30, 101 (1974)

1.7 J.E. Velazco, D.W. Setzer, J. Chem. Phys., 62, 1990 (1975)

1.8 M.J. Shaw, Prog. Quant. Elec., 6, 3 (1979), and references therein

1.9 M.H.R. Hutchinson, Appl. Phys., 21, 95 (1980)

1.10 'Excimer Lasers', ed. C.K. Rhodes, Springer-Verlag, Berlin (1979)

1.11 L.A. Levin, S.E. Moody, E.L. Klosterman, R.E. Center, J.J. Ewing, I.E.E.E. J. Quant. Elec. QE-17, 2282 (1981)

1.12 H. Hokazono, K. Midorikawa, M. Obara, T. Fujioka. J. Appl. Phys., 56, 680 (1984)

1.13 W.L. Nighan, F.K. Tittel, W.L. Wilson, Jr., N. Nishida, Y. Zhu, R. Sauerbrey. Appl. Phys. Lett., 45, 947 (1984)

1.14 R. Sauerbrieg, Y. Zhu, F.K. Tittel, W.L. Wilson, Jr., N. Nishida, F. Emmert, W.L. Nighan, I.E.E.E. J. Quant. Elec., QE-21, 418 (1985)

1.15 C.A. Brau, J.J. Ewing. J. Chem. Phys., 63, 4640 (1975)

1.16 A.E. Siegman, An Introduction to Lasers and Masers. McGraw Hill, New York (1971)

1.17 M.H.R. Hutchinson, Appl. Opt., 19, 3883 (1980)

1.18 A.J. Kearsley, D. Phil. Thesis, University of Oxford (1980)

1.19 Y. Kawamura, N.Ikegami, K. Toyoda, Paper at 3rd Keio-Riken Symposium on High Efficiency Gas Lasers, Keio University, Japan (1984)

1.20 C.B. Edwards, Ph.D. Thesis, University of London (1978)

1.21 M.R.O. Jones, Ph.D. Thesis, University of London (1981)

1.22 Rutherford Appleton Laboratory, Annual Report (1984)

1.23 A.J. Mendelsohn, R. Normandin, S.E. Harris, J.F. Young. Appl. Phys. Lett., 38, 603 (1981)

1.24 C.P. Christensen, R.W. Waynant, B.J. Feldman. Appl. Phys. Lett., 46, 321 (1985)

1.25 J.S. Townsend, The Theory of Ionisation of Gases by Collision. Constable & Co. Ltd., London (1910)

1.26 J.A. Rees, Electrical Breakdown in Gases. Macmillan, London (1973)

1.27 H. Raether, Z. fur Phys., 112, 464 (1939)

1.28 H. Raether, Arch. fur Electrotechnik, 34, 49 (1940)

1.29 J.M. Meek, The Physical Review, 57, 722 (1940)

1.30 J.M. Meek, J.D. Craggs, Electrical Breakdown of Gases. Clarendon Press, Oxford (1953)

1.31 F. Llewellyn Jones, A.B. Parker. Proc. Roy. Soc. A213, 185 (1952)

1.32 J. Dutton, W.T. Morris. Brit. J. Appl. Phys., 18, 1115 (1967)

1.33 A.J. Palmer, Appl. Phys. Lett., 25, 138 (1974)

1.34 J.I. Levatter, S.C. Lin. J. Appl. Phys., 51, 210 (1980)

1.35 L.E. Kline, L.J. Denes, J. Appl. Phys., 46, 1567 (1975)

1.36 R.R. Butcher, T.S. Fahlen, Paper ThP3, Conf. on Lasers and Electro-Optics, Anaheim, California (1984)

1.37 G.J. Ernst, Paper TUB22, Conf. on Lasers and Electro-Optics, Anaheim, California (1984)

1.38 A.J. Kearsley et al. Opt. Comm., 31, 181 (1979)

1.39 O.R. Wood, Proc. I.E.E.E., 62, 355 (1974)

1.40 R.S. Taylor, A.J. Alcock, K.E. Leopold. Opt. Lett., 5, 216 (1980)

1.41 G. Marowski, Max Planck Institut, Göttingen. Private Comm. (1985)

1.42 G.L. Clark, Applied X-rays, McGraw Hill, New York (1955)

1.43 S. Sumida, M. Obara, T. Fujioka, Appl. Phys. Lett., 33, 913 (1978)

1.44 Report No. NRTC-77-43R, Northrop Corp., Hawthorne, California (1977)

1.45 M. Casey, P.W. Smith, M.H.R. Hutchinson, Rev. Sci. Inst., 54, 458 (1983)

1.46 A. Javan, J.S. Levine, I.E.E.E. J. Quant. Elec., QE-8, 827 (1972)

1.47 P.W. Smith, Univ. of St. Andrews, Private Comm. (1985)

1.48 M.R. Osborne, P.W. Smith, M.H.R. Hutchinson. Paper VI National Quant. Elec. Conf., Univ. Sussex (1983)

1.49 M.R. Osborne, P.W. Smith, M.H.R. Hutchinson. Opt. Comm., 52, 415 (1985)

1.50 M.R. Osborne, P.W. Smith, M.H.R. Hutchinson. Paper ThP4, Conf. on Lasers and Electro-Optics, Anaheim, California (1984)

1.51 M.R. Osborne, M.H.R. Hutchinson. Submitted to J. Appl. Phys. (1985)

REFERENCES

2.1 S. Sumida, M. Obara, T. Fujioka. Appl. Phys. Lett. 33, 913 (1978)

2.2 S.C. Lin, Z. Bao, G. Gong, Y. Huo, J. Shu, S. Tang, Y. Wei, C. Zhang. Appl. Phys. Lett. 38, 328 (1981)

2.3 S.C. Lin, J.I. Levatter. Appl. Phys. Lett. 34, 505 (1979)

2.4 H. Hokazono, K. Midorikawa, M. Obara, T. Fujioka. J. Appl. Phys. 56, 680 (1984)

2.5 H. Shields, A.J. Alcock, R.S. Taylor. Appl. Phys. B, 31, 27 (1983)

2.6 R.D. Evans in Radiation Dosimetry, Vol. I, 2nd Edn., ed. F.H. Attix, W.C. Roesch. Academic Press, New York (1968)

2.7 G.L. Clark, Applied X-rays, McGraw-Hill, New York (1955)

2.8 P.E. Dyer, D.N. Raouf, Opt. Comm., 53, 36 (1985)

2.9 L.E. Kline, L.J. Denes, J. Appl. Phys., 46, 1567 (1975)

2.10 H. Bichsel in Radiation Dosimetry, Vol. I, 2nd Edn., ed. F.H. Attix, W.C. Roesch. Academic Press, New York (1968)

2.11 G.J. Rowein, Laser Focus, 16, 70 (1980)

2.12 J.C. Martin, Report SSWA/JCW/704/49, A.W.R.E. Aldermaston, U.K.

2.13 J.C. Martin, Report SSWA/JCM/759/193. A.W.R.E. Aldermaston, U.K.

2.14 L.V. Spencer, Energy Dissipation by Fast Electrons, N.B.S. Monograph 1 (1959)

2.15 A.T. Nelms, Energy Loss and Range of Electrons and Positrons, N.B.S. Circular 577 (1956)

2.16 M.L. Sentis, B.L. Fontaine, B.M. Forestier, Paper at 5th Gas Flow and Chemical Lasers Conf., Oxford (1984)

2.17 C.R. Tallman, I.J. Bigio, Appl. Phys. Lett. 42, 149 (1983)

2.18 J.I. Levatter, R.L. Sandstrom, J.H. Morris, Paper at 4th I.E.E.E. Pulsed Power Conference, Albuquerque, New Mexico (1983).

REFERENCES

3.1 Ch. Brau in 'Excimer Lasers', Ed. Rhodes. Topics in applied physics, No. 30, Springer Verlag, Berlin (1978)

3.2 J.I. Levatter, K.L. Robertson, S.C. Lin. Appl. Phys. Lett., 39, 297 (1981)

3.3 H.H. Skilling, Electric Transmission Lines. McGraw Hill, London (1951)

3.4 I.A.D. Lewis, F.H. Wells, Millimicrosecond Pulse Techniques. Pergamon Press, London (1954)

3.5 J.D. Craggs, J.M. Meek. High Voltage Laboratory Technique. Butterworths, London (1954)

3.6 B.I. Bleaney, B. Bleaney. Electricity and Magnetism, 3rd Edn. Oxford University Press (1976)

3.7 W.H. Long, Jr., M.J. Plummer, E.A. Stappearts, Appl. Phys. Lett., 43, 735 (1983)

3.8 M.R. Osborne, P.W. Smith, M.H.R. Hutchinson, Opt. Comm., 52, 415 (1985)

3.9 J.C. Martin, Report SSWA/JCM/704/49. A.W.R.E., Aldermaston, England.

REFERENCES

4.1 M. Casey, P.W. Smith, M.H.R. Hutchinson. Rev. Sci. Inst. 54, 458 (1983)

4.2 e.g. Lambda Physik EMG 101, r = 2.5

4.3 H. Shields, A.J. Alcock. Opt. Comm. 42, 128 (1982)

4.4 H. Shields, A.J. Alcock, R.S. Taylor. Appl. Phys. B. 31, 27 (1983)

4.5 W.L. Nighan, R.T. Brown. Appl. Phys. Lett. 36, 498 (1980)

4.6 H. Shields - private communication

4.7 G.L. Clark, Applied X-rays, McGraw-Hill, New York (1955)

4.8 J.I. Levatter, S.C. Lin. J. Appl. Phys., 51, 210 (1980)

4.9 A.J. Palmer, Appl. Phys. Lett., 25, 138 (1974)

4.10 H. Shields, A.J. Alcock. Opt. Comm., 42, 128 (1982) and references therein

4.11 C.R. Tallman, I.J. Bigio. Appl. Phys. Lett., 42, 149 (1983)

4.12 C.S. Lin et al. Appl. Phys. Lett., 38, 328 (1981)

4.13 J.I. Levatter, K.L. Robertson, S.C. Lin. Appl. Phys. Lett., 39, 297 (1981)

4.14 L.F. Champagne, A.J. Dudas, B.L. Wexler. Postdeadline paper Th R8-1. Conf. on Lasers and Electro-Optics, Anaheim, California, June 1984

4.15 M.R.O. Jones - Ph.D. Thesis, University of London (1981)

4.16 M. Casey, Ph.D. Thesis, University of London (1982)

4.17 R.S. Taylor, P.B. Corkum, S. Watanabe, K.E. Leopold, A.J. Alcock, I.E.E.E. J. Quant. Elec. QE-19, 416 (1983)

4.18 See, for example, 'Quantum Electronics, 2nd Ed.'. A. Yariv, John Wiley or any other Modern Optics text

4.19 Mr. Mitchell, Electro-Optic-Design, Basildon, U.K.

REFERENCES

5.1 F. Kanari, M. Obara, T. Fujioka. J. Appl. Phys. 53, 1 (1982)

5.2 T.H. Johnson, A.M. Hunter II. J. Appl. Phys. 51, 2406 (1980)

5.3 See for example Questek Inc.'s technical notes

5.4 Ch. A. Brau in 'Excimer Lasers', Ed. Ch. K. Rhodes. Topics in Applied Physics No. 30. Excimer Lasers, Springer-Verlag, Berlin, 1979

5.5 J.C. Martin, Report SSWA/JCM/704/49. A.W.R.E., Aldermaston

5.6 R.S. Taylor, P.B. Corkum, S. Watanabe, K.E. Leopold, A.J. Alcock. I.E.E.E. J. Quant. Elec., QE-19, 416 (1983)

5.7 W.H. Long, Jr., M.J. Plummer, E.A. Stappearts, Appl. Phys. Lett., 43, 735 (1983)

5.8 J.I. Levatter, K.L. Robertson, S.C. Lin, Appl. Phys. Lett., 39, 297 (1981)

5.9 C.H. Fisher, M.J. Kushner, T.E. DeHart, J.P. McDaniel, J.J. Ewing, Postdeadline Paper ThR9-1, Conference on Lasers and Electro-Optics, Anaheim, California (1984)

5.10 B.L. Wexler, Private Communication. Naval Research Labs., Washington, D.C., 1984

5.11 R.S. Taylor, K.E. Leopold, Paper ThP3. Conference on Lasers and Electro-Optics, Anaheim, California (1984)

5.12 R.R. Butcher, T.S. Fahlen, Paper ThP1, Conference on Lasers and Electro-Optics, Anaheim, California (1984)

5.13 K. Noda, T. Shimada, M. Obara. Conference on Lasers and Electro-Optics, Baltimore, Maryland (1985)

5.14 W.S. Melville, Proc. I.E.E., London, Vol. 98, Pt. 3, 185 (1951).

REFERENCES

6.1 R. Burnham, N.W. Harris, N. Djeu, Appl. Phys. Lett., 28, 635 (1977)

6.2 T.J. McKee, B.P. Stoicheff, S.C. Wallace, Appl. Phys. Lett., 30, 278 (1977)

6.3 See Ch. A. Brau in 'Excimer Lasers', Topics in applied Physics, No. 30, Springer-Verlag, Berlin (1979) and references therein

6.4 R.S. Taylor, S. Watanabe, A.J. Alcock, K.E. Leopold, P.B. Corkum, I.E.E.E. J. Quant. Elec., QE-17, 82 (1981)

6.5 S. Watanabe, A. Endoh, Appl. Phys. Lett., 41, 799 (1982)

6.6 R.C. Sze, P.B. Scott. J. Appl. Phys., 47, 5492 (1976)

6.7 D.C. Hogan, D. Phil. Thesis, University of Oxford (1983)

6.8 D.C. Hogan, A.J. Kearsley, R. Bruzzese, C.E. Webb, J. Physique, 45, 1449 (1985)

6.9 S.C. Lin, J.I. Levatter, Appl. Phys. Lett., 34, 505 (1979)

6.10 J.I. Levatter, K.L. Robertson, S.C. Lin, Appl. Phys. Lett., 39, 297 (1981)

6.11 M.R. Osborne, P.W. Smith, M.H.R. Hutchinson, Paper ThP4, Conf. on Lasers and Electro-Optics, Anaheim, California, June, 1984

6.12 R.S. Taylor, K.E. Leopold, Paper ThQ1, Conf. on Lasers and Electro-Optics, Baltimore, Maryland, May, 1985

6.13 H. Hokazono, K. Midorikawa, M. Obara, T. Fujioka, J. Appl. Phys., 56, 680 (1984)

6.14 R.S. Taylor, P.B. Corkum, S. Watanabe, K.E. Leopold, A.J. Alcock, I.E.E.E. J. Quant. Elec. Q.E.-19, 416 (1983)
and references therein

6.15 M.R. Osborne, M.H.R. Hutchinson. In press

6.16 D.C. Hogan, R. Bruzzese, A.J. Kearsley, C.E. Webb, Topical Meeting on Excimer Lasers, Incline Village, Nevada, Jan. 1983

6.17 R.T. Brown, W.L. Nighan. Appl. Phys. Lett., 32, 730 (1978); Appl. Phys. Lett., 35, 142 (1979)

6.18 J.D. Daugherty, J.A. Mangano, J.H. Jacob, Appl. Phys. Lett., 28, 581 (1976)

6.19 J. Coutts, C.E. Webb. In press.

REFERENCES

7.1 C.R. Tallman, I.J. Bigio, Appl. Phys. Lett. 42, 149 (1983)

7.2 J.I. Levatter, R.L. Sondstrom, J.H. Morris, Paper at 4th I.E.E.E. Pulsed Power Conf., Albuquerque, New Mexico (1983)

7.3 J.N. Fox, J.E.G. Wheaton, J. Phys. E, 6, 655 (1973)

7.4 W.H. Long, Jr., M.J. Plummer, E.A. Stappearts, Appl. Phys. Lett., 43, 735 (1983)

7.5 C.H. Fisher, M.J. Kushner, T.E. DeHart, J.P. McDaniel, J.J. Ewing, Postdeadline Paper ThR9-1, Conf. on Lasers and Electro-Optics, Anaheim, California (1984)

7.6 R.S. Taylor, K.E. Leopold, Paper ThP3. Conf. on Lasers and Electro-Optics, Anaheim, California (1984)

7.7 K. Noda, T. Shimada, M. Obara. Conf. on Lasers and Electro-Optics, Baltimore, Maryland (1985)

7.8 J. Coutts, C.E. Webb. To be published

7.9 T.J. Pacala, I.S. McDermid, J.B. Landenslager, Appl. Phys. Lett., 45, 507 (1984)

7.10 O.L. Bourne, A.J. Alcock, Appl. Phys. Lett., 42, 777 (1983)

7.11 M. Watanabe, S. Watanabe, A. Endoh. Opt. Lett. 8, 638 (1983)

7.12 N.P. Smith, D. Phil. Thesis, University of Oxford (1982)

7.13 Rutherford Appleton Laboratory, Annual Report (1984)

7.14 M. Latta, R. Moore, S. Rice, K. Jain, J. Appl. Phys. 56, 586 (1984)

7.15 K. Jain, R.T. Kerth, Appl. Opt. 23, 648 (1984)

7.16 J. Marshall, S. Trokel, S. Rothery, H. Schubert, Opthalmology, 92, 1 (1985)

7.17 J.M. Isner, R.H. Clarke, I.E.E.E. J. Quant. Elec., QE-20, 1406 (1984)

7.18 D. Muller, R. Svrluga, Laser Focus, 21, 7, p.70 (July 1985)

7.19 D.H. Sliney, M.L. Wolbarsht, Safety with lasers and other optical sources, Plenum Publishing Corp., New York (1980)

7.20 J. Goldhar, W.R. Rapoport, J.R. Murray, I.E.E.E. J. Quant. Elec., QE-16, 235 (1980)

7.21 R.K. Sander, T.R. Loree, S.D. Rockwood, S.M. Freund, Appl. Phys. Lett., 30, 150 (1977)

7.22 Lou Champagne, N.R.L. Washington D.C. Private communication (1984).

APPENDIX I

X-Ray Dose and Exposure Units

The unit of X-radiation used throughout this work, and most other X-ray preionised laser work, is the Roentgen (R). This is the unit of X-ray 'exposure', and is defined as that quantity of X-rays which will produce, in dry air at S.T.P., 1 e.s.u. (3.336×10^{-10}C) of charge of either sign per cubic centimetre. This is equivalent to 2.082×10^{9} ion pairs/cm^3. Clearly, an exposure of 1R could be made from a certain number of X-ray photons of a particular energy, or a different number of photons at a different energy. Therefore, an exposure of 1R in a material other than air at S.T.P. can deposit differing amounts of energy. Because of this, there is a unit of deposited energy, or dose, called the 'rad', which is equal to a deposited energy of 100 ergs/g. So, as W_{air} = 33.7 eV/ion pair, then an exposure of 1R will produce a dose of 0.869 rad. Therefore, in air (and many other gases and liquids such as He, Ne, H_2O ...) the exposure in Roentgens is numerically similar to the absorbed dose in rads. However, in higher Z materials (Xe, Ta, etc.), the two may be significantly different.

REFERENCES

A.1 Radiation Dosimetry, Vol. 1, 2nd Edn., F.H. Attix et al, Academic Press, New York (1968)

A.2 I.C.R.U. (1962) Natl. Bur. Std. (U.S.) Handbook, 84.

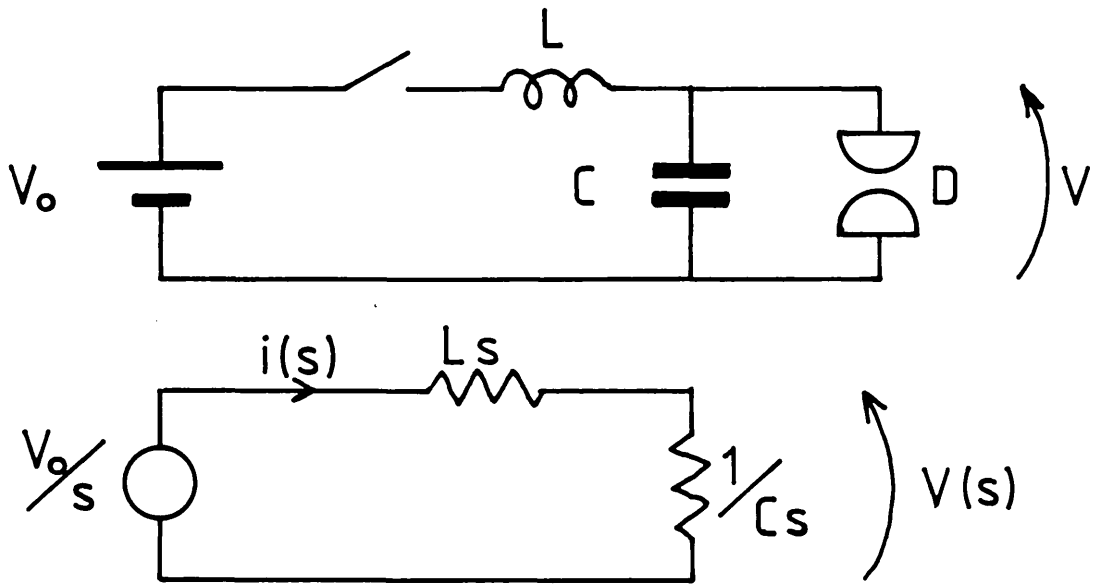

Figure 3.7 and Equivalent Circuit A.II.1

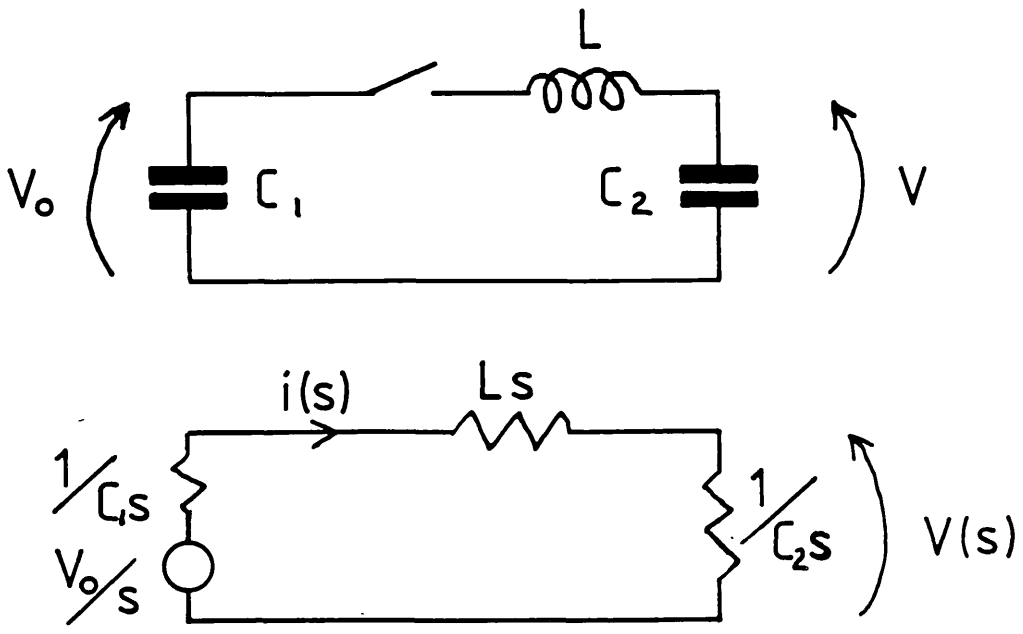

Figure 3.9 and Equivalent Circuit A.II.2

APPENDIX II

CIRCUIT ANALYSES

The circuits analysed in this Appendix are those which appear in the body of the thesis as part of, or as an approximation to, the various sections of the electrical circuits. They are all relatively simple, and the reader is referred to the standard texts for further information. The Laplace transform equivalent circuit method (A.II.1) is used throughout the following solutions.

1) Figure 3.7 and Equivalent Circuit A.II.2

$$V(s) = \frac{1}{Cs}\, i(s) = \frac{1}{Cs}\,\frac{V_o}{s}\,\frac{1}{Ls + (1/Cs)}$$

$$= V_o \frac{1}{LC}\,\frac{1}{s(s^2 + (1/LC))}$$

Taking the inverse Laplace transform

$$V(t) = V_o\ (\ 1 - \cos\omega t\ ) \qquad (\ 3.26\ )$$

where $\omega^2 = 1/LC$

2) Figure 3.9 and Equivalent Circuit A.II.2

$$V(s) = \frac{1}{C_2 s}\, i(s) = \frac{V_o}{C_2 s^2}\,\frac{1}{Ls + (1/C_1 s) + (1/C_2 s)}$$

$$= \frac{V_o}{LC_2}\,\frac{1}{s(s^2 + (1/LC_1) + (1/LC_2))}$$

which from the inverse transform gives

$$V(t) = \frac{V_0 C_1}{C_1 + C_2} \left(1 - \cos\omega t \right) \qquad (3.29)$$

where $\omega^2 = (1/LC_1) + (1/LC_2)$

The risetime, t_r, is given by

$$t_r = \frac{\pi}{\omega} = \pi\sqrt{\frac{LC_1C_2}{C_1 + C_2}} \qquad (3.30) \text{ and } (5.3)$$

It is interesting to note that taking the limit $C_1 \to \infty$ in equation 3.29 gives equation 3.26.

REFERENCE

A.II.1 A. Draper, Electrical Circuits, Longmans, London, 1964.

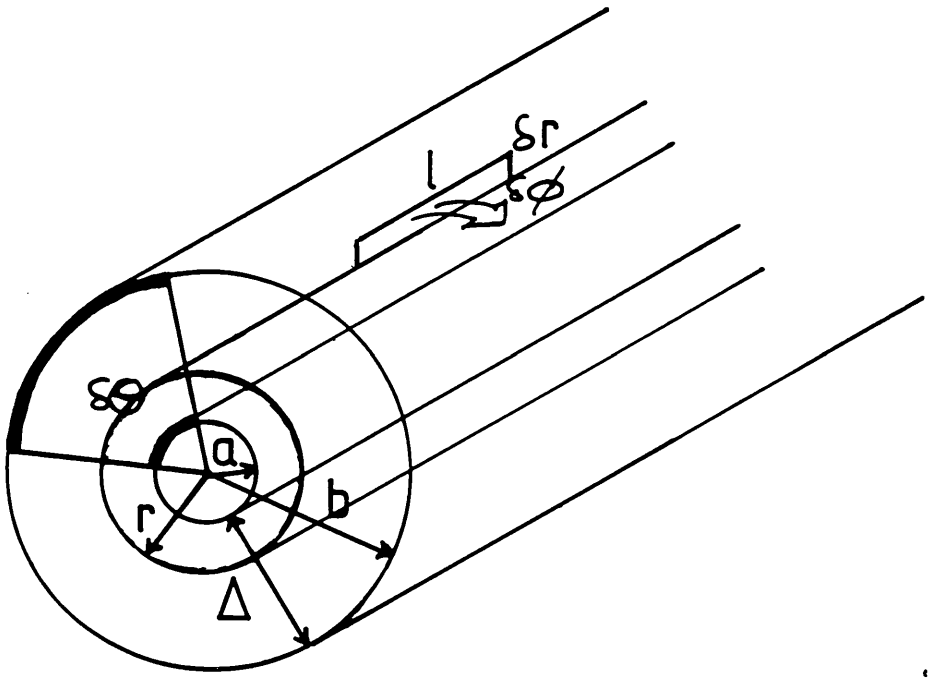

Figure A.III.1 Section of coaxial transmission line. When is very small, or alternatively a, b and r tend to infinity, the section of the conductors within the angle $\delta\Theta$ tend to flat parallel plates as used in the P.F.L.

APPENDIX III

CAPACITANCE, INDUCTANCE AND IMPEDANCE OF PARALLEL PLATE P.F.L.

The capacitance is simply given by the familiar formula

$$C = \frac{\varepsilon_r \varepsilon_0 A}{d}$$

which for plates of dimensions l x W and separation Δ gives

$$C = \varepsilon_r \varepsilon_0 \frac{l W}{\Delta} \qquad \text{(x2 for double P.F.L.)}$$

The inductance, neglecting edge effects, may be calculated in several ways. Perhaps the simplest is that given here.

Consider the section of Coax shown in figure A.III.1 with conductors at radii a and b. Ampères Law states that

$$I = \oint \underset{\sim}{H} \cdot d\underset{\sim}{s}$$

Taking only the part of this integral over the angle $\delta\Theta$ gives

$$I = H(r)\, r\, \delta\Theta = \frac{B(r)}{\mu} r\, \delta\Theta$$

$$\text{so} \qquad B(r) = \frac{I \mu}{r\, \delta\Theta}$$

Now the flux through the area shown is

$$\text{Flux} = \delta\phi = \text{field x area}$$

$$= B(r) \times l \times \delta r$$

Generally, the total flux between the conductors is given by

$$\Phi = \int_a^b \delta\phi$$

If, however, $r >> \Delta$, then B(r) may be considered as constant over this region so that

$$\underline{\Phi} = \int_a^b B(r)\, l\, \delta r = B(r)\, l\, \Delta = \frac{l\, I\, \mu\, \Delta}{r\, \delta\theta}$$

Again allowing the radii to become infinite, corresponding to zero curvature and hence flat plates

$$a\,\delta\theta = b\,\delta\theta = r\,\delta\theta = W$$

$$\underline{\Phi} = I\, l \frac{\mu\, \Delta}{W}$$

so that

$$L = \frac{\underline{\Phi}}{I} = \frac{\mu\, l\, \Delta}{W} \qquad (x\tfrac{1}{2} \text{ for double P.F.L.})$$

(3.27)

The impedance of the P.F.L. is now easily found from equation 3.11, thus

$$Z = (L/C)^{\frac{1}{2}} = \sqrt{\frac{\mu\, l\, \Delta^2}{\varepsilon\, W^2\, l}}$$

$$= (\mu/\varepsilon)^{\frac{1}{2}} \cdot (\Delta/W)$$

Now $(\mu_0/\varepsilon_0)^{\frac{1}{2}}$ is known as the impedance of free space and has the value $\sim 377\Omega$. So, in non-magnetic materials where $\mu_r = 1$ we have

$$Z = \frac{377}{(\varepsilon_r)^{\frac{1}{2}}} \cdot \frac{\Delta}{W} \qquad (x\tfrac{1}{2} \text{ for double P.F.L.})$$

(3.28)

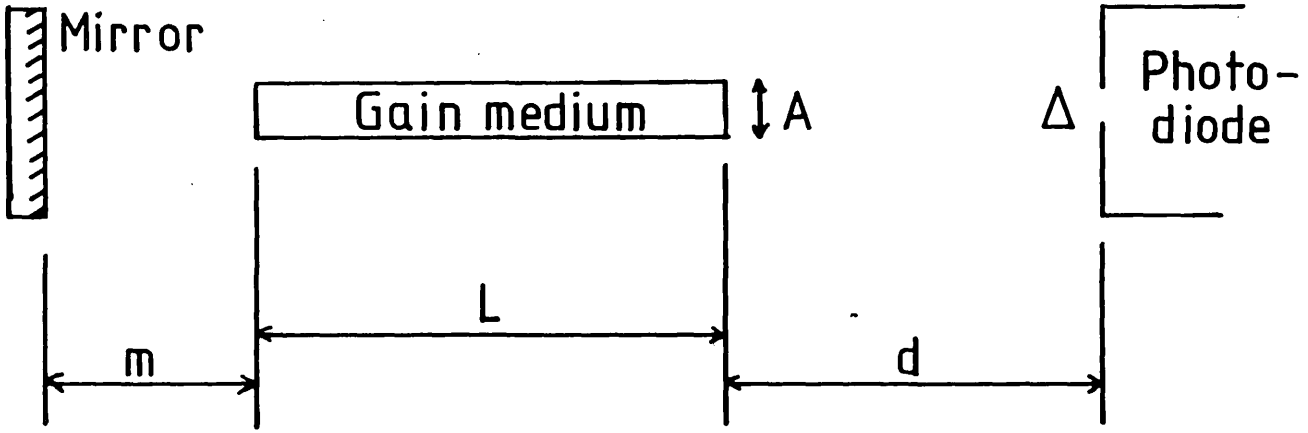

Figure A.IV.1

APPENDIX IV

GAIN MEASUREMENT

The laser gain was measured using the single pass/double pass A.S.E. method (A.IV.1,2) in which a comparison of the peak intensity of the spontaneous emission amplified through a single pass of the gain medium, with that allowed to traverse the gain medium a second time after reflection from a mirror, may be used to assess the magnitude of the small signal gain. The relevant arrangement and distances are shown on figure A.IV.1, and the following assumptions are made:

i) that the small signal gain is instantaneously constant over the length L

ii) that only one dimension need be considered as A << d,L,M, etc.

iii) that the aperture limiting the solid angle of radiation detected is close to the detector, i.e. Δ small.

Therefore, the peak measured single-pass power, S_1, will be given by

$$S_1 = K \int_0^L \frac{e^{\alpha z}}{(d + z)^2} \, dz$$

where α is the small signal gain and K a constant of proportionality. Similarly, the peak of the double-pass signal, S_2, will be

$$S_2 = S_1 + K R \int_0^L \frac{e^{\alpha (z + L)}}{(d + 2m + L + z)^2} \, dz$$

where R is the mirror reflectivity.

Hence, the ratio of the two will be

$$\frac{S_2}{S_1} = 1 + R\, e^{\alpha L} \times \frac{\int_0^L \frac{e^{\alpha z}}{(p+z)^2}\, dz}{\int_0^L \frac{e^{\alpha z}}{(d+z)^2}\, dz}$$

where $P = d + L + 2m$.

Defining $\frac{S_2}{S_1} = 1 + R\, e^{\alpha L} F(\alpha)$

and expanding $F(\alpha)$ in the series

$$F(\alpha) = F(0) + \alpha F'(0) + \frac{\alpha^2}{2!} F''(0) + \ldots\ldots$$

gives the first term as

$$F(0) = \frac{\int_0^L \frac{dz}{(p+z)^2}}{\int_0^L \frac{dz}{(d+z)^2}} = \frac{(d+L)d}{(p+L)p}$$

Similarly, $F'(0)$ is found to be

$$F'(0) = \frac{(d+L)d}{L}\left[\ln\left(\frac{1+p}{p}\right) - \frac{L}{L+p}\right] - \frac{(d+L)^2 d^2}{(p+L)pL}\left[\ln\left(\frac{L+p}{d}\right) - \frac{L}{L+d}\right]$$

Using the experimental values of $d = 420$ cm, $L = 90$ cm, $m = 35$ cm and hence $P = 580$ cm gives

$$\frac{F'(0)}{F(0)} = 0.73$$

and so, assuming a gain coefficient of $\alpha \sim 10\%\ \text{cm}^{-1}$ gives

$$\alpha F'(o) \sim 0.07\, F(0)$$

showing the first term in the expansion of $F(\alpha)$ to be dominant. Therefore, neglecting higher order terms, we have

$$\frac{S_1}{S_2} = 1 + R\, e^{\alpha L}\, \frac{(d + L)\, d}{(p + L)\, p}$$

giving the small signal gain as

$$\alpha = \frac{1}{L} \ln \left[\frac{(p + L)\, p}{(d + L)\, d} \cdot \frac{(S_2/S_1) - 1}{R} \right]$$

This is the equation used in the text to obtain the small signal gain.

REFERENCES

A.IV.1 M.R.O. Jones, Ph.D. Thesis, University of London (1981)

A.IV.2 M. Casey, Ph.D. Thesis, University of London (1982)

APPENDIX V

Publications

M.R. Osborne, P.W. Smith, M.H.R. Hutchinson. Paper presented at IVth National Quantum Electronics Conference, Univ. of Sussex, 1983

M.R. Osborne, P.W. Smith, M.H.R. Hutchinson. Paper ThP4, Conf. on Lasers and Electro-Optics, Anaheim, California, 1984

M.R. Osborne, P.W. Smith, M.H.R. Hutchinson, Opt. Comm., 52, 415 (1985)

M.R. Osborne, M.H.R. Hutchinson. Paper submitted to J. Appl. Phys., July 1985

M.R. Osborne, M.H.R. Hutchinson. Poster paper to be presented at VIIth National Quantum Electronics Conference, R.S.R.E. Malvern, Sept., 1985.

Volume 52, number 6 OPTICS COMMUNICATIONS 15 January 1985

THE EFFECT OF PULSE FORMING LINE IMPEDANCE ON THE PERFORMANCE OF AN X-RAY PREIONISED XeCl DISCHARGE LASER

M.R. OSBORNE, P.W. SMITH * and M.H.R. HUTCHINSON
The Blackett Laboratory, Imperial College, London SW7 2BZ, UK

Received 17 August 1984
Revised manuscript received 5 November 1984

The construction and performance of an X-ray preionised XeCl discharge laser is described. The laser gives an output energy of up to 4.65 J with a pulse duration ≤140 ns and a beam cross-section of 4.2 × 3.0 cm^2. Electrical efficiencies of up to 3.2% have been obtained without the use of an external prepulse circuit. This is 90% of the efficiency which is predicted to be possible using such a circuit in this laser system.

Rare gas halide lasers which are pumped by preionised avalanche electrical discharges have proved to be very convenient sources of powerful ultra-violet radiation. Although preionisation by spark arrays has proved effective for relatively small aperture systems, the use of X-radiation for preionisation has permitted the scaling of these lasers to larger volumes, longer output pulse durations and consequently higher output pulse energies [1–3].

Until recently the efficiency of avalanche discharge pumped excimer lasers has been relatively low (1~2%), considerably below the intrinsic efficiencies of 5~10% achieved in electron-beam pumped lasers [4,5]. A major cause of this inefficiency has been identified as the poor matching of the impedances of the driving circuit, usually some form of pulse forming line (P.F.L.), and the discharge plasma [6,7]. The reduction in efficiency resulting from this impedance mismatch may be quantified in the following way. When a stable glow discharge is formed, the voltage across it has been found to attain a constant value V_s. The current passing through the discharge plasma is, during the initial pulse from the P.F.L., equal to the current passing along the P.F.L. This is given by $I = (V_c - V_s)/Z$, where V_c is the voltage to which the P.F.L. is charged and Z is its characteristic impedance. Hence the impedance of the discharge plasma may be written as

$$R = V_s/I = V_s Z/(V_c - V_s) .$$

The electrical single transit time τ and the capacitance C of the P.F.L. are given by $\tau = l/s$ and $C = l/(Zs)$ where l is the physical length of the line and s is the speed of the electrical pulse along the line. Using these relations it follows that the energy deposited in the plasma during the double transit time of the line (2τ) is given by

$$E_d = I^2 R \cdot 2\tau = \frac{(V_c - V_s)}{Z} V_s \frac{2l}{s} .$$

The energy stored on the P.F.L. is

$$E_s = \tfrac{1}{2} C V_c^2 = \tfrac{1}{2}(1/Zs) V_c^2 ,$$

and the efficiency (η) of energy transfer from the line to the load during the time 2τ is

$$\eta = \frac{4V_s(V_c - V_s)}{V_c^2} = 1 - \left(\frac{2V_s - V_c}{V_c}\right)^2 . \qquad (1)$$

Thus the efficiency of energy transfer is maximal and equal to unity when the charging voltage (V_c) of the P.F.L. is equal to twice the sustaining voltage (V_s) of the discharge. This condition for impedance matching has been obtained previously by Taylor et al. [6] by equating the energy stored on the P.F.L. ($CV_c^2/2$ =

* Present address: Department of Physics, University of St. Andrews, North Haugh, St. Andrews, Fife KY16 9SS, Scotland.

0 030-4018/85/S03.30

$QV_c/2$) to that deposited in the load ($V_s It = V_s Q$) during the transit time (t) of the P.F.L. and by Long et al. [7] by equating the voltage drops across the P.F.L. and the discharge plasma.

Although the condition $V_c = 2V_s$ is necessary for impedance matching, the use of a P.F.L. charging voltage of only twice the sustaining voltage of the discharge leads to slow and non-uniform discharge formation. It is necessary therefore, to use an auxilliary high voltage prepulse circuit producing a fast rising voltage spike in order to realise the benefits of operating in the impedance matched condition. Using such techniques efficiencies over 4% have been achieved [7–9].

In order to store adequate energy at the lower charging voltages necessary for high efficiency operation, the capacitance of the P.F.L. must be relatively high. The length of the P.F.L. is governed by the length of time for which laser action can be sustained, and in many systems the width of the P.F.L. is determined by the dimensions of the laser electrodes. The only parameter of the P.F.L. which may be easily changed to increase the capacitance therefore is the separation of the plates. Increasing the capacitance by bringing the plates closer together decreases the impedance of the line. For this reason the P.F.L.'s used recently [8,10] have been of lower impedance than the 0.5–1 Ω lines used previously. We have found that in the laser system described below there is a lower limit to the impedance of the P.F.L. for which high efficiency operation can be obtained. Furthermore, relatively high efficiencies can be obtained by operating the system some way away from the impedance matched condition by taking advantage of the voltage peaking effect of a short length of transmission line between the P.F.L. and laser head. This facilitates the early formation of a uniform plasma without seriously degrading the temporal shape of the resulting laser output pulse.

A diagram of the laser system used in this study is shown in fig. 1. The X-ray source was designed to provide a uniform X-ray dose over a wide area (7.5 × 100 cm^2) and of sufficient intensity to preionise adequately the gas mixture in the laser cavity. The pulsed high voltage required th drive the e-beam diode was generated using an oil immersed, high voltage pulse transformer [11], the output from which was connected via a conventional oil to vacuum bushing to the cathode of a one metre long X-ray diode. The field emission cathode was constructed from a continuous length of uncoated razor blade mounted within a "race-track" type electrode structure and the whole cathode assembly was fixed to the anode mounting plate using perspex insulators. This enabled the distance between the blade and the anode to be set accurately so as to ensure uniform electron emission over the entire length of the blade. A tantalum foil (8 μm thick) transmission target was used as anode, separated from the e-beam

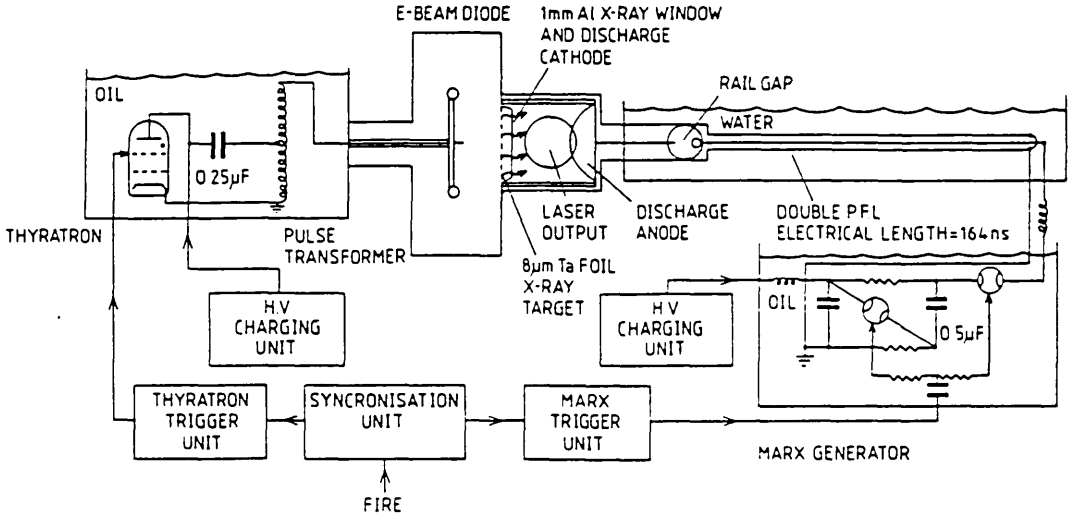

Fig. 1. Schematic diagram of the laser system.

cathode by 3 cm. The diode impedance, estimated from the decay of the voltage waveform from the pulse transformer, was 115 Ω. The voltage applied to the diode had a peak of 110 kV and a duration of 350 ns (FWHM). The resulting X-ray pulse, measured with a photomultiplier, was observed to be of similar form to the voltage pulse.

The spatial uniformity of the X-ray source was measured by means of quartz fibre dosimeters placed at varying positions over the X-ray window. Considerable care in the adjustment of anode-cathode separation was necessary to achieve acceptable uniformity of the X-ray dose. The measured value of the dose averaged along the length of the X-ray window was 55 mR with a spatial variation of ±50%. The X-rays passed into the laser cavity through a 1 mm thick aluminium window supported on a "Hibachi" grill structure.

The pulse forming line used to supply electrical energy to the discharge was a three plate double P.F.L. with deionised water as dielectric. A double P.F.L. has the advantage that its output impedance is half that of a single P.F.L. of equivalent dimensions, thus enabling very low output impedances to be achieved. The impedance of the P.F.L. could be adjusted by inserting sets of perspex spacers of varying thickness between the plates to alter their separation. The line was 2.75 m long giving an electrical double transit time of 164 ns. The width of the plates was 1.0 m, and their separation was varied in three steps, 0.6 mm, 13.5 mm, and 26.0 mm, which correspond to line impedances of 0.13 Ω, 0.28 Ω and 0.54 Ω respectively. The water resistivity was maintained at >0.5 MΩ cm by continuous circulation through a resin ion-exchange deioniser. Bubble formation between the plates, was suppressed by degassing the water.

The line was pulse charged by a two stage Marx generator with an erected output capacity of 0.25 μF. Jitter in the Marx generator was minimised by triggering both spark gaps simultaneously from a 80 kV trigger unit of low output impedance. The pulse forming line was discharged into the laser cavity via a one metre long rail gap and a short (15 ns long) transmission line section. The rail gap switch was of conventional design and consisted of a knife-edge electrode and a round electrode mounted in an annealed perspex tube. Since the P.F.L. was positively charged the knife-edge electrode was connected to the laser head side of the switch. The gap was pressurised with dry-air up to 2 atmospheres.

The body of the laser cavity was made from welded PVDF sheet. X-rays from the diode passed into the laser cavity via an earthed electrode made from 1 mm thick aluminium. The high voltage electrode was constructed from brass, the final profiling being achieved empirically by reference to the dimensions and uniformity of the laser output beam. The spacing between the two electrodes was adjusted by means of spacers behind the earthed electrode. The maximum inter-electrode spacing used was 42 mm, and the gain length was 90 cm. The optical cavity consisted of a high reflectivity (>97% at 308 nm) multi-layer dielectric plane mirror and one of the quartz end-windows.

The time dependence of the discharge current was measured using a Rogowski coil current transformer (EEV type MA459) which surrounded part of one of the feeds from the P.F.L. to the laser cavity. Accurate absolute current measurement, although attempted using a series current viewing resistor made from low resistance foil, proved to be impossible due to calibration problems resulting from contact resistances. The voltage across the cavity was measured using a calibrated ammonium chloride potential divider. The energy stored on the PFL was calculated from its voltage just prior to laser breakdown. This was measured close to the rail gap using a second calibrated ammonium chloride potential divider.

The laser gas was a mixture of Ne, Xe and HCl. The output energy was found to be strongly dependent on the pressure of HCl, being optimum at 4 mbar with a decrease of 50% at 2 mbar and 7 mbar. However, the output energy was independent of the pressure of Xe over the range 15–100 mbar, but was found to increase almost linearly with buffer gas pressure up to the safe working limit of the PVDF laser cavity (3.5 atm), where 4.65 J was obtained. The replacement of the neon by argon resulted in a slight decrease in laser output at low voltages, but at higher voltages arcing resulted in no laser output being produced.

The quality of the laser beam, as measured from burn marks, was good over the majority of the operating range with only a slight blurring at the cathode visible. However at the lowest pumping voltages the beam did not fill the inter-electrode gap, being concentrated at the anode. Broad diagonal stripes which occasionally appeared in the burn marks could be removed by adjusting the quartz windows for all but the highest pumping rates.

By varying the time delay between the X-ray preionisation pulse and the discharge pulse, the influence of preionisation on laser performance could be studied. When the discharge pulse preceded the X-ray pulse, no laser action was observed. At the X-ray doses used, when the start of the discharge pulse overlapped the X-ray pulse the output power of the laser was independent of their relative synchronisation, but a delay of 40 ns of the discharge pulse relative to the end of the X-ray preionisation was sufficient to prevent laser action. This is in marked contrast to the results of Shields et al. [12] where delays of up to 2 μs could be tolerated before laser action ceased.

The short section of transmission line and electrical feeds between the rail gap and laser head act in a manner similar to a peaking capacitor and produce a large initial voltage spike of more than twice the charging voltage of the P.F.L. This facilitates early and uniform discharge formation even for rather low charging voltages (V_c). However, this section also causes the voltage to oscillate, producing a 20% modulation in the discharge current which results in a 10% ripple in the optical output. Unfortunately, this voltage oscillation makes it impossible to measure accurately the value of the discharge sustaining voltage V_s, although as shown below a value can be estimated from the laser efficiency data.

The dependence of the laser efficiency on the energy stored on the P.F.L. is shown in fig. 2 for lines of differing impedances. It is clear that in this system the

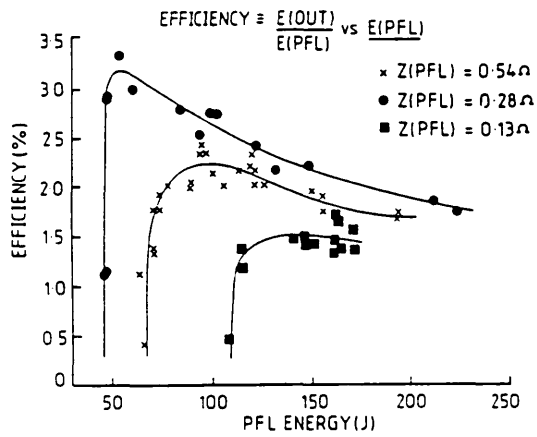

Fig. 2. Laser efficiency as a function of pumping rate for pulse forming lines of impedance 0.13 Ω, 0.28 Ω and 0.54 Ω.

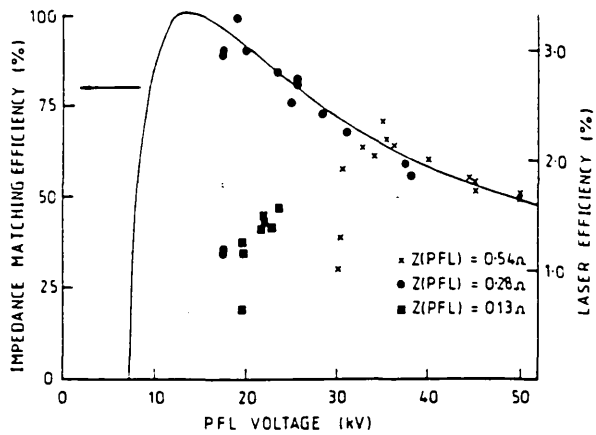

Fig. 3. Laser efficiency as a function of voltage on the P.F.L. The solid curve is the theoretical prediction of the impedance matching efficiency, i.e. the efficiency of transfer of energy from the P.F.L. to the laser plasma during the electrical transit time of the P.F.L. The curve drawn for a constant value of V_s of 7 kV.

0.28 Ω line produces significantly higher efficiencies than the 0.13 Ω or 0.54 Ω lines. The sharp decline in efficiency at low P.F.L. energies, and hence voltages, corresponds to conditions where the spark gaps fail to operate satisfactorily.

The same data is shown in fig. 3 where the efficiency is plotted against the voltage to which the P.F.L. was charged, rather than the energy stored on it. The solid curve represents the impedance matching efficiency, that is the efficiency of energy transfer from the P.F.L. to the plasma during the transit time of the P.F.L. (1). It is drawn for a constant value of V_s, as it has been found by other authors [6] that V_s varies only slowly as a function of the charging voltage of the line over a large range of $V_c > 2V_s$. The form of the curve on the low voltage side of the efficiency peak is less reliable as there is no experimental data for the dependence of V_s on V_c in this region.

The data from the 0.28 Ω and 0.54 Ω lines most closely follow the form of eq. (1) for a value of V_s of 7 kV. It can be seen from fig. 3 that for V_s = 7 kV, the efficiency of energy transfer achieved in this laser is as much as 90% of that predicted to be obtainable under conditions of perfect impedance matching (V_c = $2V_s$) although in this case V_c = 2.7 V_s. At the impedance matched condition an efficiency of 3.4% is predicted, which, from a 3.5 atm laser system, compares

well with the 4% achieved by others from 5 atm systems [8].

The efficiencies produced by the 0.13 Ω line are much lower than would be predicted by this simple impedance matching theory. It has been found that the inductance of the electrical driving circuit is similar for the three impedances of P.F.L. used in this study. Therefore the reactive component of the impedance will be relatively larger in the case of the lowest impedance line resulting in inefficient energy deposition in the plasma.

For the P.F.L. to behave as a pure transmission line it is necessary for the inductance in the circuit to be sufficiently small to allow current risetimes significantly shorter than the transit time of the line. In this system the current risetime was observed to be of the order of 40 ns, which is comparable to the P.F.L. transit time of 164 ns. Under these circumstances the P.F.L. behaves partly as a lumped capacitor. This lumped capacitance gives rise to a component of current oscillation at frequency $1/2\pi\sqrt{LC}$ from which the series inductance L can be calculated. Fig. 4 shows the variation of this inductance for the experimental conditions under which the efficiency results were obtained. The inductance introduced by the rail gap varies inversely with the number of spark channels in the gap and this in turn increases as the rate of rise of voltage (dV/dt) on the P.F.L. is increased. When charging to a higher voltage, and hence higher stored energies, dV/dt is increased, the number of spark channels is also increased and hence the inductance is decreased. The rate of rise of voltage, (dV/dt), is also affected by the risetime of the voltage on the P.F.L. This is given by the equation

$$t_r = \pi[L_m C_m C_Q/(C_m + C_Q)]^{1/2} ,$$

where C_m and C_Q are the capacitances of the erected Marx bank and P.F.L. respectively, and L_m is the series inductance of the Marx and feeds to the P.F.L. L_m has been measured to be 200 nH, giving typical P.F.L. charging times of about 600 ns. Similarly, when using a higher impedance (lower capacitance) P.F.L., the voltage risetime is decreased and the inductance of the line connecting the rail gap to the laser head is also increased. The limiting inductance which is approached for an increasing number of spark channels represents that of the laser head and the line connecting the P.F.L. to the laser cavity, and the results obtained are consistent with the expected increase of this inductance with line separation. The number of spark channels in the rail gap was obtained by open shutter photography and is shown in fig. 4, to increase with increasing stored energy as expected. It should be noted that, for the majority of the operating range, and particularly at the point of maximum efficiency ($E_{P.F.L.}$ = 50 J) the 0.28 Ω line feeds a less inductive load than either of the other two lines.

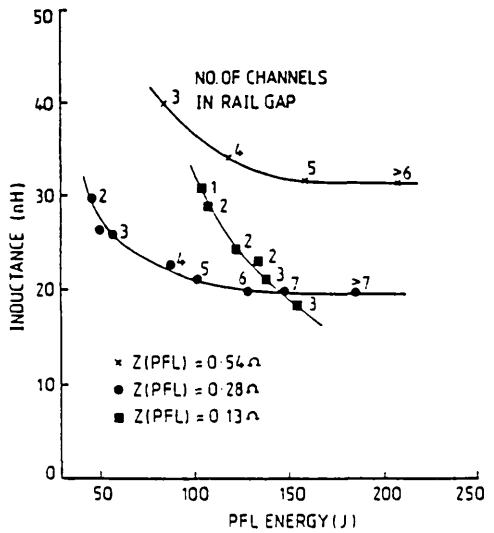

Fig. 4. Total inductance of load (rail gap, feeds and laser head) as a function of pumping rate for the three pulse forming line impedances. The number of spark channels in the rail gap is shown next to each experimental point.

In conclusion, it has been shown that the output power of the X-ray preionised laser increases monotonically with the total gas pressure up to 3.5 atm, and this suggests that higher powers and efficiencies may be achieved at higher pressures using laser cavities of greater mechanical strength. The importance of impedance matching between the P.F.L. and discharge plasma has been described quantitatively, and the experimental data has been shown to be consistent with the simple theory. High-efficiency operation away from the impedance matched condition has been demonstrated without the need for an external prepulse circuit. However, successful operation with a very low impedance P.F.L. has not proved possible with this laser system.

The authors would like to acknowledge the technical assistance of Mr. J.A. Bean, and the financial support of the Science and Engineering Research Council.

References

[1] S.C. Lin and J.I. Levatter, Appl. Phys. Lett. 34 (1979) 505.
[2] J.I. Levatter, K.L. Robertson and S.C. Lin, Appl. Phys. Lett. 39 (1981) 297.
[3] L.F. Champagne, A.J. Dudas and B.L. Wexler, Postdeadline paper ThR8-1, Conf. on Lasers and electro-optics, June 1984, Anaheim, California.
[4] F. Kannari, M. Obara and T. Fujioka, J. Appl. Phys. 53 (1982) 1.
[5] T.H. Johnson and A.M. Hunter II, J. Appl. Phys. 51 (1980) 2406.
[6] R.S. Taylor, P.B. Corkum, S. Watanabe, K.E. Leopold and A.J. Alcock, IEEE J. Quant. Elec. QE-19 (1983) 416.
[7] W.H. Long, Jr., M.J. Plummer and E.A. Stappaerts, Appl. Phys. Lett. 43 (1983) 735.
[8] C.H. Fisher, M.J. Kushner, T.E. DeHart, J.P. McDaniel and J.J. Ewing, postdeadline paper ThR9-1, Conf. on Lasers and electro-optics, June 1984, Anaheim, California.
[9] R.S. Taylor and K.E. Leopold, paper ThP3, Conf. on Lasers and electro-optics, June 1984, Anaheim, California.
[10] M.R. Osborne, P.W. Smith and M.H.R. Hutchinson, paper ThP4, Conf. on Lasers and electro-optics, June 1984, Anaheim, California.
[11] G.J. Rowein, Laser Focus 16 (1980) 70.
[12] H. Shields, A.J. Alcock and R.S. Taylor, Appl. Phys. B31 (1983) 27.